

Polymer Chemistry

Accepted Manuscript

This article can be cited before page numbers have been issued, to do this please use: M. Adeli and H. Ghibi, *Polym. Chem.*, 2015, DOI: 10.1039/C4PY01437E.



This is an *Accepted Manuscript*, which has been through the Royal Society of Chemistry peer review process and has been accepted for publication.

Accepted Manuscripts are published online shortly after acceptance, before technical editing, formatting and proof reading. Using this free service, authors can make their results available to the community, in citable form, before we publish the edited article. We will replace this *Accepted Manuscript* with the edited and formatted *Advance Article* as soon as it is available.

You can find more information about *Accepted Manuscripts* in the [Information for Authors](#).

Please note that technical editing may introduce minor changes to the text and/or graphics, which may alter content. The journal's standard [Terms & Conditions](#) and the [Ethical guidelines](#) still apply. In no event shall the Royal Society of Chemistry be held responsible for any errors or omissions in this *Accepted Manuscript* or any consequences arising from the use of any information it contains.

ARTICLE

Supramolecular Anticancer Drug delivery Systems
Based on Linear-Dendritic CopolymersHoma Gheybi^a and Mohsen Adeli^{*ab}

Cite this: DOI: 10.1039/x0xx00000x

Received 00th January 2012,
Accepted 00th January 2012

DOI: 10.1039/x0xx00000x

www.rsc.org/

Current cancer chemotherapy often suffers severe side-effects of the administered cancer drugs on the normal tissues. In addition, poor bioavailability due to the low water solubility of the anticancer drugs, limits their applications in chemotherapy. New delivery technologies could help to overcome this challenge by improving the water solubility and achieving the targeted delivery of the anticancer drugs. Linear-dendritic hybrid nanomaterials, which combine the highly branched architectures and multifunctionality of dendrimers with the processability of traditional linear-linear block copolymers, have been introduced as ideal carriers in anticancer drug delivery applications. This review presents the recent advances in the investigational aspects of linear-dendritic copolymers to be applied as anticancer drug delivery vehicles. We highlight the structures, synthesis of linear-dendritic block copolymers, interaction mechanisms between linear-dendritic copolymers and anticancer drug molecules, and findings on their drug release behavior and anticancer efficacies in vitro and in vivo.

Table of contents

1.	Introduction.....
2.	Strategies employed for loading anticancer drugs into linear-dendritic vehicles.....
2.1.	Linear-dendritic copolymers/drug conjugates produce vehicles.....
2.2.	Linear-dendritic copolymer produces vehicles upon encapsulation drugs.....
3.	Classification according to loaded drug.....
4.	Paclitaxel.....
4.1.	Paclitaxel-encapsulated linear-dendritic block copolymers.....
4.1.1.	Physicochemical properties.....
4.1.2.	In vitro evaluations.....
4.1.3.	In vivo evaluations.....
4.2.	Paclitaxel-conjugated linear-dendritic block copolymer.....
4.2.1.	Physicochemical properties.....
4.2.2.	In vitro evaluations.....
4.2.3.	In vivo evaluations.....
5.	Doxorubicin.....
5-1.	Doxorubicin-encapsulated linear-dendritic block copolymers.....
5.1.1.	Physicochemical properties.....
5.1.2.	In vitro evaluations.....
5.1.3.	In vivo evaluations.....
5-2.	Doxorubicin-conjugated linear-dendritic block copolymers.....
5.2.1.	Physicochemical properties.....
5.2.2.	In vitro evaluations.....
5.2.3.	In vivo evaluations.....
6.	Cisplatin.....
6.1.	Cisplatin-conjugated linear-dendritic block copolymers.....

6.1.1.	Physicochemical properties.....
6.1.2.	In vitro evaluations.....
7.	Camptothecin.....
7.1.	Camptothecin-conjugated linear-dendritic block copolymers.....
7.1.1.	Physicochemical properties.....
7.1.2.	In vitro evaluations.....
7.1.3.	In vivo evaluations.....
8.	Conclusion.....
9.	Acknowledgement.....
10.	References.....

Abbreviations

CMC: critical micelle concentration; PEG: poly(ethylene glycol); TEM: Transmission electron microscopy; DLS: dynamic light scattering; PBS: phosphate buffered saline; LDP: linear-dendritic copolymers; PTX: paclitaxel; DTX: docetaxel; DOX: doxorubicin; Cispt: cisplatin; CPT: camptothecin; HCPT: hydroxycamptothecin; PAMAM: polyamidoamine; CA: cholic acid; ALN: alendronate; bis-MPA: 2,2-bis(hydroxymethyl) propanoic acid; MWCNTs: multi-walled carbon nanotubes; PG: polyglycerol; Bz: benzylidene; DNQ: diazonaphthoquinone; NIR: near-infrared light-responsive; PDMAEMA: poly(2- dimethylaminoethyl methacrylate); PNIPAM: poly(N-isopropylacrylamide); PDMAEMA: poly(2-(dimethylamino)ethyl methacrylate); PPEGMA: poly(poly(ethylene glycol) methyl ether methacrylate); PCL: poly(ϵ -caprolactone); LA: lipoic acid; PCA: polycitric acid; ENH: enhanced value; ASGP: asialo-glycoprotein receptor; FR: folate receptor; GSH: glutathione; LA: lipoic acid; HNDDSs: hybrid nanomaterial-based drug delivery systems; PDI: polydispersity index; NIRF: near infrared fluorescence imaging; EPR: enhanced permeation and retention effect; MTD: most tolerated dosage; RES: reticuloendothelial system;

1. Introduction

Cancer is one of the leading causes of morbidity and accounts for approximately 20% of all deaths world-wide (World Health Organization). When a cell acquires enough mutations to become cancerous, it will be replicate at a rate higher than normal cells. After tumor mass formation, it is not possible for the normal cells to compete with the cancerous ones for the adequate supply of nutrients from the blood vessels [1–4]. Clinical surgery to remove cancerous tumor is considered as the primary method for fighting cancer. However, surgery may have undesirable side effects such as changing the growth rate of the remaining cancer cells by triggering a faster metastatic process. Following the surgical resection, radiotherapy, chemotherapy and immunotherapy are the common methods currently employed in the clinical management of cancer [5,6]. One of the major problems facing cancer chemotherapy is the lack of mandatory selectivity of chemotherapeutic drugs to direct the cytotoxicity to tumor cells, leading to undesirable side effects [7,8]. A promising approach to overcome this problem is the application of nanomaterial based drug delivery systems [9] including inorganic or other solid nanoparticles (gold [10,11], iron oxide [12,13], quantum dots [14,15] and carbon nanotubes [16,17,18]), polymeric micelles [19,20,21], dendrimers [22,23,24], and liposomes [25,26]. Ability to improve drug solubility, slow down the metabolism of the drug and prolong the circulation time, tumor specific delivery, higher accumulation in tumors via the enhanced permeability and retention (EPR) effect resulting in enhanced efficacy and reducing side effects are the advantages of such nanocarriers [27–29]. Use of nanomaterial based drug delivery systems for biomedical applications is one of the constituents of an emerging field called nanomedicine that has shown great promise for the development of novel diagnostic, imaging, and therapeutic agents for a variety of diseases, including cancer [30–35]. Among the nanomaterials, linear-dendritic hybrid materials are a growing class of nanoscopic carriers which combine the highly branched architecture and multifunctionality of dendrimers with the processability of traditional linear-linear block copolymers [36,37]. The concept of linear-dendritic block copolymer was announced by Fréchet group in the early 1990's for the first time including a polystyrene and a dendritic poly(benzyl ether) block [38], and later on, a PEG block and a hydrophobic dendritic poly(benzyl ether) block [39]. Because of their unique self-assembly properties, linear-dendritic systems have received increasing attention to use as a versatile platform for drug delivery applications [40–42]. Dendrimers offer a plenty of advantages compared to other architectural forms of polymers that have been used in drug-delivery systems. Unique characteristics such as highly branched globular architecture, narrow polydispersity, nanometer size range, periphery groups, physicochemical, and self-assembly properties make dendrimers promising candidates in nanomedicine. The main successes of dendrimers in nanomedicine resulted in their appropriate, reproducible and optimized design parameters addressing physicochemical limitations of classical drugs (e.g. solubility, specificity, stability, biodistribution and therapeutic efficiency) and their ability to overcome biological issues to reach the right target(s) (e.g. first-pass effect, immune clearance, cell penetration, off-target interactions, etc.) [43–47]. However, several drawbacks limit transportation of small guest molecules by perfect dendrimers. Perfect dendrimers have a relatively rigid molecular structure with interior cavities, which are not flexible, and have certain dimensions for accepting guest molecules with a certain and defined size. For encapsulation and release of guest molecules from perfect dendrimers, a protection and deprotection reaction series is necessary. In contrast to drawbacks of perfect dendrimers, linear-dendritic copolymers have flexible interiors and can encapsulate

variety of small guest molecules[48–51]. Recently, it has been shown that transport capacity of some of linear-dendritic copolymers is much more than perfect dendrimers[52,53]. These advantages and interesting properties of linear-dendritic polymers have stimulated investigation in this area.

Three strategies have been reported for synthesis of linear-dendritic copolymers [54]: (a) "coupling" method: coupling of dendron with a functionalized linear polymer [39]; (b) "chain-first" method: growth of dendritic segment from the terminal group of a linear polymer [55]; (c) "dendron-first" method: polymerization of linear segment from the dendron macroinitiator by controlled/"living" radical routes [56]. These synthetic strategies lead to low polydispersity and a great deal of control over molecular architecture of obtained linear-dendritic copolymers [43,57–59].

Gitsov has described detailed architectures of linear-dendritic hybrids in a valuable review [41]. The building blocks of the linear-dendritic copolymers can be positioned in several distinct configurations due to the presence of multiple anchoring points in blocks. According to Gitsov's classification, the first general group contains a single monodendron or dendrimer (D) and one (A), two (B), or multiple (C) linear segments (L) attached at the "focal" point or at the peripheral functional groups in the D fragments, Figure 1.

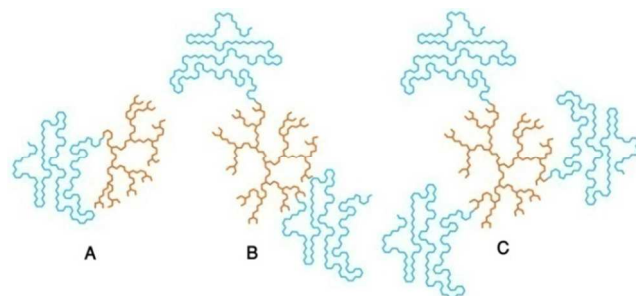


Figure 1. Linear-dendritic architectures; First group: A, B, and C. Structures were first published in ref 41.

The characteristic feature of the second group is the attachment of two monodendrons to the extremities of a single linear chain (E) or the incorporation of dendrimers into the main linear chain (F), Figure 2.

The third group unifies the structures, where monodendrons are attached like "pendants" to a main linear chain through short (G) or long spacers (H). When the linear chain is "shrunk" (H) is transformed into a star-like macromolecule with the monodendrons anchored at the extremities of the star arms (K), Figure 3. A special case of (K) arises when the core of the star is not a small multifunctional unit, but a dendrimer.

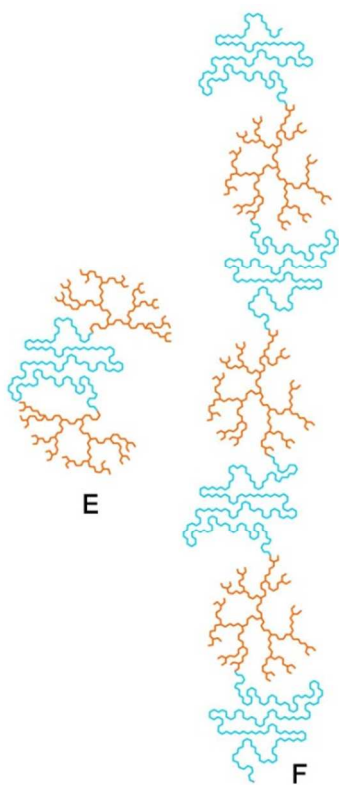


Figure 2. Linear-dendritic architectures; second group: E, and F. Structures were first published in ref 41.

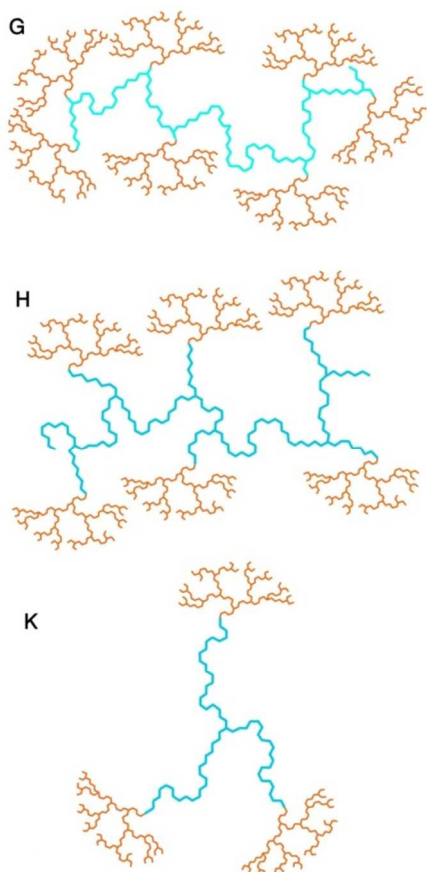


Figure 3. Linear-dendritic architectures; Third group: G, H, and K. Structures were first published in ref 41.

A network constructed by dendrimers as the crosslinking moieties and linear blocks as the interjunction fragments constitutes a special case of "infinite" linear-dendritic copolymer, Figure 4.

Finally, the dendritic-linear-dendritic super dendrimer shown in Figure 5 represents the ultimate challenge in synthetic organic and polymer chemistry.

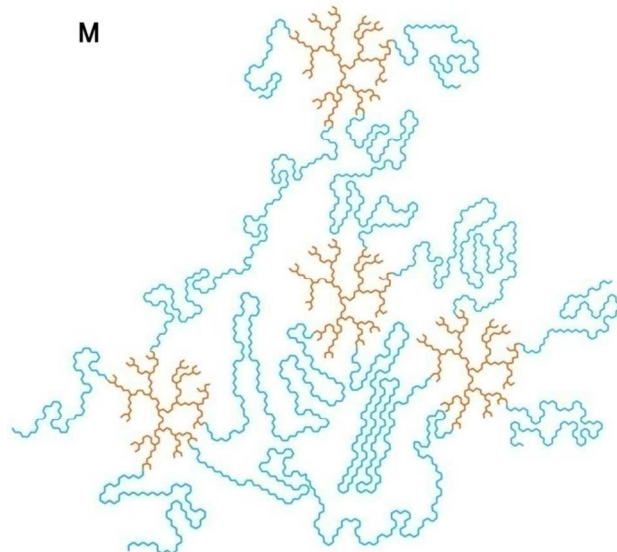


Figure 4. Linear-dendritic architectures; Forth group: M. Structures were first published in ref 41.

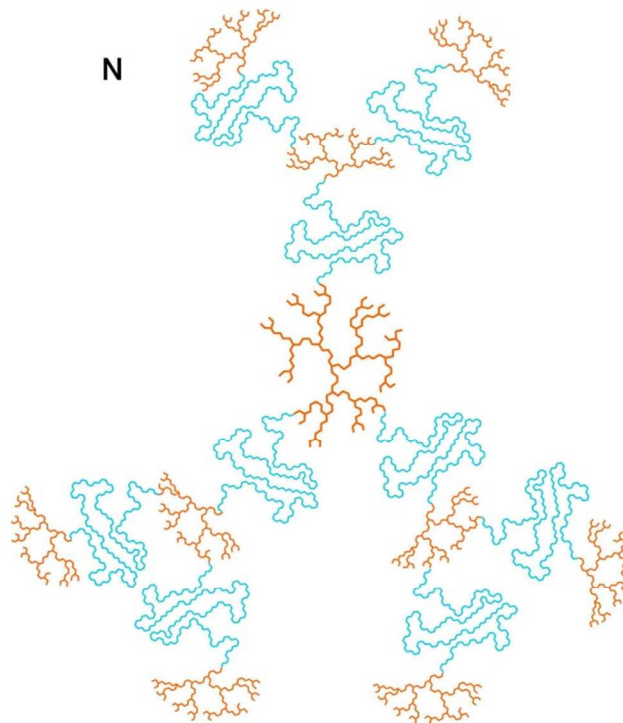


Figure 5. Linear-dendritic architectures; Fifth group: N. Structures were first published in ref 41.

Besides improving the water solubility of the hydrophobic drugs, encapsulated by hydrophobic interior of dendritic segments [60-62], the reactive surface end groups of dendritic blocks can be covalently attached to variety of drugs and therapeutic agents [63,64], targeting and imaging moieties [65-67], and bioactive molecules [68] to achieve targeting, imaging, and therapeutic treatment of cancer. Several articles reviewed the research activities generated on linear-dendritic hybrids from different point of views such as discovery and synthetic strategies, PEG-dendritic block copolymers applications, and DNA-protein-dendritic biohybrids in nanobiotechnology [41, 43, 58, 69, 70]. This review will focus on the potential of several (A), (E), and (K) typelinear-dendritic hybrids as nanosized carriers for anticancer drug delivery systems. Specifically, we will describe the synthesis methods of related linear-dendritic hybrids, loading/conjugating of anticancer agents onto linear-dendritic carriers, and the associated in vitro and in vivo anticancer activity.

2. Strategies employed to load anticancer drugs into linear-dendritic vehicles

Currently used cancer chemotherapeutics are often inadequate to cure tumors because of the nonselectivity of these drugs, resulting in dose-limiting side effects. Strategies for reducing this toxicity and side effects without sacrificing efficacy could greatly improve treatment and quality of life issues for those besieged. Drug delivery systems that are specific to tumor cells offer both an increased therapeutic index and reduced harmful side effects [71-73]. Several attempts have been made to design linear-dendritic copolymers as drug carriers. Drug molecules can be transferred either as conjugated to the functional groups on the dendritic structure or encapsulated by the hydrophobic interior of the dendritic blocks. These two approaches have been developed substantially although each approach has its own advantages and drawbacks [74-78].

2-1. Linear-dendritic copolymers/drug conjugates produce vehicles

By conjugating appropriate targeting moieties, drugs, and imaging agents to linear-dendritic polymers, 'smart' drug-delivery nanodevices can be developed that can target, deliver, and monitor the progression of therapy [8, 79]. However, the conjugation generally requires multi-step organic reactions and the covalent conjugation chemistry has to be optimized in order for the drug molecules to be cleaved and released at the specific biological conditions [75].

Drugs can be conjugated to linear-dendritic polymers either directly or via a linker/spacer including:

- acid labile hydrazone linkages, which are stable at physiological pH but readily cleaved under mildly acidic conditions, e.g., inside of endosomes and lysosomes [78];
- ester linkages, which are hydrolyzed inside the cell by esterase enzymes [8];
- disulfide bonds, which are reduced by glutathione inside the cytosol [80];
- amide bond, but this bond is known to be very stable chemically under biological environments [81].
- Acid sensitive acetal bonds, which are stable at pH > 7, can be an interesting option. At mildly acidic pH, hydrolysis of the acetals is expected to occur, generating hydroxyl groups [82].

2-2. Linear-dendritic copolymers produce vehicles upon encapsulation of drugs

In the physical encapsulated or complex form, the drugs can be loaded to the dendritic blocks by non-covalent interactions such as

van der Waals forces, hydrophobic interactions, hydrogen bonding and electrostatic interactions between oppositely charged fragments of drug molecule and dendritic blocks [42,74,83]. The latter approach is relatively simple; however, in spite of significantly improving the water solubility and bioavailability of the drugs, the in vivo stability of the copolymer/drug complexes could be a challenging issue [75,84].

3. Classification based on the loaded drug

The present review focus on the application of linear-dendritic vehicles for delivery of four anticancer drugs: paclitaxel, doxorubicin, cisplatin, and camptothecin. The following listing of drugs associated with carriers composed of linear-dendritic copolymers provides an overview of the potential of the linear-dendritic platform to serve as anticancer drug carriers.

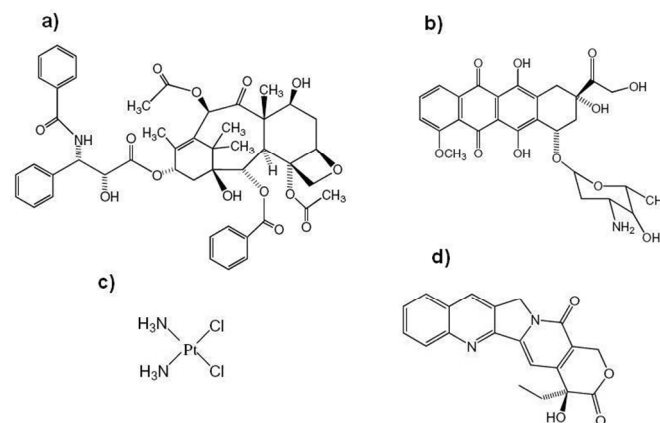


Figure 6. Structures of a) Paclitaxel, b) Doxorubicin, c) Cis-platin, and d) Camptothecin

4. Paclitaxel

Paclitaxel (PTX), also known as Taxol (trade mark of Bristol-Myers-Squibb), is one of the most effective anticancer agents against a wide spectrum of cancers including ovarian, breast, and colon cancer. It exerts its antitumor effect by binding to microtubules and interfering with the normal growth of microtubules during cell division, which especially affects fast growing cancer cells [61, 85-89]. However, systemically administered PTX causes serious side effects, such as neutropenia and peripheral sensory neuropathy. On the other hand, to overcome its limited solubility in water, paclitaxel (Taxol) is formulated in an oily solution of Cremophor EL (polyethoxylated castor oil) and absolute ethanol (1:1 v/v). This is known to create such effects as anaphylaxis and other severe hypersensitivity reactions attributable to Cremophor EL and ethanol [85, 86, 90].

4-1. Paclitaxel-encapsulated linear-dendritic block copolymers

4.1.1. Physicochemical properties

In attempts to overcome mentioned limitations, paclitaxel has been encapsulated into micelle-based formulations. An interesting study has reported micellar linear-dendritic block copolymer composed of polyethylene glycol (PEG, Mw=5 KDa) and third generation of polylysine terminated with 8 units of cholic acid (CA), named PEG^{5k}-CA₈ telodendrimer (Figure 7), for delivery of PTX in the treatment of nude mice bearing ovarian cancer xenografts (Compound 1) [84].

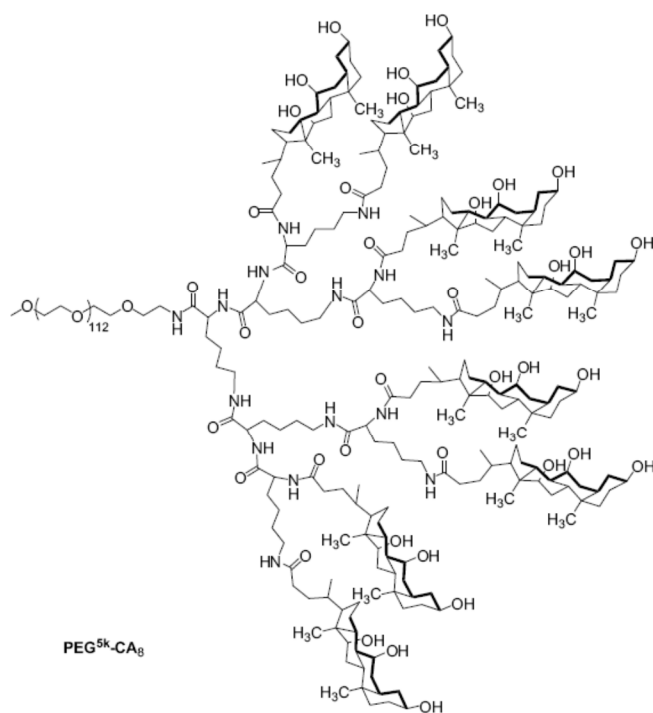


Figure 7. The chemical structure of PEG^{5k}-CA₈ (Compound 1). Reprinted with permission from ref. 84. Copyright (2009) Elsevier Ltd.

Physical entrapment of paclitaxel in linear-dendritic micelles has been done utilizing hydrophobic interactions between PTX and dendritic cholic acid cluster resulted to high loading capacity (7.3 mg PTX/mL) through evaporation method. The particle size of PEG^{5k}-CA₈ nanoparticles loaded with PTX was 56 nm as measured by the dynamic light scattering (DLS) method. Cryo-TEM images showed the particles were spherical in situ, and the sizes were 50–60 nm, which was consistent with the results obtained by DLS. PTX-PEG^{5k}-CA₈ NPs have also been found to be very stable at 4 °C, showing no significant changes in average particle size over 6 months. Whereas, Abraxane® (the FDA-approved Albumin nanoparticle-bound Paclitaxel) was unstable and start to form larger aggregates and precipitate 4 days after dissolving the white powder of Abraxane with saline. The obtained PTX-PEG^{5k}-CA₈ NPs exhibited sustained drug release into surrounding PBS, rapid release of 20% of the drug in the first 2 h, cumulative release of 35% of the drug by 12 h, and a slow linear release of 75% of the drug by 156 h [84]. In order to better define the relation between the structures of the PEG^{mk}-CA_n telodendrimers and their physicochemical properties for drug delivery, this group prepared a series of stable micelle systems with tuneable particle sizes by varying the PEG chain length and the number of cholic acid in the dendritic core [90]. Other natural lipophilic molecules such as cholesterol formate (CF), lithocholic acid (LA) (both with planar steroid scaffold), and heptadecanoic acid (HA) (linear fatty acid) have been also substituted instead of cholic acid in PEG^{5k}-CA₈ linear-dendritic structure. The resulting micelles, with low critical micelle concentrations (CMC) at approximately 1 μM, tended to form precipitate in aqueous solution, and their PTX loading capacities were rather low [90], indicating the essential role of facial amphiphilic cholic acid for stabilizing telodendrimer micelles. Also by varying the PEG chain length and the number of cholic acid in the dendritic core, it has been determined that larger numbers of

cholic acids led to low CMC, larger micelles with a heterogeneous size distribution, and significant precipitation after PTX loading. PEG^{5k}-CA₈ with a medium particle size of 61 nm and the highest PTX loading capacity (7.3 mg PTX loaded in 20 mg PEG^{5k}-CA₈/mL, 36.5% (w/w) of drug/polymer ratio) has been found to be the optimized structure for carrying the drug [90]. The stability of the PTX-loaded PEG^{5k}-CA₈ micelles was followed by the DLS particle sizer. The particle size of these PTX-loaded micelles in aqueous solution was found to be highly stable at 4 °C for over 6 months, no further aggregations and no needle crystals of PTX were observed. As mentioned before, Abraxane tends to precipitate 24 h after reconstituted with saline. Upon dilution with PBS to 125-fold to mimic the dilution by the blood pool through intravenous (iv) injection, needle-like crystals of PTX were observed in the diluted Taxol (Cremophor formulation of PTX) the diluted PTX-loaded PEG^{5k}-CA₈ micelle solutions even for 12 months, indicating that the PTX complex inside these micelles is very stable [90].

Later Li et al. [80] introduced a cross-linked micelle system for specific delivery of paclitaxel to tumor sites composed of a dendritic oligomer of cholic acids attached to one terminus of the linear PEG through a poly(lysine-cysteine-Ebes) backbone (Compound 2). Cysteine has been inserted in linear-dendritic structure to achieve a self assembling disulfide-crosslinking system so that micelles can be further stabilized to avoid premature release of the loaded drugs during circulation. At the tumor sites, the intracellular reductive agents such as glutathione cleaved the intra-micellar disulfide bonds and the drug release occurred. PTX loading into the micelles was done by the solvent evaporation method. PTX and the polymeric structure were first dissolved in chloroform. Then, the chloroform was evaporated under vacuum to form a thin film. PBS buffer (1 mL) was added to re-hydrate the thin film, followed by 30 min of sonication. The PTX-loaded micelles were then cross-linked via O₂-mediated oxidization. CMC value of 0.67 μM was determined for PTX loaded cross-linked micelles. The morphology of the PTX loaded cross-linked micelles was observed to be spherical with uniform sizes under a TEM. The size of the micelles observed under TEM was consistent with those measured by DLS (27 nm) [80]. Loading capacity of PTX in the cross-linked system was 7.1 mg/mL, which was equivalent to 35.5% (w/w) of drug/micelle ratio. PTX loaded disulfide cross-linked micelles have been found to be very stable at 4 °C, showing no significant changes in average particle size and drug contents over 8 months. The stability of the micelles in physiological conditions including blood was demonstrated by monitoring the particle sizes of micelles over time. The PTX loaded DCMs micelles retained the average particle size around 30 nm, with uniform and narrow size distribution, in human plasma for 24 h. Drug release studies indicated that the PTX release was gradually facilitated as the GSH concentration increased from its extracellular level (2mM) up to the intracellular level (10 mM). This drug release strategy indicated that premature drug release can be minimized during circulation in vivo, and accelerated release occurred upon internalization of the micelles into cancer cells [80].

There is one interesting study employing biodegradable amphiphilic linear-dendritic block copolymers that present folate in clusters for cell targeting, as a means of selectively targeting drug-loaded nanocarriers for chemotherapeutics [91]. PTX has been loaded into the polymeric micelles noncovalently via self-assembly of amphiphilic linear-dendritic copolymers (LDP) composed of the hydrophobic linear polypeptide block [poly(β-benzyl-L-aspartate)] (Mw=3000 Da) and the hydrophilic dendritic polyester-PEG block (Mw= 12000 Da) (Figure 8) (Compound 3). Folate occupied approximately 10% of the surface (~4–5 wt% of micelle), leaving the other 90% exposed as PEG. During assembly, hydrophobic PTX is entrapped within the micelle core and the polyester-PEG dendron

ARTICLE

forms a dense antifouling shell around the micelle. The PTX-loaded micelles have a hydrodynamic diameter of ~ 90 nm and a negative surface charge of -20 mV. It was shown that PTX remained within the LDP carrier for at least 2 hours following systemic injection, which is sufficient time to allow their distribution to tumors in significant quantity via EPR. The longer stability observed can be attributed to the low micelle CMC (CMC of $\sim 10^{-8}$ M) for LDP micelles, making the system more resistant to dilution effects and destabilization by in vivo conditions. Increased effective solubility of PTX was achieved by PTX loading into the linear-dendritic micellar system with drug-loading weight efficiencies up to 40 wt%. Drug release studies showed enhanced release at lower pH, caused by breakdown and destabilization of micelle structure [91].

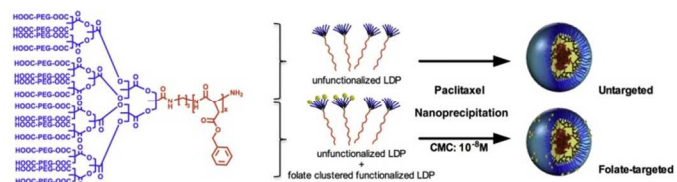


Figure 8. Chemical structure of the linear dendritic polymer (LDP) made from biocompatible and degradable elements (linear polypeptide-[poly(β -benzyl-L-aspartate)] block and dendritic polyester-PEG block) ($X_n = 12-15$). Blue, hydrophilic; red, hydrophobic. Schematic showing the preparation of paclitaxel (PTX)-encapsulated LDP micelles that do not present folate or present folate clusters for enhanced cell targeting (compound 3). Reprinted with permission from ref. 91. Copyright (2011) Elsevier Inc.

Qiao et al. have reported a novel linear-dendritic block copolymer micelles semi-polyamidoamine-b-poly(d,l-lactic acid) encapsulating hydrophobic docetaxel, a semisynthetic structural analogue of paclitaxel (Compound 4) [92]. Hydroxyl-tailed semi-polyamidoamine dendron (sPA-OH) has been synthesized by a divergent method, in which the growth of a dendron has been originated from a core site. Then, ring-opening polymerization (ROP) of d,l-lactide has been carried out using hydroxyl-tailed sPA-OH G4.5 (or G3.5) and catalytic amount of $\text{Sn}(\text{Oct})_2$. DTX has been encapsulated to obtain linear-dendritic copolymer by co-solvent evaporation method. Hydrophobic linear PLA block formed a micelle inner core that acted as a container for insoluble drug DTX, which was subsequently stabilized by hydrophilic capped polyamidoamine shell. The highest DTX loading efficacy (80.4%) was achieved for the copolymer with molecular weight of 11500 g/mol bearing semi-PAMAM G4.5. CMC of 5.01 mg/L and particle size of 87.4 nm was determined for these DTX loaded micelles. Based on drug release experiments, it was determined that approximately 100% of encapsulated DTX was released at pH 5.0, however this value was about 75% at pHs 6.8 and 7.4, indicating a facilitated DTX release under acidic conditions that can be beneficial to specific drug targeting in vivo (Figure 9). This pH dependent manner was described by protonation of tertiary amine groups of semi-PAMAM dendritic block that leads to conformational changes and triggers the drug release [92].

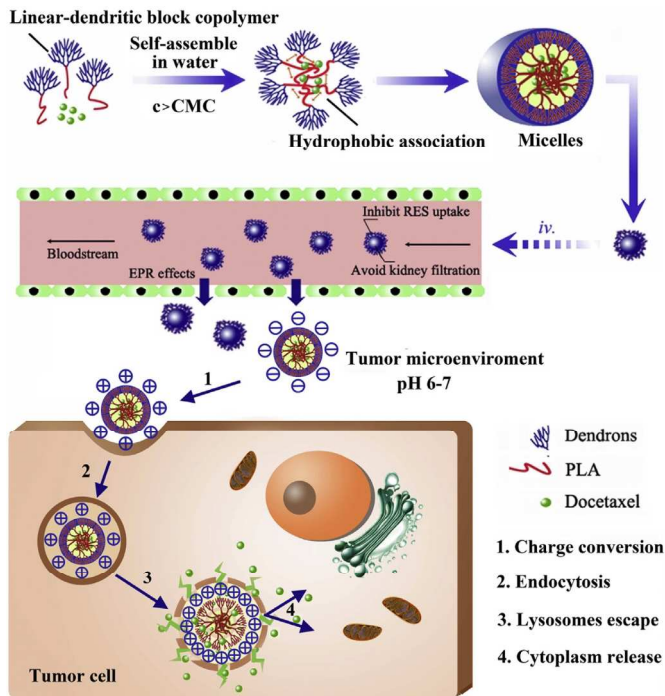


Figure 9. Self-assembly and multifunctional target delivery of DTX-loaded polyamidoamine-b-poly(d,l-lactic acid) micelles (Compound 4). Reprinted with permission from ref. 92. Copyright (2013) Elsevier B.V.

4.1.2. In vitro evaluations

Investigations of in vitro anticancer activity of the PTX-PEG^{5k}-CA₈ NPs (Compound 1), performed on SKOV3-luc-D3 ovarian cancer cells, demonstrated similar cytotoxic activity against cancer cells as the free drug [84]. In vitro cytotoxicity studies of PTX-loaded linear-dendritic micelles including PEG^{5k}-CA₈, PEG^{3k}-CA₄, and PEG^{3k}-CA₈ and the two clinical formulations of PTX (Taxol and Abraxane) on SKOV-3 cells demonstrated the IC₅₀ in the range of 4.3 to 6.2 ng/mL (Figure 10) [90].

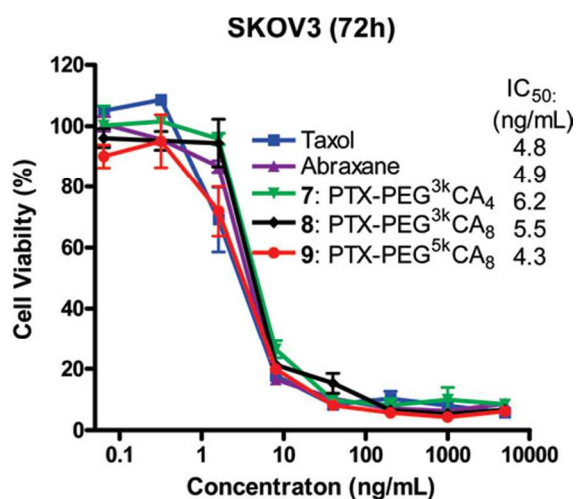


Figure 10. Tumor cell killing of the PTX-loaded PEG^{mK}-CA_n micelles in the SKOV-3 ovarian cancer cells, very similar IC₅₀ values were observed for all the formulations in in vitro tumor cell

killing. Reprinted with permission from ref. 90. Copyright (2010) American Chemical Society

Investigation of in vitro antitumor effect of PTX loaded PEG-poly(lysine-cysteine-Ebes)-cholic acid crosslinked system (Compound 2), evaluated on SKOV-3 cells, showed less cytotoxicity than Taxol [80]. This was attributed to the slower release of PTX within the cell culture media. However, enhanced cytotoxicity was achieved through studies on SKOV-3 cells with an enriched GSH level that facilitates intracellular drug release by cleavage of intracellular disulfide bridges [80].

Cytotoxicity studies of docetaxel encapsulated semi-polyamidoamine-b-poly(d,l-lactic acid) (Compound 4) on human breast cancer cell lines (MCF-7) [92] showed no inhibition of cellular growth for blank micelles attributed to reduction/shielding of the positive charge on dendrimer surface by terminal ester while, DTX-loaded micelles showed equipotent anticancer efficacy as control Taxotere® (IC_{50} 2.23 ± 0.15 vs 1.58 ± 0.11 $\mu\text{g/mL}$) (incubation time: 72 h) confirming semi-PAMAM-b-poly(d,l-lactic acid) as a promising anticancer drug carrier [92].

4.1.3. In vivo evaluations

Evaluation of the anti-tumor effects of PTX-PEG^{5k}-CA₈ NPs (Compound 1) after intravenous injection in subcutaneous SKOV3-luc tumor bearing mice showed inhibition of tumor growth for all PTX formulations and for PTX-PEG^{5k}-CA₈ NPs at 30 mg PTX/kg being the most [84]. However, a second treatment cycle was initiated on day 38 because of tumor progression noted. Decreased tumor growth rate was demonstrated after the intravenous administration of PTX-PEG^{5k}-CA₈ NPs and free drug, PTX-PEG^{5k}-CA₈ exhibited superior anti-tumor activity as compared with Taxol. Based on near infrared fluorescence (NIRF) imaging, it was found that PTX-PEG^{5k}-CA₈ nanoparticles post i.v. injected in cancer bearing mice had a prolonged blood circulation time, and preferentially accumulate in tumors, possibly as a result of EPR effects [84]. In vivo biodistribution (evaluated in nude mice bearing the SKOV-3 ovarian cancer xenografts) was greatly influenced by the size of the micelles [90]. Demonstrated by NIRF images, PTX-loaded PEG^{3k}-CA₄ micelles with larger sizes (154 nm) had very high uptake in liver and lung, but low uptake in tumor. On the other hand, PEG^{2k}-CA₄, PEG^{5k}-CA₈ micelles having smaller particle sizes (17 and 64 nm) showed more ability to carry the loaded drug to the tumor sites attributed to EPR effects. In vivo antitumor effects for PTX-loaded PEG^{5k}-CA₈ was found to be superior to those of Abraxane and Taxol, and the cure of the disease was achieved in the group treated with PTX-loaded PEG^{5k}-CA₈ at its MTD dosage (45 mg/kg). No weight loss was observed in mice treated with this nanoformulation, while consistent weight loss was observed in those treated with Taxol [90]. This system concludes some significant advantages such as nontoxicity of carrier in contrast to commercial vehicle of PTX, high drug loading capacity, relatively small sustained drug release profile, superior stability, preferential accumulation in tumors, similar in vitro cytotoxic activity with Taxol, and superior in vivo anti-tumor activity as compared with Taxol [84, 90]. Enhanced efficacy of PTX encapsulated PEG^{5k}-CA₈ NPs after intravenous injection can be explained as follows: First, the PEG^{5k}-CA₈ nanocarrier may improve the pharmacokinetic profile of PTX, prolonging its circulation time, thus resulting in a higher accumulation in tumors due to EPR effects. Secondly, since PTX encapsulated PEG^{5k}-CA₈ NPs accumulate in tumor, PTX is released in a sustained manner so that tumor cells can be exposed to PTX for longer time period. Thirdly, PTX encapsulated PEG^{5k}-CA₈ NPs have a relatively small size (50 nm) compared to Abraxane (130 nm), which may result in deeper penetration into tumor nodules.

This is important regarding that although some nanoparticles with larger size such as liposomes can be delivered effectively to a solid tumor via the EPR effect, they would not be distributed sufficiently to cancer cells distant from tumor vessels [91]. These promising features make PTX encapsulated PEG^{5k}-CA₈ NPs suitable for more investigations [84,90].

For PTX encapsulated PEG-poly(lysine-cysteine-Ebes)-cholic acid crosslinked system (Compound 2) [80], according to noninvasive NIRF optical images, a significant contrast of fluorescence signal has been observed between tumor and background at 4 h after administration and sustained up to 72 h (Figure 11, Top). Ex vivo imaging at 72 h post injection further confirmed the preferential uptake of crosslinked micelles in tumor compared to normal organs (Figure 11, Bottom). This is due to the prolonged in vivo circulation time of the micelles and the size mediated EPR effect. A relatively high uptake in the liver was observed compared to other organs, which is likely attributed to the nonspecific clearance of nanoparticles by the reticuloendothelial system (RES). Similar biodistribution and tumor uptake of PTX loaded crosslinked micelles were observed via EPR effects [80].

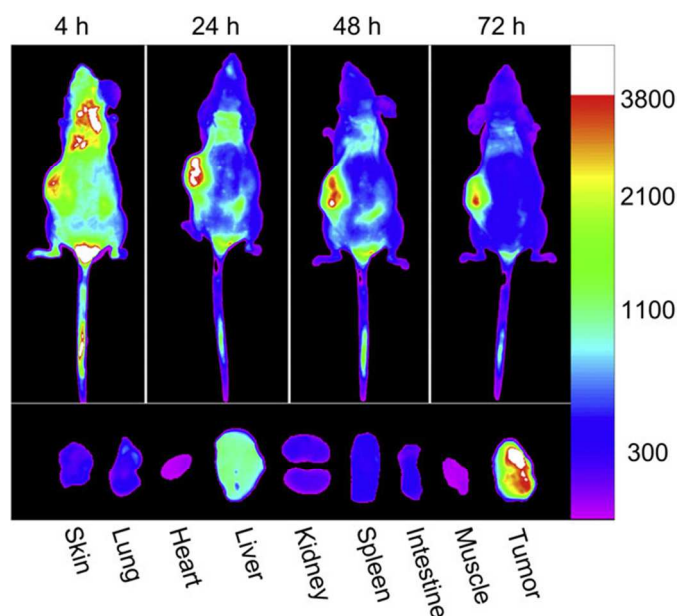


Figure 11. In vivo and ex vivo near infra-red fluorescence (NIRF) optical imaging. Top: In vivo NIRF optical images of SKOV-3 xenograft bearing mouse were obtained with Kodak imaging system at different time points after i.v. injection of PEG-poly(lysine-cysteine-Ebes)-Cholic acid co-loaded with PTX and DiD; Bottom: Ex vivo NIR image of dissected organs and tumor was obtained at 72 h after injection. (For interpretation of the references to colour in this figure legend, the reader is referred to the web version of this article.) Reprinted with permission from ref. 80. Copyright (2011) Elsevier Ltd.

Based on in vivo studies evaluated in the subcutaneous SKOV-3 tumor bearing mice, increased in vivo therapeutic efficacy has been shown for PTX-loaded crosslinked micelles compared to the equivalent dose of free drug. This has been corresponded to the higher amount of PTX that reached the tumor site via their prolonged circulation time. In addition, the high glutathione level of the tumor site and particularly inside the tumor cells caused to facilitate drug release and increase cytotoxicity [80]. Uniform size around 27 nm for PTX encapsulated PEG-poly(lysine-cysteine-Ebes)-cholic acid crosslinked system enables these PTX loaded

micelles to take full advantage of the EPR effect and accumulate at tumor sites. In addition, the system has the characteristics of superior drug loading capacity, enhanced micellar stability, prolonged in vivo circulation time, preferential tumor targeting, and superior in vivo anti-tumor activity as compared with Taxol. However, a relatively

high uptake in the liver was observed compared to other organs, which is likely attributed to the nonspecific clearance of nanoparticles by the reticuloendothelial system (RES) [80].

Table 1. Paclitaxel-encapsulated linear-dendritic block copolymers

Carrier	Size (nm)	CMC	In vitro activity	In vivo activity	advantages	ref
PEG ^{5K} -CA ₈	56	1 μM	IC ₅₀ = 4.3 ng/mL on SKOV3-luc-D3 ovarian cancer cells	superior anti-tumor activity for PTX-PEG ^{5K} -CA ₈ as compared with Taxol after intravenous injection in subcutaneous SKOV3-luc tumor bearing mice	High drug loading level, nontoxic carrier, high drug loading capacity, relatively small sustained drug release profile, superior stability, preferential accumulation in tumors, superior anti-tumor activity as compared with Taxol	84, 90
PEG- poly (lysine-cysteine-Ebes)-CA	27	0.67 μM	less cytotoxicity compared to Taxol on SKOV-3 cells, but higher cytotoxicity compared to Taxol with an enriched GSH level	increased in vivo therapeutic efficacy compared to the equivalent dose of free drug in the subcutaneous SKOV-3 tumor bearing mice	Superior drug loading capacity, enhanced micellar stability, prolonged in vivo circulation time, preferential tumor targeting, and superior in vivo anti-tumor activity as compared with Taxol	80
[poly(β-benzyl-l-aspartate)]-polyester-PEG	90	10 ⁻⁸ M	enhanced uptake of ligand-clustered micelles in ovarian tumor cells	Higher in vivo antitumor efficacy for the folate-bearing linear-dendritic micelles compared to free PTX in FR-expressing KB xenograft model in nude mice	Suitable circulation half-life, resistance to dilution effects and destabilization by in vivo conditions, increased targeting of the micelles to FR-expressing cells, increased accumulation	91
semi-PAMAM-b-poly(d,l-lactic acid)	87.4	5.01 mg/L	IC ₅₀ =2.23 ± 0.15 μg/mL on human breast cancer cell lines (MCF-7), equipotent anticancer efficacy as control Taxotere	1.53 fold higher half-life of DTX in micelles compared to Taxotere®	biocompatibility, improved cellular uptake, facilitated anticancer drug release under acidic conditions	92

In the case of polymeric vehicle composed of hydrophobic linear polypeptide block [poly(β -benzyl-L-aspartate)] and hydrophilic dendritic polyester-PEG block (Compound 3) [91], after intravenous injection in BALB/c mice without tumors, distribution half-lives ($t_{1/2}$, distribution) of the encapsulated PTX (2.5 wt%) and free PTX (2.5 wt% equivalent) were 1.72 ± 0.2 hour, and 0.61 ± 0.4 hour, and their elimination half-lives ($t_{1/2}$, elimination) were 9.06 ± 2 hours, and 4.32 ± 3 hours, respectively, indicating a much higher bioavailability of the PTX-loaded LDP micelles compared to free drug. This can be attributed to the low CMC of micelles, making the system more resistant to dilution effects and destabilization by in vivo conditions. Also 10–12% weight loss was revealed in mice receiving free-PTX and signs of hair loss were shown after six injections. No signs of toxicity were shown in mice receiving PTX-encapsulated injections. In vivo antitumor efficacy investigations, evaluated in FR-expressing KB xenograft model in nude mice, showed that the folate-bearing linear-dendritic micelles (PTX dosage = 2.5 mg/kg) is as effective as a higher dose of free PTX (10 mg/kg). Comparison of tumor killing effects between folate-targeted and untargeted micelles (PTX dosage = 2.5 mg/kg) determined the higher antitumor efficacy for folate-targeted LDP system. This was attributed to more efficiently entering of folate targeted micelles into tumor cells from the extracellular space, through FR-mediated uptake, and subsequent intracellular releasing of drug [91]. The measured circulation half-life of PTX encapsulated [poly(β -benzyl-L-aspartate)]-block-dendritic polyester-PEG was significantly higher than values reported in preclinical trials for PTX loaded PEG-block-poly(d,l-lactide) linear block copolymers in the literature [94]. The longer stability due to low micelle CMC, more resistance to dilution effects and destabilization by in vivo conditions, increased targeting of the micelles to FR-expressing cells, increased accumulation over a 5-day period, and potency of therapy with a low PTX dose of 2.5 mg/kg make this system promising for antitumor treatment. For achieving a relatively similar effect, this dosage regimen is much lighter in comparison to other studies involving folate-mediated therapy [95–97]. However, data also suggest a gradual loss of PTX from the micelles at longer time points via slow leakage of drug from the interior of the micelle, and future design of the system may be applied to further address this issue [91].

Pharmacokinetic study in Sprague-Dawley (SD) rats illustrated that semi-polyamidoamine-b-poly(d,l-lactic acid) micelles (Compound 4) prolonged DTX retention in blood circulation (1.737 h) in comparison to Taxotere® (commercial vehicle of DTX) (1.231 h), and the half-life of DTX in micelles was 1.53 fold higher than that of Taxotere® control [92]. A plausible explanation was that ester-terminated hydrophilic dendrons and dense micelle structure were capable of preventing drug molecules from being easily eliminated from the physiological environment. Investigation of intracellular uptake capacity evaluated in MCF-7 cells demonstrated that fluorescent dye C6 labeled semi-polyamidoamine-b-poly(d,l-lactic acid) micelles had been internalized into cytoplasm. Previous studies indicated that multivalent dendrimers enhanced membrane adhesion and disruption [98]. Multivalent dendritic surface of linear-dendritic semi-polyamidoamine-b-poly(d,l-lactic acid) might also increase binding sites with membrane and facilitate micelles uptake. Further studies are needed to elucidate the uptake mechanisms of semi-polyamidoamine-b-poly(d,l-lactic acid) micelles. Generally, low CMC would be beneficial to semi-polyamidoamine-b-poly(d,l-lactic acid) micelles in order to avoid dilution in the blood circulation. Some other advantages such as biocompatibility, improved cellular uptake, and facilitated anticancer drug release under acidic conditions make linear-dendritic semi-polyamidoamine-b-poly(d,l-lactic acid) benefit for anticancer drug delivery. However, its safety and efficacy in chemotherapy should be further studied [92].

4-2. Paclitaxel-conjugated Linear-dendritic block copolymers

4.2.1. Physicochemical properties

A linear-dendritic targeting system for PTX delivery has been reported by Clementi et al. [8] employing alendronate (ALN), a bone-targeting agent used for the treatment of osteoporosis and bone metastases. PEG–dendrimer–ALN structure has been designed using β -Glutamic acid as symmetric bicarboxylic branching unit and linking of ALN to carboxylic groups of PEG–dendrimer. Coupling of PTX to PEG–dendrimer–ALN through ester linkage yielded the linear-dendritic ALN-mediated bone targeting prodrug (Compound 5) (Figure 12).

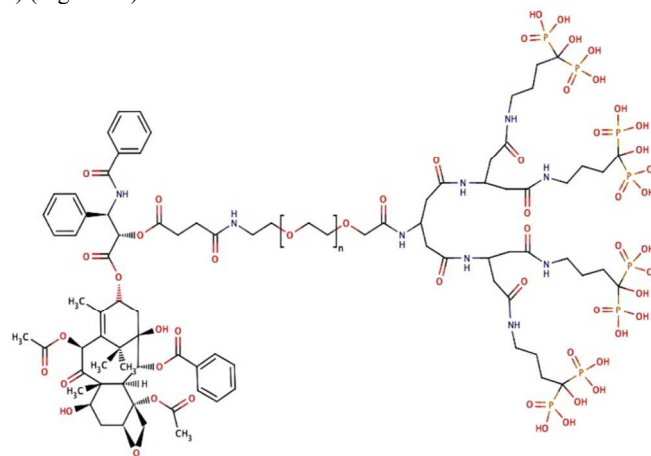


Figure 12. Chemical structure of PTX conjugated PEG–(β -Glu) dendrimer–ALN (Compound 5). Reprinted with permission from ref. 8. Copyright (2011) American Chemical Society

This design leads to an amphiphilic conjugate, being PTX highly hydrophobic and ALN hydrophilic. The spatial separation of these drugs, besides offering the possibility to form self-assembled micelles, will maintain all ALN molecules exposed to the water, promptly available for binding to the bone mineral HA [8]. The content of ALN and PTX in PEG–(β -Glu) dendrimer was determined as 11% w/w and 4.7% w/w respectively. The mean hydrodynamic diameter of PTX–PEG–(β -Glu) dendrimer–ALN conjugates was 200 nm. Investigation of drug release showed that the hydrolysis rate of the ester bond between PTX and the polymer was higher in both plasma and buffer solution at physiological pH (7.4), compared to that in buffer solution at lysosomal pH (pH 5). This phenomenon indicated that PTX is released by a hydrolytically based mechanism without a significant contribution of esterases. The stability of PTX–PEG–(β -Glu) dendrimer–ALN was evaluated in buffer solutions at physiological pH (7.4), at lysosomal pH (5), and in mice plasma. At pH 7.4 and in plasma, about 50% of the PTX-PEG-ALN conjugate was degraded within the first 1 h; the remaining conjugate was degraded within 24 h. The stability of the conjugates micelles, monitored at 37 °C for 24 h by DLS, was in line with the kinetics of PTX release. The micelles of PTX-PEG-ALN conjugates preserved the same size for 24 h when incubated in buffer at pH 5, whereas at pH 7.4 the same micelles were stable for 3 h, then the PTX release from the conjugates destabilized the system [8].

4.2.2. In vitro evaluations

ALN-mediated binding capacity of PEG–(β -Glu) dendrimer–ALN and PTX conjugated PEG–(β -Glu) dendrimer–ALN (Compound 5) to bone mineral was evaluated in vitro employing HA mineral

mimicking bone tissue [8]. By Fast protein liquid chromatography (FPLC) analysis, it was revealed that following 5 min of incubation, 80% or 90% of PTX-PEG-dendrimer-ALN or PEG-ALN conjugates, respectively, were bound to HA and reached a plateau. On the other hand, non-targeting PEG could not bind to HA after 60 min of incubation confirming the role of ALN in bone targeting process. Illustrated by in vitro rat red blood cell (RBC) hemolysis assay, PTX-PEG-(β -Glu) dendrimer-ALN showed no hemolytic activity at up to 5 mg/mL. Regarding significant hemolytic activity of commercial solubilizing vehicle of PTX, PEG-(β -Glu) dendrimer-ALN can be suggested as a promising carrier for PTX. In vitro cytotoxicity assay on PC3 human prostate cancer cells exhibited similar IC_{50} for PTX-PEG-dendrimer-ALN and free PTX (25–60 nM) [8].

4.2.3. In vivo evaluations

The pharmacokinetic studies of PTX dissolved in 1:1:8 ethanol/Cremophor EL/saline and PTX-PEG-(β -Glu) dendrimer-ALN (Compound 5) Showed an improved Pharmacokinetic Profile in Mice [8]. After administration of free PTX, high levels of the drug were recorded, however at 5 min post-injection, the PTX concentration decreased dramatically, and it was not detectable at 60 min. On the contrary, the conjugates showed a marked half-life prolongation, with detectable levels of PTX after 24 h for PTX-PEG-(β -Glu) dendrimer-ALN. In particular, elimination half-lives ($T_{1/2\beta}$) were 15.1 and 85.5 min for PTX and PTX-PEG-(β -Glu) dendrimer-ALN, respectively [8].

PTX-PEG-(β -Glu) dendrimer-ALN conjugate was designed for a strong bone tropism and a fast drug release. Therefore, with PTX-PEG-(β -Glu) dendrimer-ALN conjugate, a cathepsin B-cleavable linker might not be suitable because the derivative in vivo will bind to the bone HA matrix. The high affinity to the bone originating from the presence of a bisphosphonate in the conjugate can affect the conjugate internalization into cancer cells and consequently slow the rate of PTX release, if a cathepsin B-cleavable linker is used. Cathepsin B is over-expressed in lysosomes of many types of tumor cells, but also secreted to the extracellular matrix. In general, enzymatic cleavage is efficient when slow and controlled drug release is required. When a fast release is desired, a different mechanism, such as hydrolysis, is necessary. Therefore, a PTX-polymer hydrolysis at physiological conditions has been preferred because it allows drug release in the surroundings of bone metastasis, where the conjugate will fast accumulate.

PTX was linked to PEG through an ester linkage exploiting a succinimidyl spacer, which releases the drug at physiological pH. The hydrolysis rate of the ester bond between the drug and the polymer was higher in buffer at pH 7.4 than in pH 5. Interestingly, the incubation in plasma showed a drug release comparable to that in buffer at pH 7.4, suggesting that PTX is released by a hydrolytically based mechanism without a significant contribution of esterases. Besides nontoxic building blocks, the derivative can target bone neoplasms by dual-targeting as follows: (1) through ALN (active mechanism), and (2) by exploiting the EPR effect (passive mechanism), which is due to the atypically leaky tumor blood vasculature that enhances tumor accumulation of the conjugate thanks to its increased size with respect to the free drug [8].

Table 2. Paclitaxel-conjugated Linear-dendritic block copolymers

Carrier name	size	CMC	In vitro activity	In vivo activity	advantages	ref
PEG-poly (β -glutamic acid) – ALN	200	n	similar IC_{50} for PTX-PEG-dendrimer-ALN and free PTX (25–60 nM) on PC3 human prostate cancer cells	n	nontoxic carrier building blocks, half-life prolongation of conjugates, targeting bone neoplasms, fast drug release in the surroundings of bone metastasis	8

n: not reported

5. Doxorubicin

Doxorubicin (DOX) is a widely used anticancer drug in the treatment of many types of cancer, including hematological malignancies, many types of carcinoma, and soft tissue sarcomas. DOX is known to interact with DNA by intercalation and to inhibit the biosynthesis of macromolecules [67, 99–101].

However, drawbacks such as poor water solubility, poor penetration in vitro and in vivo, and dose dependent side-effects such as cardiotoxicity, caused by lack of tumor selectivity, limit its application in chemotherapy [101–103]. Several techniques have been used to enhance tumor targeting and reduce the toxicity without sacrificing efficacy. The use of macromolecular drug carriers such as liposomes [104], polymeric micelles [105], dendrimers [106] and linear-dendritic copolymers [107] is the focus of research. One clinical example is Doxil[®], a polyethylene glycol (PEG) containing liposomal formulation of DOX that limits the cardiotoxicity while maintaining the same survivability as the free drug [102].

5-1. Doxorubicin-encapsulated linear-dendritic block copolymers

5.1.1. Physicochemical properties

Gillies and Fréchet has reported DOX encapsulation in acid-sensitive linear-dendritic micelles. The linear-dendritic structure has been composed of a PEO block and a G3 polyester dendrimer of 2,2-bis(hydroxymethyl) propanoic acid units bearing cyclic acetals of 2,4,6-trimethoxybenzaldehyde (Compound 6 in Figure 13). DOX was loaded into micelles of by an oil/water emulsion method in which chloroform was used as the organic phase, and 3 equiv of NEt_3 was used relative to DOX, as the drug is known to partition most effectively into the chloroform phase and into the micelle upon deprotonation of the glycosidic amine. Release of drug occurred through disruption of the micelle caused by hydrolysis of the cyclic acetals at acidic pH and change in micelle solubility [107].

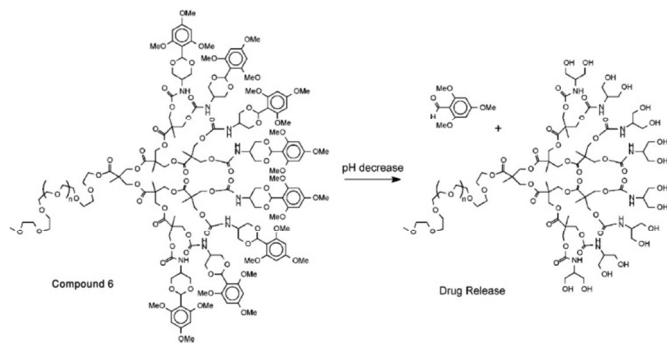


Figure 13. Hydrolysis of acetals on the dendrimer periphery of the micelle-forming copolymer **6** leads to a solubility change designed to disrupt micelle formation and trigger the release of drug. Reprinted with permission from ref. 107. Copyright (2005) American Chemical Society

A drug loading of approximately 12 wt % was determined according to absorbance using UV-visible spectroscopy. The DOX-loaded micelles demonstrated the particle size of 35 nm and a small fraction of aggregates in the size range of 200–400 nm was observed. Additionally, CMC value of 40 mg/L was determined for this system. At pH 7.4, the micelles were stable over several days, with no significant changes in the size distribution over this time period. In contrast, over several h at pH 5.0, the size of the DOX-loaded micelles increased and the fraction of aggregates in the population became greater. This aggregation probably occurred upon disruption of the micelles due to acetal hydrolysis and was facilitated by the tendency of DOX to form aggregates by π -stacking. Investigation of drug release at different pH's demonstrated a pH-dependent manner for release of DOX from copolymer **1**. After 24 h, more than 80%, about 40% and about 30% drug release was observed at pH of 4.0, 5.0 and 6.0, respectively, while at pH 7.4 the system was very stable with less than 10% of the DOX released over 72 h. These results indicated that the hydrolysis of the pH-sensitive acetals likely plays a role in drug release manner leading to the selective release of DOX in mildly acidic physiological environments (such as tumor tissues). In addition, the increased stability of the pH-sensitive system at pH 7.4 is advantageous so that DOX will not be released during blood circulation, thus avoiding the undesirable organ accumulation and toxicity associated with the free drug [107].

A newly developed telodendrimer platform, consisting of PEG as linear block and cholic acid attached to amine terminus of lysine as dendritic block, has been employed to prepare DOX micellar formulations for the targeted delivery of DOX to lymphoma [108]. As mentioned before [84], PEG^{5k}-CA₈ micellar NPs provided a suitable drug delivery system for PTX (a hydrophobic drug) in the treatment of cancer. In their study, Xiao et al showed that the delivery of DOX using this nanocarrier is limited by the relatively low drug loading capacity and poor stability [108]. Using the dry-down method, PEG^{5k}-CA₈ telodendrimers can efficiently encapsulate hydrophobic drug DOX into the core of micelles (Compound **7**). PEG^{5k}-CA₈ telodendrimer along with different amount of neutralized DOX were first dissolved in CHCl₃/MeOH, mixed, and evaporated on rotavapor to obtain a homogeneous dry polymer film. The film was reconstituted in 1 mL phosphate buffered solution (PBS), followed by sonication for 30 min, allowing the sample film to disperse into micelle solution [108].

Based on their report, PEG^{5k}-CA₈ micelle was found to have DOX loading capacity of 8.2% w/w. Another telodendrimer with the similar structure, PEG^{2k}-CA₄, was suggested to encapsulate DOX which resulted in higher drug loading capacity of 14.8% w/w. The

particle sizes of DOX-loaded PEG^{5k}-CA₈ and PEG^{2k}-CA₄ micelles were in the range of 12–17 nm in diameter. Drug release profiles illustrated biphasic patterns for both DOX-loaded PEG^{2k}-CA₄ and PEG^{5k}-CA₈ micellar formulations. It was indicated that 50% DOX cumulative release occurred from DOX-PEG^{5k}-CA₈ during the first 6 h. This value was 35% for DOX-PEG^{2k}-CA₄ during the same time. After the initial fast release, the slow linear release was observed for both systems in the next 7 days. However, the DOX release rate from DOX-PEG^{2k}-CA₄ micelles was significantly slower than that from DOX-PEG^{5k}-CA₈ micelles reflecting the better stability and stronger interaction between the nanocarrier and drug in DOX-PEG^{2k}-CA₄. Particle size monitoring confirmed the stability of DOX-PEG^{2k}-CA₄ in physiological conditions. As shown by DLS measurements (Figure 14), DOX-PEG^{2k}-CA₄ micelles as well as Doxil[®] were able to maintain their initial particle sizes over 72 h incubation in the presence of 50% FBS. In contrast, DOX-PEG^{5k}-CA₈ micelles started to form bigger aggregates (around 300 nm) after a 6-hour incubation with 50% FBS [108].

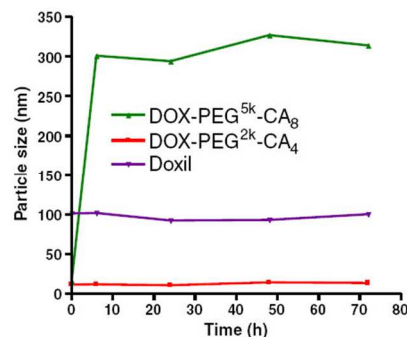


Figure 14. DLS measurement of particle size change of DOX-loaded PEG^{5k}-CA₈ micelles, and Doxil[®] in 50% FBS over time at 37 °C. DOX loading level was 2 mg/ml DOX in 20 mg/ml telodendrimer, respectively. Reprinted with permission from ref. 108. Copyright (2011) Elsevier B.V.

Wu et al. developed dendritic-linear block copolymer-modified magnetic iron oxide nanoparticles as a carrier for DOX that display thermosensitive drug release behaviors [109]. In their study, magnetic iron oxide (Fe₃O₄) nanoparticles were first prepared by the method of the organic solution-phase decomposition of the iron precursor at high temperature. The prepared magnetic iron oxide nanoparticle surfaces were capped by the propargyl focal point poly(amideamine) (PAMAM)-type dendron, having four carboxylic acid end groups. Then, by a click reaction, the surface initiator was introduced onto the propargyl group, and using two-step surface-initiated ATRP, poly(2-dimethylaminoethyl methacrylate) (PDMAEMA) chains and poly(N-isopropylacrylamide) (PNIPAM) chains were sequentially introduced onto the magnetic nanoparticle surfaces resulting in PAMAM-b-PDMAEMA-b-PNIPAM block copolymer-modified magnetic iron oxide nanoparticles. At the final step, to increase stability of the nanoparticles and reverse aggregation, a cross-linking reaction between PDMAEMA block and 1,2-bis(2-iodoethoxy)ethane (BIEE) was carried out (Figure 15). After the crosslinking reaction, the magnetic nanoparticles were stabilized in water, forming a stable brown solution and no precipitation occurred for 4 months. However, non-crosslinked Fe₃O₄-PAMAM-b-PDMAEMA-b-PNIPAM nanoparticles could be only stabilized in water for 2 months. It was also verified that the cross-linking reaction could be helpful to stabilize magnetic iron oxide nanoparticles. DLS measurements of freshly cross-linked block copolymer-modified nanoparticles diluted in water provided

an average hydrodynamic diameter of particles in solution equal to ~32 nm. DOX has been loaded into the PAMAM-b-PDMAEMA-b-PNIPAM shell of the modified nanoparticles with the loading efficiency of 22.7% (Compound 8) [109].

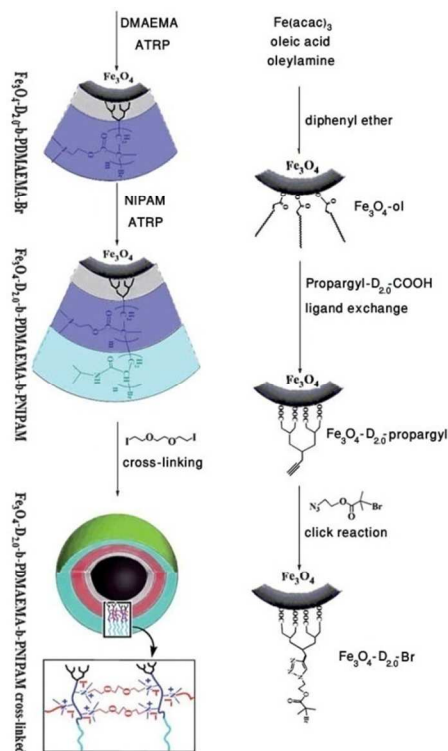


Figure 15. Synthesis and surface modification of superparamagnetic Fe_3O_4 nanoparticles (Compound 8). Reprinted with permission from ref. 109. Copyright (2011) The Royal Society of Chemistry

Investigation of drug release behaviour of DOX-loaded nanoparticles demonstrated the cumulative release amounts of 26.8% and 13.7% at 25 °C and 37 °C, respectively (pH = 7.4, 5 h). This phenomenon was also observed after 24 h with the cumulative release amounts of 41% and 26% at 25 °C and 37 °C, respectively. It was noted that the cumulative release amount was higher at 25 °C than at 37 °C, confirming thermosensitive release manner caused by PNIPAM block chains that are in the collapsed and hydrophobic conformation at 37 °C above the LCST, which can retard drug release [109].

Also it has been reported a DOX-loaded water-soluble dendritic-linear-brush-like triblock copolymer, polyamidoamine-b-poly(2-(dimethylamino)ethyl methacrylate)-b-poly(poly(ethylene glycol) methyl ether methacrylate) (PAMAM-b-PDMAEMA-b-PPEGMA)-grafted superparamagnetic iron oxide nanoparticles (SPIONs) as a pH-sensitive drug delivery system (Compound 9) [110]. Immobilization of ATRP macroinitiator, containing PAMAM G2-typed dendron, on the surface of Fe_3O_4 nanoparticles has been carried out according to the reported procedure in the literature [109]. Then, water soluble dendritic-linear-brush-like triblock copolymer (PAMAM-b-PDMAEMA-b-PPEGMA)-grafted SPIONs has been prepared by gradually growing of PDMAEMA and PPEGMA from nanoparticle surfaces using the ATRP "grafting from" approach. After removal of Fe_3O_4 cores with hydrochloric acid, M_n and PDI of the grafted copolymers PAMAM-b-PDMAEMA-Br were 3900 g mol^{-1} and 1.08, respectively. For final

grafted copolymers PAMAM-b-PDMAEMA-b-PPEGMA, M_n and PDI were 26300 g mol^{-1} and 1.25, respectively. DLS measurement confirmed that the obtained dendritic-linear-brush-like triblock copolymer-grafted SPIONs had a uniform hydrodynamic particle size of average diameter less than 30 nm. In order to drug loading, DOX-HCl (2.0 mg) was dissolved in methanol (4.0 mL), and triethylamine (25 μL) was then added into the solution to remove hydrochloride. Drug loading was done by drop-wise adding the DOX solution with stirring to 3 mL Fe_3O_4 -PAMAM-b-PDMAEMA-b-PPEGMA nanoparticles in methanol (concentration of 2.5 mg/mL). The mixture was shaken for 24 h in the dark at room temperature to allow the drug partition into the polymer shell. The modified Fe_3O_4 -PAMAM-b-PDMAEMA-b-PPEGMA nanoparticles possessed the thicker shell of polymers, which is beneficial to enhance hydrophobic interactions and hydrogen binding with DOX and improve the loading capacity [110]. In vitro drug release experiments showed a pH-responsive drug release behavior for DOX-loaded nanoparticles. The cumulative release amounts of DOX within 48 h at pH 4.7, 7.4 and 11.0 are 83.1%, 64.7% and 8.3%, respectively. The higher release at pH 4.7 has been attributed to decreased hydrogen bond interaction between PDMAEMA and DOX due to protonation of PDMAEMA chains and DOX at pH 4.7. On the other hand, PDMAEMA chains tend to swell due to the protonated tertiary amino groups at pH 4.7, which is beneficial to accelerate DOX release [110].

The antitumor effect of doxorubicin encapsulated into amphiphilic linear-dendritic hybrids of PEG-G#n-PCL (G = 0, 1, 2) (Compound 10) has been evaluated in MDA-MB-231 and MDA-MB-468 breast adenocarcinomas [102]. Linear component of PEG has been employed as the hydrophilic block and a dendron branched poly(ϵ -caprolactone) (PCL) as the hydrophobic one. The dendrons have been prepared from the 2,2-bis(methylol)propionic acid (bisMPA) building block, bearing click chemistry moieties in the focal point to attach PEG (Figure 16).

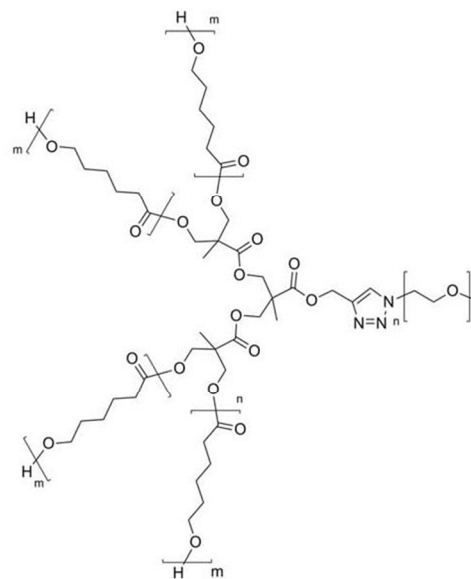


Figure 16. Chemical structure of PEG-G#2-PCL (Compound 10). Reprinted with permission from ref. 102. Copyright (2011) Wiley Periodicals, Inc.

The amphiphilic PEG-G#n-PCL structures were capable of forming self-assembled micelles with diameters of about 100 nm. Sequestering doxorubicin achieved the loading efficiency up to 22% for PEG2k-G1-PCL30. It has been demonstrated that the loading of DOX resulted in aggregation of the smaller particles into larger ones suggesting that some PEG components used in these linear-dendritic hybrids are not sufficiently large to effectively shield the particle from particle-particle interactions. Also increasing the generation of the dendron to two resulted in a substantial loss of loading efficiency down to 8% (PEG5k-G2-PCL30) [102]. This has been attributed to effect of lower crystallinity due to the effect of the dendritic branching, resulting in a less densely packed hydrophobic core. Also, the incorporation of DOX in a nanoscale confined crystalline core will reduce the crystallinity further. Drug release studies revealed that release manner was independent of blocks portions and dendrimer generation employed in the micelle construction suggesting that the core material did not influence the diffusion path of the drug from the core. The release of about 60% at 6h and more than 80% at 24 h has been shown for all evaluated systems [102].

Recently carbon nanotubes have been introduced as promising materials for delivery of drugs, RNA, DNA, peptides and other biological active molecules into cells because of the ability to cross cell membranes [111–114]. Despite the great potential of carbon nanotubes (CNTs) in anticancer drug delivery, concerns regarding their carcinogenicity, inefficient dispersion in aqueous solutions and biological activity in vivo still remain. One important and feasible route to overcome these problems is modification of CNTs with polymers, which are widely studied and play a vital role in biological and biomedical fields, especially in drug delivery [115]. Two methods are used to modify the CNTs by polymers based on either physical interactions or chemical bonding and are so called “noncovalent” or “covalent” approaches respectively. Noncovalent approach is based on poor VanderWaals interactions between CNTs and polymers and includes dispersion with the low molar mass polymers, polymer wrapping and polymer adsorption [116–118]. In the covalent approach, molecules or macromolecules are grafted onto the surface of CNTs through chemical linkages raising the solubility of CNTs even with a low degree of functionalization. Covalent attachment of polymer chains to the surface of CNTs can be accomplished by either “grafting to” or “grafting from” methods [114,115,119–124]. We proved that polymers not only raise the functionality, biocompatibility and water solubility of CNT but also are able to change the CNTs conformations dramatically. A drug carrier composed of polyglycerol-poly(ethylene glycol)-polyglycerol (PG-PEG-PG) ABA linear-dendritic copolymer and CNTs was designed and potential application of obtained structure to load and transport anticancer drug DOX was investigated (Compound 11) [125]. Figure 17 illustrates schematic structure of the used linear-dendritic copolymer. It has been observed that noncovalent interactions between (PG-PEG-PG) linear-dendritic copolymer and CNTs lead to the conformation alteration of CNTs from an extended toward a closed state due to liposome-like nanocapsules (LLNs) formation. The size of the PG-PEG-PG/MWCNT LLNs filled with DOX molecules was estimated to be 350 nm.

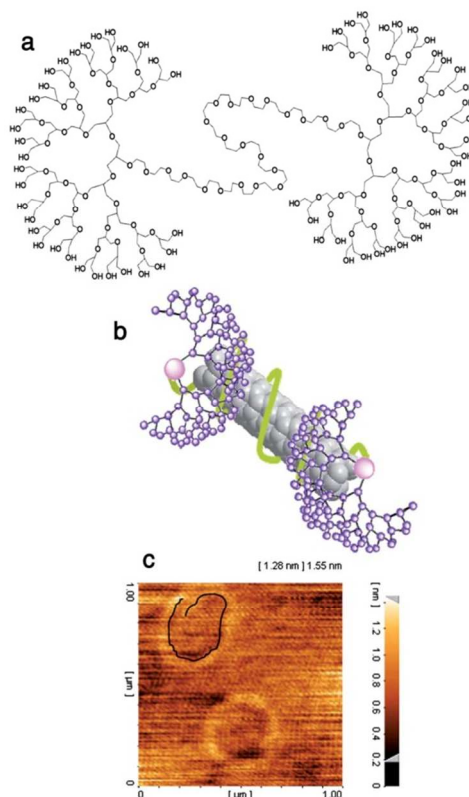


Figure 17. (a) Schematic representation of PG-PEG-PG ABA type linear dendritic copolymer, (b) schematic representation of noncovalent interactions between linear-dendritic copolymers and surface of CNTs that lead to new hybrid nanomaterials with improved properties, (c) AFM image of PG-PEG-PG/MWCNT liposome-like nanocapsules containing encapsulated DOX molecules. The highlighted object in the top-left part of image, by a black line, shows the MWCNTs (Compound 11). Reprinted with permission from ref. 125. Copyright (2012) The Royal Society of Chemistry.

Loading capacities for the PG-PEG-PG/MWCNT LLNs were determined by HPLC as 2.2 grams to one gram of LLNs [125].

Poor water solubility and low functionality are two critical factors that limit biomedical applications of CNT/ γ -Fe₂O₃NP hybrid nanomaterials. Non-covalent method for improving solubility is based on supramolecular interactions between CNTs and polymers and includes polymer wrapping or adsorption. In this method, structure of CNTs does not damage as much as the covalent method, but its disadvantage is the low functionality of the final product. A new method to improve the functionality and water solubility of CNT/ γ -Fe₂O₃NP hybrid nanomaterials without damaging their structure has been reported by using linear-dendritic copolymers [126–128].

An example of non-covalent interactions between CNTs and linear-dendritic copolymers is hybrid nanostructure-based magnetic drug delivery systems (HNMDSSs) including carbon nanotubes, magnetic iron oxide nanoparticles, and linear-dendritic PAMAM-PEG-PAMAM copolymer [32]. PAMAM-PEG-PAMAM was employed to solubilize and functionalize carbon nanotubes through supramolecular interactions. The resulted Fe₃O₄-MWCNTs/PAMAM-PEG-PAMAM hybrid nanomaterials were utilized to encapsulate DOX (through π - π stacking) with the loading

capacity of about 3.3% (Compound 12). According to dynamic light scattering, the average diameter of DOX loaded Fe_3O_4 -MWCNTs/PAMAM-PEG-PAMAM nanomaterials in water was 207 nm and aqueous solutions of hybrid nanomaterials were stable over several weeks at room temperature [32].

Based on VSM curves, the saturation of magnetization of Fe_3O_4 -MWCNTs/PAMAM-PEG-PAMAM and DOX/ Fe_3O_4 -MWCNTs/PAMAM-PEG-PAMAM were little smaller than that of Fe_3O_4 -MWCNTs, but both had similar properties that were close to the superparamagnetic behavior, indicating that the magnetic properties of Fe_3O_4 -MWCNTs did not lose by the non-covalent interaction of DOX and PAMAM-PEG-PAMAM on their surfaces. With this unique property, DOX/ γ - Fe_3O_4 -MWCNTs/PAMAM-PEG-PAMAM can be used as a promising material in many fields such as cancer diagnosis and therapy [32].

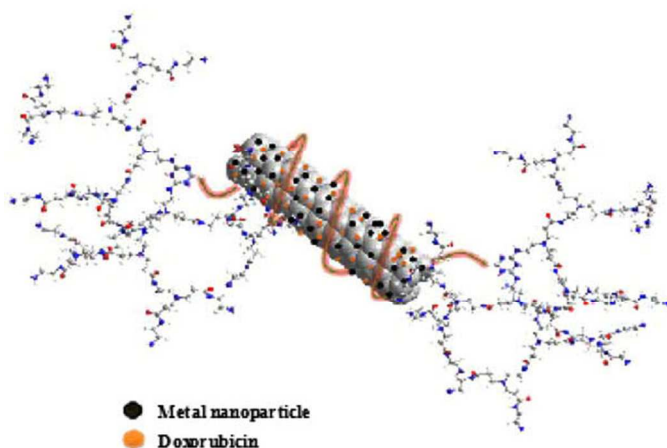


Figure 18. The schematic representation of HNMDSDs including carbon nanotubes, magnetic iron oxide nanoparticles, and linear-dendritic PAMAM-PEG-PAMAM copolymer (Compound 12). Reprinted with permission from ref. 32. Copyright (2013) Iranian Chemical society

Using copper (I)-catalyzed azide-alkyne cycloaddition (CuAAC)-based click chemistry and "dendrone-first" method, Hed et al. synthesized a set of dendritic linear hybrid materials composed of linear PEG and dendritic aliphatic bis-MPA polyesters (G4) [129]. To achieve amphiphilic structures, the bis-MPA layer also introduced hydrophobicity, using benzylidene-protected bis-MPA anhydride. Finally, the convergent coupling was carried out between monofunctional PEG5k-acetylene and azide functional dendrons Azide-[G4]-(Bz)₈ by CuAAC click chemistry (Figure 19).

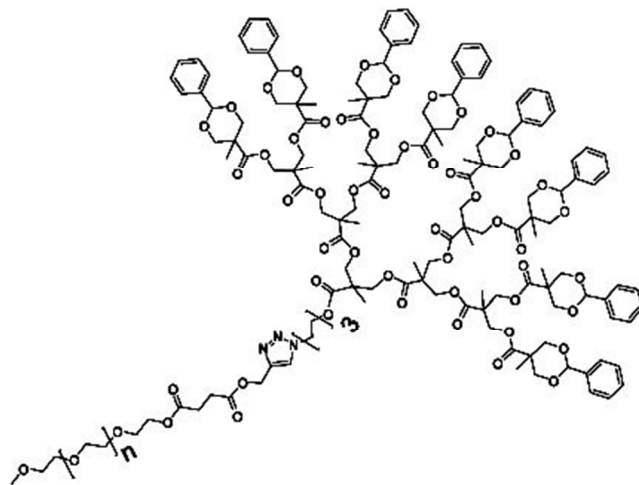


Figure 19. Schematic structure of DL PEG-[G4]-(Bz)₈ (Compound 13). Reprinted with permission from ref. 129. Copyright (2013) Wiley Periodicals, Inc.

Increased sizes of the micelles has been demonstrated after encapsulation of DOX into the amphiphilic PEG-[G4]-(Bz)₈ (diameters reported for the intensity average DLS data: 88 nm for PEG-[G4]-(Bz)₈, and 300 nm for DOX loaded PEG-[G4]-(Bz)₈ (Compound 13)) indicating that the PEG length used for these materials is not sufficient to suppress aggregation. Loading efficiency of 51% has been found for DOX-loaded PEG-[G4]-(Bz)₈. Drug release studies exhibited a burst release during the first 12 h under which at least 80% of the DOX was released, and around 90% of the content was released within 72 h. This phenomenon has been attributed to the low capacity of the hydrophobic domain to act as a diffusion barrier. It was suggested that increasing of PEG molecular weight should be noted to restrict aggregation and achieve better controlled release kinetics [129].

Recently, the stimuli-responsive polymeric micelles and assemblies that are triggered by the light as external stimuli have been widely investigated for "on-off" drug delivery systems and "on-demand" nanomedicines because of their assembly/disassembly switch. Compared with UV light, the near infrared (NIR) light between 750 and 1000 nm can penetrate up to centimetre depth of tissues with less damage and scattering, which makes the NIR-sensitive nanomedicines promising as noninvasive and on-demand therapeutic candidates [130,131].

Sun et al. have reported near-infrared (NIR) light-responsive linear-dendritic amphiphiles consisting of linear PEO and dendritic PAMAM (third-generation, D3) decorated with diazonaphthoquinone (DNQ) employed for NIR-triggered release of the anticancer drug doxorubicin (Compound 14) [132]. In their synthetic route, the reaction between alkyne focal point PAMAM Dendron (D3: bearing eight primary amine groups) and DNQ sulfonyl chloride has been utilized to afford the clickable dendron D3DNQ (having eight DNQ groups), which then has been click conjugated with azide-terminated PEO (5K) to produce the final linear-dendritic amphiphiles (Figure 20). It has been demonstrated that under NIR (e.g., 808 nm) irradiation, the hydrophobic diazonaphthoquinone (DNQ) molecule transforms into the hydrophilic photoproduct 3-indenecarboxylic acid (pKa = 4.5) via Wolff rearrangement [132], which would result in the disassembly and/or disruption of DNQ-containing micelles in PBS (e.g., pH 7.4) [133–135].

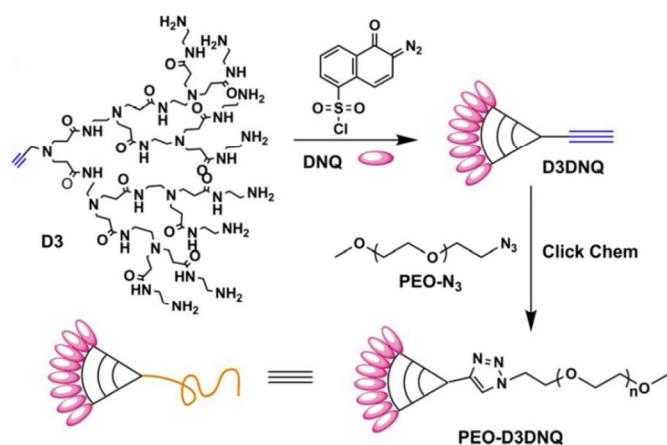


Figure 20. Synthesis of linear-dendritic amphiphiles PEO-PAMAM (D3) DNQ by click chemistry (Compound 14). Reprinted with permission from ref. 132. Copyright (2013) The Royal Society of Chemistry.

Besides a common spherical morphology, PEO5K-D3DNQ micelles had a DLS-determined diameter of ~ 90 nm. In addition, the average size of the micelles slightly changed over 25 days in PBS (10 mM, pH 7.4) at 37 °C, suggesting that they were dynamically stable in vitro. DOX-loading capacity of about 20 wt% has been determined for PEO5K-D3DNQ micelles. Determined by DLS, the DOX-loaded PEO5K-D3DNQ micelles increased from 90 nm (blank micelles) to 160 nm. These results also suggested that the hydrophobic DOX drug was indeed encapsulated into the hydrophobic core of the micelles. Similar to their blank counterparts, the DOX-loaded micelles presented a nearly spherical morphology. In vitro drug release studies demonstrated NIR-triggered drug release profile for DOX-loaded PEO5K-D3DNQ micelles. The accelerated drug-release was exhibited after 10 min of 808 nm irradiation. It was found that 90% of DOX was released within about 210 h compared with that without irradiation (about 420 h). Moreover, the apparent drug-release rate of DOX-loaded PEO5K-D3DNQ micelles accelerated nearly 8 times after 30 min of 808 nm irradiation compared to that of 10 min indicating NIR-responsive DOX release from the nanomedicines [132].

5.1.2. In vitro evaluations

Based on in vitro cytotoxicity investigations evaluated on MDA-MB-231 breast cancer cells, IC_{50} of approximately 3 $\mu\text{g}/\text{mL}$ and 0.8 $\mu\text{g}/\text{mL}$ has been determined for DOX-loaded PEO-block-G3 polyester dendrimer of 2,2-bis(hydroxymethyl)propanoic acid units bearing cyclic acetals of 2,4,6-trimethoxybenzaldehyde micelles (Compound 6) and free drug, respectively [107]. The somewhat lower toxicity of the micelle system may result from the gradual release of DOX within the cell and from differences in the released drug's cellular localization relative to the free drug. However, IC_{50} of 3 $\mu\text{g}/\text{mL}$ for DOX-loaded micelles indicated the release of free and active DOX in the cells and encouraged for the therapeutic potential of the system. Drug localization in intracellular organelles has been proved for DOX-loaded micelles by Laser scanning confocal microscopy images, while free DOX was localized in the cell nucleus after 24 h (Figure 21) [107]. Drug localization in intracellular organelles has been proved for DOX loaded micelles by Laser scanning confocal microscopy images. As

shown in Figure 21a, MDAMB-231 cells exposed to free DOX show significant accumulation of DOX in the nucleus after 24 h. In contrast, cells exposed to DOX-loaded pH-sensitive micelles have a punctate fluorescence that is concentrated in the cytoplasm after 24 h as shown in Figure 21b. These observations are important for several reasons. First, the absence of DOX fluorescence in the nucleus suggests that the micelles are stable in the presence of cells and serum-containing cell medium, as the rapid destabilization of the micelles in the extracellular environment and subsequent release of DOX outside the cell would be expected to result in an image similar to that observed for free DOX. In addition, the fluorescence in the cytoplasm suggests that the DOX-loaded micelles are indeed taken up by cells, and its punctate nature is consistent with the localization of the drug in subcellular organelles [107]. The increased stability of the pH-sensitive system at pH 7.4, and controlled release of therapeutics in mildly acidic physiological environments make DOX-loaded PEO-block-G3 polyester (bis-MPA) dendrimer bearing cyclic acetals of 2,4,6-trimethoxybenzaldehyde promising for anticancer drug delivery. The somewhat lower toxicity of the micelle system was observed in comparison with free DOX. However, the potential for the selective accumulation of the micelle system in tumor tissue by the enhanced permeation and retention effect may enhance its overall therapeutic efficacy in vivo relative to free DOX [107].

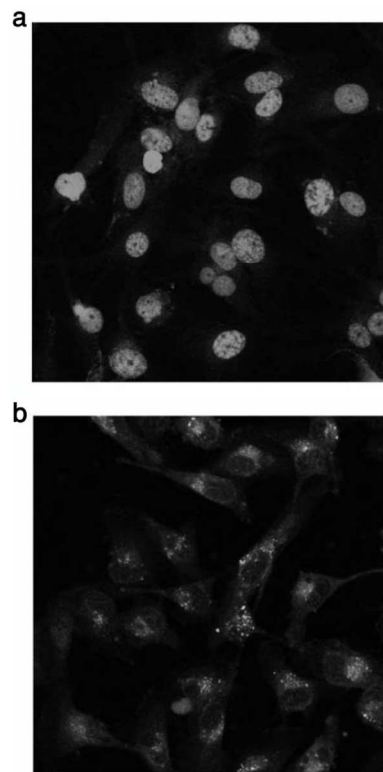


Figure 21. Laser scanning confocal microscopy images of (a) DOX and (b) DOX-loaded pH-sensitive micelles (PEO-block-G3 polyester dendrimer of 2,2-bis(hydroxymethyl)propanoic acid units bearing cyclic acetals of 2,4,6-trimethoxybenzaldehyde) incubated with MDAMB-231 cells for 24 h. Reprinted with permission from ref. 107. Copyright (2005) American Chemical Society.

Cellular uptake evaluations on Raji lymphoma cells indicated that cells treated with DOX-PEG^{5k}-CA₈ (Compound 7) and DOX-PEG^{2k}-CA₄ micelles showed MFI (median fluorescence intensity) of 1.8-fold and 1.9-fold higher than free DOX, respectively, proving efficient internalization of drug loaded micelles in mentioned cells [108]. Similar *in vitro* cytotoxicities have been found for drug loaded micelles against T- and B-lymphoma cells as the free drug, exhibiting the IC₅₀ values of 20 – 50 ng/ml DOX. Higher value of maximum tolerated dose (MTD) found for DOX-PEG^{2k}-CA₄ micelles (15 mg/kg) compared to free DOX (10 mg/kg) in non-tumor bearing BLAB/c mice has been attributed to the prolonged circulation time and the controlled drug release property [108]. In the case of DOX-loaded PAMAM-b-PDMAEMA-b-PNIPAM block copolymer-modified magnetic iron oxide nanoparticles (Compound 8) [109], *in vitro* cytotoxicity studies revealed higher inhibition on HeLa cells for free DOX (IC₅₀ = 0.66 mg mL⁻¹) in comparison with the loaded DOX in the modified nanoparticles (IC₅₀ = 1.49 mg mL⁻¹) at the same concentrations of DOX. This result has been explained by the slow release of the drug from the drug-loaded nanoparticles. At the same time, the result confirmed that the DOX-loaded nanoparticles were beneficial to decrease the side effects of DOX on cells [109]. *In vitro* cytotoxicity of blank Fe₃O₄-dendritic-linear-brush-like copolymer PAMAM-b-PDMAEMA-b-PPEGMA nanoparticles on NIH 3T3 cells demonstrated cell viability of almost 100% [110]. Also *in vitro* hemolysis assay with rabbit erythrocytes confirmed high biocompatibility of the Fe₃O₄-modified nanoparticles. *In vitro* cytotoxicity investigations on Hella cells showed IC₅₀ values of 2.72 µg/mL and ~0.72 µg/mL for DOX loaded in the modified nanoparticles (Compound 9) and free DOX, respectively. This result demonstrated that dendritic-linear-brush-like structures retard the toxic effect of DOX on the cells due to the slow release of the drug from the drug-loaded nanoparticles indicating that the modified nanoparticles can delay drug release, in which more compact brush structure possibly result in a lower diffusion rate of drug molecules [110]. This system offers preparing water soluble and biocompatible modified Fe₃O₄ nanoparticles for physical encapsulation of DOX. A pH-sensitive and delayed drug release manner was reported which can be beneficial to further facilitate potential biomedical applications of magnetic nanoparticles. Of course, biodistribution investigations and *in vivo* studies are necessary [110]. It has been shown that all of drug loaded PEG-G#n-PCL systems (Compound 10) delivered an effective dose of DOX to the breast cancer cells comparable to that of the free drug [102]. Determined by *in vitro* cytotoxicity studies, cell viability was decreased to 60–80% for MDA-MB-231 cells at 1 µg mL⁻¹ concentration of loaded DOX, while at lower concentrations than 1 µg mL⁻¹ the cell viability was 60% for MDA-MB-468 cells. The higher toxicity of free and loaded DOX on MDA-MB-468 cells contributes to the greater sensitivity of MDA-MB-468 cells to DOX. As proved by confocal imaging the intensity of DOX fluorescence, released from DOX-loaded micelles, increased with time, and the fluorescence became more concentrated in the cell nuclei at the later time-point (Figure 22).

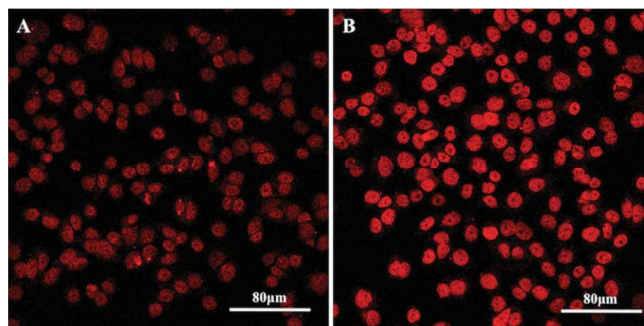


Figure 22. Confocal microscopy of DOX in MDA-MB-468 cells. Cells were cultured in medium with DOX-PEG^{5k}-G1-PCL₆₀ (containing 2 µg mL⁻¹ DOX) for 4 h (A) and 24 h (B). Both images were captured with same parameters on confocal microscopy and adjusted to the same the contrast level and brightness. Reprinted with permission from ref. 102. Copyright (2011) Wiley Periodicals, Inc.

According to flow cytometry investigations, in spite of less cellular uptake of DOX from carrier-loaded DOX, the level of apoptosis of cells was comparable for free DOX and carrier-loaded DOX confirming PEG-G#n-PCL system as a promising anticancer drug carrier [102]. Biocompatibility of empty micelles, good drug loading efficacy and efficient killing of the breast cancer cells in spite of less cellular uptake are significant advantages of DOX loaded PEG-G#n-PCL system. However, to reduce the release rates and potentially the observed aggregation of the drug-loaded micelles, a longer PEG component is most likely necessary. Pharmacokinetics and other *in vivo* investigations are also necessary [102].

In vitro cytotoxicity assays on murine colon adenocarcinoma tumor C26 line demonstrated higher anticancer effects for DOX/PG-PEG-PG/MWCNTs (Compound 11) in comparison with free DOX in equal concentrations. With respect to this point that equal concentrations of free DOX and the DOX/PG-PEG-PG/MWCNT drug delivery system means a much lower concentration of DOX in the latter case, toxicity of DOX molecules loaded inside LLNs against cancer cells is much higher than those shown in Figure 23 [125]. Hydrophilic dendritic polymers not only raise the functionality, biocompatibility and water solubility of CNTs but also change their conformations from a linear to a packed state. Changes in the conformation of the CNTs upon noncovalent interactions with PG-PEG-PG ABA type linear-dendritic copolymer led to liposome-like nanocapsules (LLNs). Since one of the proposed reasons for the carcinogenicity of carbon nanotubes is their long lengths and rigid structures, flexible liposome-like nanocapsules prepared by this strategy could be safer and far from the asbestos like physicochemical properties of CNTs and therefore their potential health hazards. Avoiding these health hazards, it is possible to develop CNTs for biomedical applications [125].

Journal Name

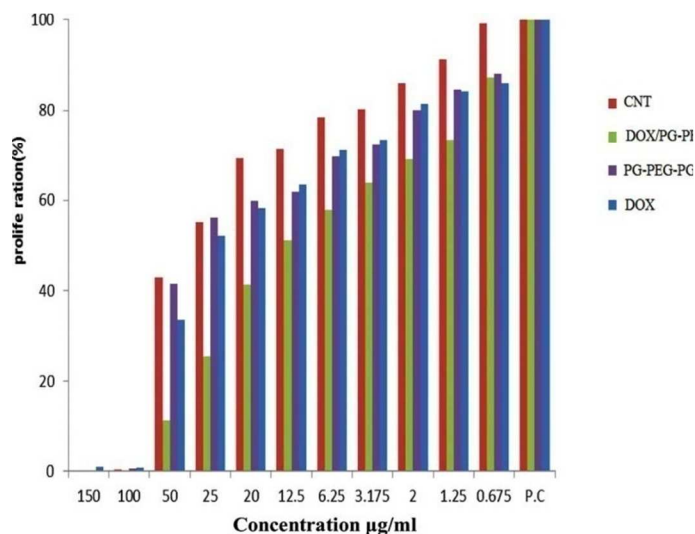


Figure 23. The MTT assay results for opened MWCNT, PG-PEG-PG linear-dendritic copolymer, DOX/PG-PEG-PG/MWCNT drug delivery system and free DOX incubated with murine colon adenocarcinoma tumor C26 line. Reprinted with permission from ref. 125. Copyright (2012) The Royal Society of Chemistry.

By in vitro cytotoxicity tests conducted on mouse tissue connective fibroblast adhesive cell line (L929), it was found that in low concentrations the toxicity of DOX-loaded Fe_3O_4 -MWCNTs/PAMAM-PEG-PAMAM hybrid nanomaterials (Compound 12) was much higher than other systems and even free DOX, indicating critical role of carbon nanotube in transferring hybrid nanomaterials drug delivery systems, and therefore loaded DOX, from the cell membrane [32]. Since PEG improves the processability, water solubility and long blood circulation of CNTs through non-covalent interactions, supramolecular interactions between linear-dendritic PAMAM-PEG-PAMAM copolymers and CNTs leads to water soluble and high functional hybrid nanomaterials. Additionally, high loading capacity, higher toxicity compared to free DOX, and good supramagnetic behavior make DOX/ γ - Fe_3O_4 -MWCNTs/PAMAM-PEG-PAMAM promising material for anticancer drug delivery [32].

By in vitro cytotoxicity assays in the breast cancer cells (MDA-MB-231), the PEG-block-bis-MPA polyesters (G4)-(Bz)₈ has been found nontoxic [94]. Also reduced cell viability of 55% has been determined for DOX-PEG-(G4)-(Bz)₈ (Compound 13) containing 10 μgml^{-1} DOX in comparison with 73% cell viability obtained at the same concentration of free DOX, showing that DOX-loaded micelles delivered the therapeutic with the high efficacy [129]. In summary, DOX encapsulated PEG-block-bis-MPA polyesters (G4)-(Bz)₈ showed some advantages such as nontoxicity of linear-dendritic carrier and higher cytotoxic effect against MDA-MB-231 cancer cells in comparison with free DOX. However, higher molecular weights of PEG are necessary to provide sufficient stealth or steric repulsion during DOX loading and to avoid aggregation. Additionally, strategies for achieving better controlled release kinetics should be noticed. Pharmacokinetics studies and in vivo tests can help this system develop for cancer therapy [129].

By flow cytometry profiles it has been proved that the DOX-loaded PEO5K-PAMAM (D3)-diazonaphthoquinone (DNQ) micelles (Compound 14) could quickly enter into HeLa cells with a time-independent manner compared with free DOX (Figure 24) [132]. This phenomenon has been attributed to the nanomedicines of <200 nm internalization by HeLa cells in an endocytosis process

compared with a diffusion process for the cellular uptake of free DOX [135]. In vitro cytotoxicity studies evaluated in HeLa cells at 6 $\mu\text{g/mL}$ DOX dosage showed the cell viability of ~65% and ~18% for the DOX-loaded PEO5K-D3DNQ micelles and free DOX, respectively. This lower cytotoxicity of DOX-loaded micelles has been corresponded to the sustained drug-release behaviour of them. Interestingly, the cell viability for the DOX-loaded micelles decreased to ~35% after 30 min of 808 nm irradiation exhibiting a NIR-triggered cytotoxicity [132]. Collectively, DOX-loaded PEO5K-PAMAM (D3)-diazonaphthoquinone (DNQ) micelles demonstrated some interesting advantages including stability of drug-free micelles in PBS at 37 °C and pH=7.4, tuned release of DOX by the NIR light irradiation, quick entrance into HeLa cells compared to free DOX, DOX releasing inside the cells, and then killing the cells in a NIR-triggered manner. Disrupting the micelles by 808 nm NIR irradiation may be a challenge for this system, however, biodistribution studies and in vivo tests can develop this promising anticancer system [132].

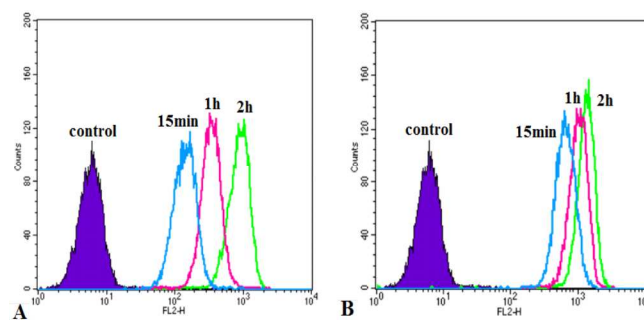


Figure 24. Flow cytometry histogram profiles of HeLa cells incubated with free DOX (A) and DOX-loaded micelles of PEO5K-PAMAM (D3) DNQ (B) for different time intervals. Reprinted with permission from ref. 132. Copyright (2013) The Royal Society of Chemistry.

5.1.3. In vivo evaluations

Biodistribution studies showed 2.0-fold and 2.2-fold higher drug uptake for DOX-PEG^{5k}-CA₈ and DOX-PEG^{2k}-CA₄ micelles than that for free DOX in the tumor tissue of treated mice [108]. This enhanced accumulation corresponded to the prolonged circulation and the EPR effect in linear-dendritic micelle formulations (Compound 7). Compared to free DOX, significantly reduced drug distribution in the heart has been achieved by both DOX-PEG-CA formulations. However, relatively higher uptake in the liver and spleen has been exhibited for DOX-micellar systems caused by nonspecific elimination of micellar NPs via the reticuloendothelial system (RES) such as macrophage in the liver and spleen. Better inhibition of tumor growth was shown for DOX-PEG^{2k}-CA₄ micelles because of their longer retention time and slower drug release rate. By day 28 post-injection, relative tumor volume (RTV) of 7.7 and 6.8 was achieved for Raji lymphoma bearing mice treated with DOX-PEG^{5k}-CA₈ and DOX-PEG^{2k}-CA₄, respectively. This value was 9.9 for free DOX treated mice [108]. Besides stability in physiological condition, DOX encapsulated PEG^{mk}-CA_n micelles offered some significant advantages in comparison to free DOX, such as higher in vitro cellular uptake, higher maximum tolerated dose, increased retention time in the blood, higher uptake in tumor tissue in vivo, higher antitumor efficacy in vivo, and reduced drug distribution in the heart. These all make PEG^{mk}-CA_n micelles attractive for cancer therapy [108].

Table 3. Doxorubicin-encapsulated linear-dendritic block copolymers

Carrier name	Size (nm)	In vitro activity	In vivo activity	advantages	ref
PEO–Poly(bis-MPA)– 2,4,6- trimethoxybenzaldehyde	35 nm 200-400* (cmc=40 mg/L)	Lower cytotoxicity on MDA-MB-231 breast cancer cells for DOX- loaded carrier (IC ₅₀ = 3 μg/ mL) compared to free DOX (IC ₅₀ = 0.8 μg/mL)	n	stability at pH 7.4, controlled release of therapeutics in mildly acidic physiological environments, potential for the selective accumulation of the micelle system in tumor tissue by EPR effect	107
PEG ^{5k} -CA ₈	12–17	Similar in vitro cytotoxicities (IC ₅₀ = 20 – 50 ng/ml) of drug loaded micelles and free drug against T- and B- lymphoma cells	Higher antitumor activity compared to free drug on Raji lymphoma bearing mice	stability in physiological condition, higher in vitro cellular uptake, higher maximum tolerated dose, increased retention time in the blood, higher uptake in tumor tissue in vivo, higher antitumor efficacy in vivo	108
Fe ₃ O ₄ -PAMAM-b- PDMAEMA-b-PNIPAM cross linked	32	Less cytotoxicity (IC ₅₀ = 1.49 mg mL ⁻¹) on Hela cells compared to free DOX (IC ₅₀ = 0.66 mg mL ⁻¹)	n	stabilized magnetic iron oxide nanoparticles, thermosensitive release manner, decrease the side effects of DOX on cells	109
Fe ₃ O ₄ -PAMAM-b- PDMAEMA-b-PPEGMA	30	Less cytotoxicity on Hella cells (IC ₅₀ of 2.72 μg/mL) compared to free DOX (IC ₅₀ of 0.72 μg/mL)	n	Water soluble and biocompatible modified Fe ₃ O ₄ nanoparticles as carrier, pH-sensitive and delayed drug release manner	110
PEG–G2 (bis-MPA)–PCL	865	greater sensitivity of MDA-MB- 468 cells to DOX released from micelles, comparable level of apoptosis of cells for free DOX and carrier-loaded DOX	n	Biocompatibility of carrier micelles, good drug loading efficacy and efficient killing of the breast cancer	102
PG-PEG-PG/MWCNTs	350	higher anticancer effects in comparison with free DOX on murine colon adenocarcinoma tumor C26 line	n	functionality, biocompatibility and water solubility of CNTs, higher anticancer effects compared to free DOX	125
Fe ₃ O ₄ – MWCNTs/PAMAM– PEG–PAMAM	207	Higher cytotoxicity than free DOX on mouse tissue connective fibroblast adhesive cell line (L929)	n	Water solubility and high functionality of hybrid nanomaterials. high loading capacity, higher toxicity compared to free DOX, and good supramagnetic behavior	32
PEG-poly(bis-MPA)-(Bz) ₈	300	Higher cytotoxicity effects on MDA-MB- 231 breast cancer cells	n	nontoxicity of linear-dendritic carrier and higher cytotoxic effect in comparison with free	129

		compared to free DOX		DOX in vitro	
PEO-PAMAM-DNQ	160 (cac=0.0206 mg/mL)	lower cytotoxicity of DOX-loaded micelles in comparison with free drug in HeLa cells	n	Stability in physiological conditions, tuned release of DOX by the NIR light irradiation, quick entrance into HeLa cells compared to free DOX, DOX releasing inside the cells	132

*a small fraction of aggregates

n: not reported

5-2. Doxorubicin-conjugated linear-dendritic block copolymers

5.2.1. Physicochemical properties

Padilla De Jesús et al. [136] have designed a soluble carrier for DOX consisted of a 3-arm poly(ethylene oxide) (PEO) and three [G-2] dendritic polyester with 2,2-bis(hydroxymethyl)propanoic acid monomer units (Compound 15), providing the multivalency necessary for drug attachment (Figure 25). DOX has been covalently linked to the linear-dendritic structure via an acidlabile hydrazone which can remain stable under physiological conditions, and can be cleaved in the vicinity of a tumor prior being internalized by the cancer cell because of more acidic environment around tumor tissue [136].

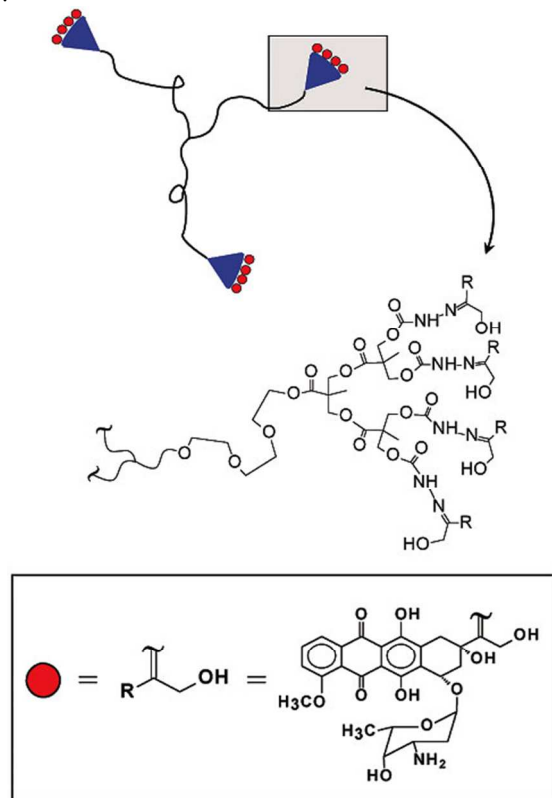


Figure 25. Polymer drug conjugate consisting of 3-arm PEO-polyester dendrimer and doxorubicin using a hydrazone covalent bond as a linker (Compound 15). Reprinted with permission from ref. 136. Copyright (2002) American Chemical Society.

Drug release studies indicated that a 100% release would be achieved after 10 min, 3 h, 26.5 h, and 10 days for pH 2.5, 4.5, 5.5, and 6.5, respectively. This confirms suitability of the hydrazone linkage for a pH-dependent release that is compatible with conditions found in tumors [136].

Gillies and Frechet also reported interesting polyester dendrimer-PEO bow-tie hybrids consisting of 2,2-bis(hydroxymethyl) propionic acid based polyester dendrimers and PEO in which PEO was linked to the dendritic scaffold via carbamate bonds [137, 138].

Later, [G-3]-(PEO_{5k})₈-[G-4]-(OH)₁₆ bow-tie structure (Molecular mass of ~45 kDa) was utilized to provide the dendrimer-DOX conjugates by coupling of hydrazide linkers to the hydroxyl groups of the bow tie (Compound 16), followed by hydrazone formation with DOX hydrochloride and subsequent chromatographic separation from free DOX. DOX loading was consistently found to be 8–10 wt % for different batches [139, 140]. Notably, the bow-tie DOX conjugate was readily dissolved in water at DOX concentrations as high as 6 mg/ml (~60 mg/ml polymer), indicating that the PEO arms of the bow-tie dendrimer can shield the hydrophobic drug moieties at the core of the molecule, perhaps in a structure similar to that of a unimolecular micelle. A volume average hydrodynamic diameter of 8 nm for the conjugate was determined by using dynamic light scattering, indicating that intermolecular aggregation did not occur [139]. The release of drug from DOX-conjugated bow-tie polymer at pH 5.0 and 7.4 buffers at 37 °C was monitored chromatographically. At pH 5, drug was released from the dendrimer rapidly, and the concentration of free doxorubicin in solution increased steadily with $t_{1/2} = 6 \pm 1$ h, reaching 100% release within 48 h. Only a small amount (<10%) of the same compound was released after 48 h at pH 7.4 [139,140].

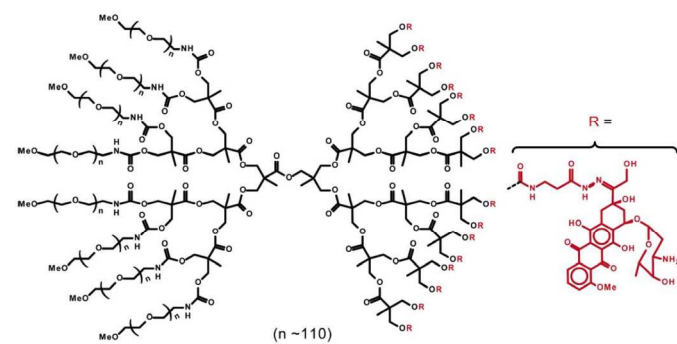


Figure 26. [G-3]-(PEO_{5k})₈-[G-4]-(OH)₁₆-Doxorubicin Conjugates (Compound 16). Reprinted with permission from ref 140. Copyright (2006) American Chemical Society.

Huang et al. [141] have reported a liver-targeting potential of polymeric prodrug of doxorubicin bearing Galactose conjugated linear dendritic block copolymers. Galactose as targeting ligand has been conjugated to linear PEG, and DOX has been coupled to PAMAM dendritic section via an acid-labile hydrazone linker to produce Gal-PEG-b-PAMAM-DOX_n drug delivery system (Compound 17) (Figure 27). It has been demonstrated that galactosylated drug carrier could reach hepatocytes via receptor-mediated active targeting due to the high affinity of asialoglycoprotein (ASGP) receptor to galactosyl residues [142]. Determined by HNMR, the molar ratio of DOX to copolymer was 5.5:1, which was lower than the theoretic value (8:1) because of the steric hindrance that leads to the lower drug loading.

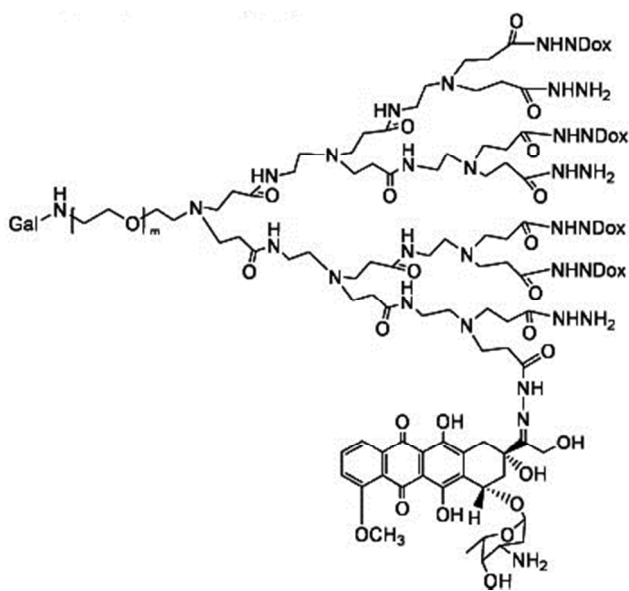


Figure 27. Gal-PEG-b-PAMAM-DOX_n prodrug (Compound 17). Reprinted with permission from ref. 141. Copyright (2010) Society of Chemical Industry

The acid-sensitive degradation of hydrazone linker between DOX and Gal-PEG-b-PAMAM carrier caused to a pH-triggered drug release profile. It has been determined that 14 and 32% of DOX was released at pH of 8.0 and 7.4, respectively in 30 h. On the other hand, at pH=5.6, 97% of DOX release was observed in 15 h. This indicates the stable circulation of the polymeric drug in the bloodstream (pH = 7.4), and triggered drug release in endosomes and lysosomes (pH=5.6–6.5) of cancer cells [141].

In a recent study, She et al. have demonstrated the use of mPEGylated peptide Dendron-DOX conjugate (Compound 18) as pH-stimuli drug delivery system for breast tumor therapy [143]. In their study, the tail of L-lysine dendron has been functionalized with two alkynyl groups. Then, mPEG (2 kDa) with azido group at one end has been covalently linked to the peptide dendron via Cu^I-catalyzed azide-alkyne cycloaddition (CuAAC). DOX has been conjugated to the dendron through pH-sensitive hydrazone bond, resulting in compact nanoparticle via the self-assembly governed by Dendron-DOX itself, as shown in Figure 28.

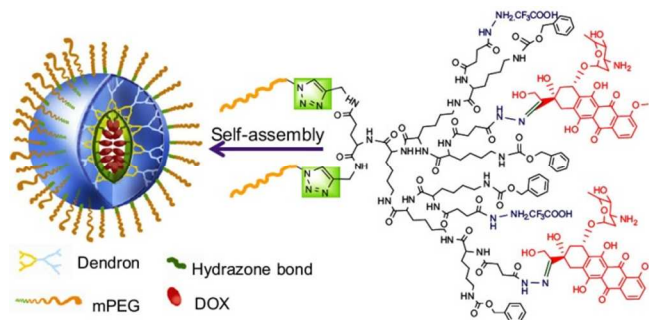


Figure 28. Structures of mPEGylated peptide dendron, and the illustration of the dendron-DOX conjugate based nanoparticle (Compound 18). Reprinted with permission from ref. 143. Copyright (2012) Elsevier Ltd.

UV-vis spectrophotometry indicated the presence of 2 DOX molecules for each mPEGylated peptide Dendron-doxorubicin (14 wt%). The mPEGylated peptide Dendron-DOX conjugate aggregated to particle with nanoscale size in water (pH = 7.4), displaying average hydrodynamic sizes around 220 nm [143]. Generally, producing drive force segments are needed to introduce to the PEGylation and functionalization of dendron for the self-assembly [144]. For this designed dendron, self-assembly behavior was mediated by mPEGylated peptide Dendron-DOX itself. The primary driving force responsible for the self-assembly behavior is the minimization of the interfacial energy governed by the balance between the hydrophilic interaction of the linear mPEG and the hydrophobic interaction of the Dendron-DOX block [144]. Secondly, the driving forces governed self-assembly of prepared mPEGylated peptide Dendron-DOX, such as π - π stacking, dipole interactions, H-bonding and the pre-organized branched architecture of the dendritic block should also be considered, since the DOX is composed of multiple domains of different chemical composition, e.g., hydrophobic, aliphatic and aromatic [145]. At predetermined time points, higher release amounts (80%) at pH 5, in comparison with release amounts at pH 7.4 (20%) revealed the pH-sensitive manner of drug release for mPEGylated peptide Dendron-doxorubicin nanoparticles. This accelerated release has been attributed to cleavage of hydrazone linkers at lower pH values [143]. In other study She et al. also have used Cu^I-catalyzed azide-alkyne cycloaddition (CuAAC) click chemistry for covalently attaching of L-lysine peptide dendron to heparin, resulting in the water-soluble dendronized heparin [146]. Then, DOX has been conjugated to the surface of dendron through pH-sensitive hydrazone bond, resulting in compact nanoparticle via the self-assembly in water (pH = 7.4), displaying average hydrodynamic sizes around 90 nm and PDI of 0.140 (DOX content 9 wt %) (Compound 19), (Figure 29).

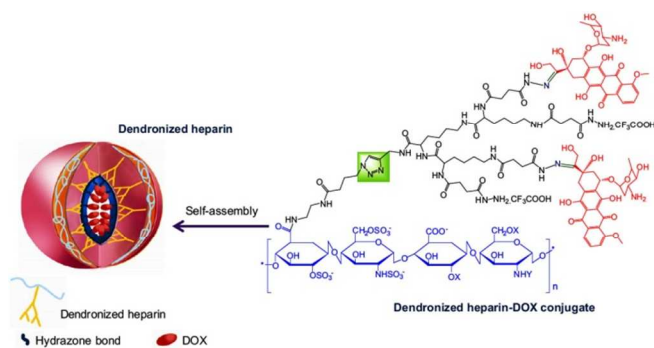


Figure 29. The illustration of dendronized heparin-DOX conjugate based nanoparticle (Compound 19). Reprinted with permission from ref. 146. Copyright (2012) Elsevier Ltd.

Self-assembly behavior was mediated by dendronized heparin-DOX conjugate itself. As mentioned before [146], the primary driving force responsible for the self-assembly behavior is the minimization of the interfacial energy governed by the balance between the hydrophilic interaction of the linear polymer and the hydrophobic interaction of the dendronized heparin-DOX block. Secondly, the driving forces governed self-assembly of prepared dendronized heparin-DOX, such as π - π stacking, dipole interactions, H-bonding and the preorganized branched architecture should also be considered, since the DOX is composed of multiple domains of different chemical composition, e.g., hydrophobic, aliphatic and aromatic. Based on drug release profiles, showing 20% DOX release at pH 7.4 after 56 h incubation, it was concluded that dendronized heparin-DOX system was stable in circulation system (pH 7.4). In contrast, cleavage of acid-labile hydrazone bonds of DOX-conjugated nanoparticles accelerated the release of drug at pH 5.0 (> 80%) indicating the ability of nanoparticles to release the DOX in the acidic endosomes and/or lysosomes where the pH ranges is 4.0-6.0 [146].

In a research work reported by Zhang et al. [147], a co-delivery strategy for anti-cancer treatment has been employed utilizing 10-hydroxycamptothecin (HCPT) encapsulated MPEG-b-PAMAM-DOX amphiphilic linear-dendritic prodrug. In the preparation route, MPEG-b-PAMAM G2.5 has been hydrazinolysized to MPEG-b-PAMAM G3X by hydrazine hydrate. Then, DOX as the hydrophobic part of the amphiphilic copolymer has been conjugated to PAMAM via an acid-labile hydrazone linkage by reacting with the keto groups of DOX. UV absorbance studies gave DOX content of 52.9 wt% for MPEG2000-b-PAMAM-DOX and 31.0 wt% for MPEG5000-b-PAMAM-DOX. HCPT loading into DOX-conjugated nanoparticles has been carried out by solvent displacement method with pH adjusted to 6.5 in which the hydrazone bond was stable while HCPT could maintain its lactone form [148,149]. HCPT content has been determined to be 19.2 and 21.6 wt% for MPEG2000-b-PAMAM-DOX and MPEG5000-b-PAMAM-DOX (Compound 20) nanoparticles, respectively. The nanoparticles were of uniform size and spherical shape. The radii of nanoparticles formed by MPEG2000-b-PAMAM-DOX and MPEG5000-b-PAMAM-DOX were about 50 and 60 nm, respectively. As a hydrophobic molecule, HCPT was wrapped in the core of the nanoparticles which were formed by the self-assembly of MPEG-b-PAMAM-DOX prodrugs. The radii of the HCPT loaded nanoparticles formed by MPEG2000-b-PAMAM-DOX and MPEG5000-b-PAMAM-DOX were 88 nm and 122 nm, respectively. The increase of nanoparticles size after HCPT loading indicates the successful incorporation of HCPT in the hydrophobic

core [147]. A pH-dependent manner of release has been demonstrated for both drugs released from HCPT loaded MPEG-b-PAMAM-DOX. There has been no initial DOX burst release from DOX-conjugated nanoparticles because of chemical combination of DOX to the copolymer. The release of DOX molecules was negligible at pH 7.4, indicating the stability of hydrazone bond at this pH. Lowering the pH to 5.5 and 4.5 caused to increased DOX release of about 30% and 60% in 48 h, respectively. Also faster release of HCPT has been demonstrated in pH 4.5 compared to pH 5.5, attributed to the faster cleavage of DOX and faster disassembly of the self-assembled nanoparticles in lower pH [147].

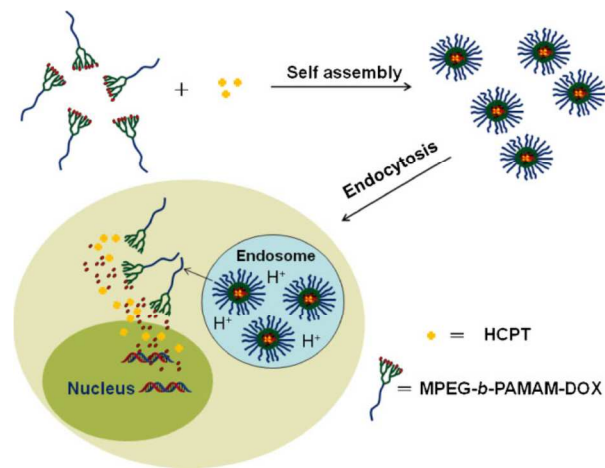


Figure 30. Illustration of MPEG-b-PAMAM block copolymer conjugated with DOX and its self-assembled HCPT loaded nanoparticles for the pH-responsive intracellular release (Compound 20). Reprinted with permission from ref. 147. Copyright (2013) Wiley-VCH Verlag GmbH & Co. KGaA, Weinheim

Another pH-responsive prodrug formulation based on linear-dendritic MPEG-b-PAMAM has been recently reported by Zhang et al. [78]. Firstly, linear-dendritic MPEG-b-PAMAM has been modified with lipoic acid (LA) and then, doxorubicin was conjugated to the modified structure by an acid-labile hydrazone bond resulting in amphiphilic structures that could be self-assembled to the nanosized micelles (Compound 21) (Figure 31). Due to the significant glutathione (GSH) concentration difference between the extracellular milieu (2–20 mM) and the cytoplasm (2–10 mM), the reduction responsive cross-linked micelles are attracting more and more attention. Therefore, the obtained MPEG-b-PAMAM-LA/DOX micelles have been cross-linked by disulfide bonding through introducing 10 mol% DTT relative to the lipoyl units in borate buffer (pH 8.5). With the MPEG segment as the hydrophilic moiety and LA and DOX as the hydrophobic moieties, the amphiphilic prodrug self-assembled into spherically shaped micelles. The particle size of the cross-linked prodrug particles was ~140 nm. The stability of the cross-linked MPEG-b-PAMAM-LA/DOX NPs was evaluated in 20 mM PB solution for different time intervals. After standing for 4 days, 8 days and 16 days, the particle size of the NPs only slightly changed from the original 144 nm to 161 nm after 16 days of incubation, also suggesting the good stability of the cross-linked NPs. The change in the particle size in response to 10 mM GSH was monitored over time in 20 mM PB solution to investigate whether cross-linked NPs can be de-cross-linked in a reductive environment. It was shown that the addition of GSH led to a dramatic increase and wide distribution of the particle size, implying the cleavage of disulfide bonds by reduced GSH. The DOX loading

ARTICLE

content of cross-linked MPEG-b-PAMAM-LA/DOX micelles has been determined to be 25.6 wt%. The high drug loading content has been ascribed to the multiple amine groups on the PAMAM backbone [78].

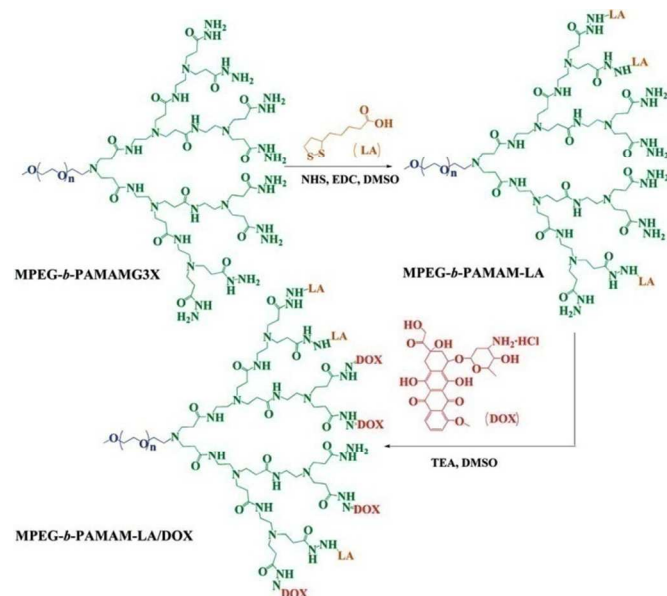


Figure 31. Synthesis pathway of MPEG-b-PAMAM-LA/DOX (Compound 21). Reprinted with permission from ref. 78. Copyright (2014) the Royal Society of Chemistry

A pH-dependent release for DOX from core-cross-linked MPEG-b-PAMAM-LA/DOX nanoparticles has been demonstrated. At pH 7.4, only about 6% of the loaded DOX was released in 72 h while about 35% of DOX was released at pH 5.5. These results indicate that the hydrazone bond is stable at the physiological pH of 7.4, but would be cleaved at the endosomal pH of 5.5. Also reduction-sensitive release behavior has been found for cross-linked MPEG-b-PAMAM-LA/DOX. At the same pH value, higher DOX release has been achieved with a higher GSH concentration. This has been attributed to the cleavage of the disulfide bonds by GSH leading to de-cross-linking of the nanoparticles and the rapid release of DOX [78].

5.2.2. In vitro evaluations

Based on in vitro cytotoxicity of drug-polymer conjugate, evaluated on three cell lines B16F10, MDA-MB-435, and MDA-MB-231, free drug has been more potent than DOX-conjugated 3-arm (PEO) star-three [G2] polyester dendritic block with bis-MPA units (Compound 15); 6-fold in the B16F10 cells, 50-fold in the MDA-MB-231, and 9-fold in the MDA-MB-435 cells. Cell uptake of the polymer-drug conjugate (monitored via fluorescence confocal microscopy) proved the cell uptake of the conjugate by endocytosis, through fluorescence observation in the cytosol. On the other hand, both the cytoplasm and the nuclei were highly fluorescent after exposition to free doxorubicin [136].

In spite of substantial intratumoral concentrations of polymer and drug, the attempts at chemotherapy utilizing the doxorubicin functionalized 3-armed (PEO) star-three [G2] polyester bis-MPA dendrimer in murine tumor models (B16F10) were largely unsuccessful [140]. This was attributed to hydrazone carboxylate linkages which were utilized in this system to attach doxorubicin

topolymeric structure [Figure 25]. Lee et al. [140] investigated the hydrolysis kinetics of hydrazone carboxylate linked doxorubicin and proposed intramolecular nucleophilic attack of the C-14 hydroxyl of doxorubicin on the carbonyl group of the hydrazone carboxylate linker [Figure 32].

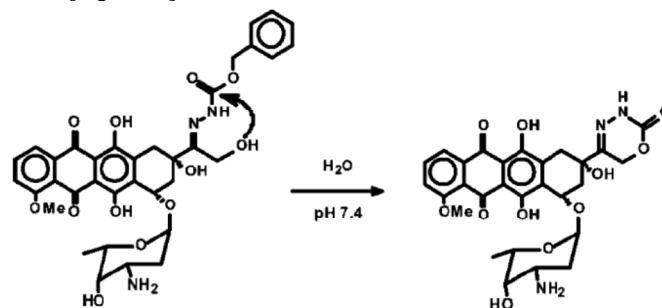


Figure 32. Intramolecular cyclization in hydrazone carboxylate linked doxorubicin system. Reprinted with permission from ref. 140. Copyright (2006) American Chemical Society

The proposed intramolecular cyclization reaction involving doxorubicin's C-14 hydroxyl and the carboxylate-substituted hydrazone rationalizes the seemingly anomalous hydrolysis kinetics seen for hydrazone carboxylate linked doxorubicin, and provides a possible explanation for the poor antitumor activity exhibited by polymer-doxorubicin conjugates utilizing this specific type of linkage [140].

In Vitro Cytotoxicity studies of polyester dendrimer-PEO bow-tie hybrids, with a range of MWs 20 – 100 KDa as well as low and high degrees of branching, on MDA-MB-231 cancer cells showed no significant toxicity up to 10 mg/mL, the highest concentration evaluated, with cell viabilities exceeding 85% relative to controls at all concentrations [138]. Cytotoxic activity of DOX-conjugated bow-tie polyester dendrimer-PEO (Compound 16) on C-26 cells was found to be considerably less than that for the free DOX on an equimolar basis (IC_{50} , DOX = $0.08 \pm 0.02 \mu\text{g/ml}$; IC_{50} , hydrazone bow-tie DOX = $1.4 \pm 0.2 \mu\text{g/ml}$). This result was attributed to the slower rate of cellular uptake for the dendrimers when compared with the free drug and to the gradual release of free drug from the polymers due to hydrolysis of the linkers and the polyester dendrimer backbone [139].

By in vitro cytotoxicity studies against Bel-7402 cells, the cell viability has been determined as 11%, 60% and 50% in cells treated with free DOX, non-targeting PEG-b-PAMAM-DOX_m, and targeting Gal-PEG-b-PAMAM-DOX_n (Compound 17) respectively, at DOX concentration of $40 \mu\text{g mL}^{-1}$ [141]. Compared to free DOX, decreased cytotoxicity of the polymeric prodrugs has been attributed to their gradual drug release profiles. Also higher cytotoxicity of galactose conjugated prodrug in comparison with the non-targeting one has been explained by receptor-mediated higher cell uptake of Gal-PEG-b-PAMAM-DOX_n. ASGP receptors in Bel-7402 and galactosyl residue in prodrug are responsible for increased intracellular drug concentration [141].

In vitro cytotoxicity, evaluated on mouse breast cancer cell line (4T1), showed lower cytotoxicity for mPEGylated peptide Dendron-DOX conjugate nanoparticles (Compound 18) (IC_{50} = 151 ng/mL) compared with free DOX (IC_{50} = 25.9 ng/mL) [143]. It has been explained by amphipathic properties of DOX and higher ability of small molecule to cross the cell membrane. Cell viability of 95% for non-drug conjugated nanoparticles indicated that mPEGylated peptide dendron was nontoxic and DOX released from DOX-conjugated nanoparticle in the acidic environment of endosomes was responsible for cytotoxicity [143].

Dendronized heparin-DOX (Compound 19) showed IC_{50} of 300 ng/mL against mouse breast cancer cell line (4T1), approximately 11 fold of free DOX with IC_{50} of 27 ng/mL [146]. This lower cytotoxicity of dendronized heparin-DOX has been due to amphipathic properties of free DOX and its ability to easily cross the cell membrane. More than 90% of 4T1 cells have been still alive after the treatment with drug-free dendronized heparin showing non-cytotoxicity of dendronized heparin nanoparticle. So it is clear that the cytotoxicity of nanoparticle with drug would not be due to dendronized heparin block, but the drug DOX, proving the release of DOX from nanoparticle in the acidic environment of endosomes [146].

Flow cytometric analysis demonstrated the HCPT loaded MPEG-b-PAMAM-DOX nanoparticles (Compound 20) could be effectively taken up by MCF-7 cells [147]. After 10 h incubation with MCF-7 cells, about 80% HCPT has been internalized by MCF-7 cells from both HCPT loaded MPEG-b-PAMAM-DOX nanoparticles, much higher than the internalization content of free HCPT indicating that DOX conjugated nanoparticles increased the solubility of free HCPT and delivered HCPT efficiently to MCF-7 cells. Higher in vitro cytotoxicity has been determined for HCPT loaded MPEG-b-PAMAM-DOX nanoparticles compared to free DOX and free HCPT in MCF-7 and HepG2 cell lines. Moreover the HCPT loaded MPEG-b-PAMAM-DOX exhibited better cytotoxicities than the physical mixtures of MPEG-b-PAMAM-DOX and HCPT [147]. This confirmed that the DOX conjugated prodrugs could effectively encapsulate HCPT and subsequent release it in cell, leading to enhanced drug activity and exhibited better in vitro antitumor effect for co-delivery system. Enhanced cell apoptosis has been demonstrated for co-delivery system. Evaluated by flow cytometry in MCF-7 cells, HCPT loaded MPEG2000-b-PAMAM-DOX and MPEG5000-b-PAMAM-DOX caused 13.3 and 13.4% late apoptotic cells and 81.7 and 81.3% normal cells, respectively. Both HCPT loaded nanoparticles resulted in more apoptotic cells than the blank MPEG-b-PAMAM-DOX nanoparticles (4.7% late apoptotic cells and 89.2% normal cells for MPEG2000-b-PAMAM-DOX, 4.9% late apoptotic cells and 88.6% normal cells for MPEG5000-b-PAMAM-DOX) and free HCPT (6.1% late apoptotic cells and 88.8% normal cells) with concentration of $1 \mu\text{g mL}^{-1}$ [147]. Having advantages of co-delivery of two anticancer drugs (DOX and HCPT), high drug loading content, pH-dependent manner of drug release, higher cellular uptake compared to free HCPT, higher in vitro cytotoxicity compared to free HCPT and free DOX make HCPT loaded MPEG-b-PAMAM-DOX nanoparticles attractive for drug delivery. More investigations, especially pharmacokinetic studies and in vivo antitumor efficacy, can help this system develop in cancer therapy [147].

By comparison of CLSM results in HeLa cells, after 3 and 16 h incubation with cross-linked MPEG-b-PAMAM-LA/DOX micelles (Compound 21) (Figure 33), it has been determined that the effective cellular uptake of the nanoparticles and efficient DOX release had taken place after a longer period of incubation [78]. In fact, after cellular uptake, the acidic environment and the relatively higher GSH concentration in both endosomes and the cytoplasmic matrix triggered the cleavage of the hydrazone bonds and disulfide bonds of cross-linked MPEG-b-PAMAM-LA/DOX causing to the slow release of DOX. Also the weaker DOX fluorescence observed for the cells treated with cross-linked MPEG-b-PAMAM-LA/DOX nanoparticles in comparison with that of free DOX has been explained by slower internalization and the self-quenching effect of DOX in the nanoparticles [78].

By in vitro cytotoxicity studies it has been found that cross-linked nanoparticles have been more effective after a longer period of incubation. The IC_{50} value of the cross-linked nanoparticles

decreased from $18.9 \mu\text{g mL}^{-1}$ to $2.5 \mu\text{g mL}^{-1}$ for HeLa cells with the elongation of the incubating time from 24 to 72 h. The decrease of IC_{50} has also been shown for A549 cells from more than $20 \mu\text{g mL}^{-1}$ to $6.3 \mu\text{g mL}^{-1}$ at the same incubation conditions. Enhanced inhibition of the cell proliferation has been demonstrated for cross-linked nanoparticles incubated with GSH pretreated HeLa and A549 cells. This higher cytotoxicity has been attributed to the cleavage of disulfide cross-linking by GSH and faster release of DOX [78]. Because of high drug loading content, pH and reduction-sensitive DOX release behavior (regarding the acidic environment and the relatively higher GSH concentration in both endosomes and the cytoplasmic matrix), higher in vitro cytotoxic effect with the elongation of the incubating time, the core cross-linked MPEG-b-PAMAM-LA/DOX NPs showed bright prospects for anti-cancer therapy. However, investigations of in vivo efficacy, tolerable doses, and biodistribution studies are needed to complete cross-linked MPEG-b-PAMAM-LA/DOX system [78].

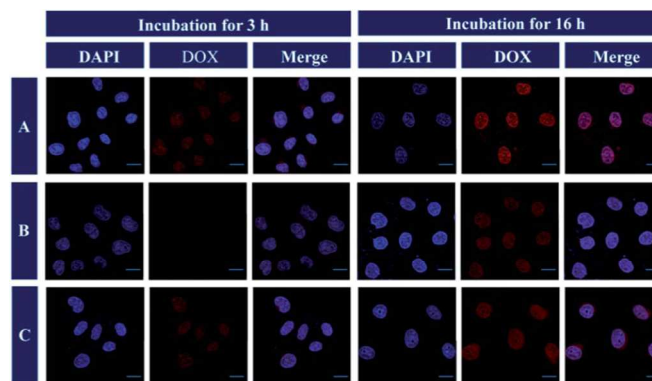


Figure 33. Confocal laser scanning microscopy of HeLa cells (1.0×10^5 cells per well) after incubation with (A) free DOX, (B) cross-linked MPEG-b-PAMAM-LA/DOX NPs (the cells were not pretreated) and (C) cross-linked MPEG-b-PAMAM-LA/DOX NPs (the cells were pretreated with 10mM GSH) for 3 h and 16 h at 37°C (DOX equivalent concentration: $0.5 \mu\text{g mL}^{-1}$ for all formulations). The scale bars represent 20 μm . Reprinted with permission from ref. 78. Copyright (2014) The Royal Society of Chemistry

5.2.3. In vivo evaluation

Biodistribution Studies of the DOX-conjugated 3-arm (PEO) star – three [G2] polyester dendritic blocks with bis-MPA units (Compound 15) performed on CD-1 female mice demonstrated no significant accumulation in any vital organ, including the liver, heart, and lungs (Figure 34) [136]. This is a preferred distribution pattern compared with free drug which partitions into a variety of organs such as the liver and heart. Also polymer-DOX conjugate exhibited a longer circulatory half-life (72 min) as compared to the half-life of the free drug (8 min), demonstrating influence of 3-arm PEO-polyester dendritic system in the pharmacokinetics and the distribution of the drug [136].

According to reported results, it is concluded that DOX-conjugated 3-arm (PEO) star – three [G2] polyester dendritic block with bis-MPA units (Compound 16) shows advantages including biocompatibility of carrier, pH-dependent release which is compatible with conditions found in tumors, no significant accumulation in vital organs, and longer circulatory half-life than free drug. But its lower cytotoxicity in comparison with free drug

arises from hydrazone carboxylate linkages which lead to intramolecular cyclization reaction and subsequent poor antitumor activity [136, 140].

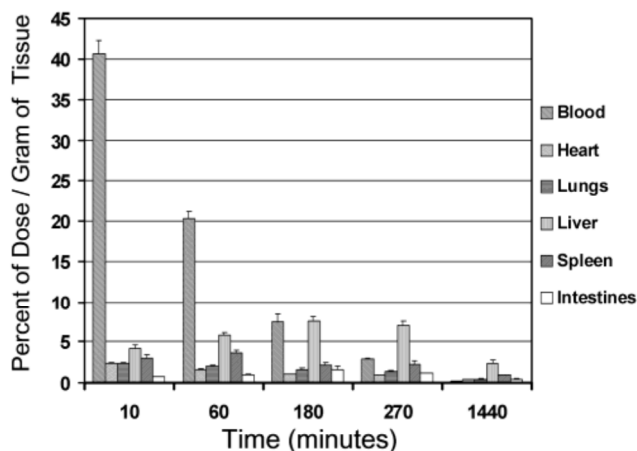


Figure 34. Biodistribution of 3-arm PEO-polyester dendrimer/DOX conjugate. Reprinted with permission from ref. 136. Copyright (2002) American Chemical Society

According to biodistribution studies of bow-tie polyester dendrimer-PEO [138] on CD-1 female mice at a dose of approximately 40 mg/kg, no specific organ accumulation was observed for these bow-tie polymers, with a significant portion of the dose (35-46%) found in the carcass after 48 h. Less than 4% of the dose was found in the urine for each of these polymers, indicating that their effective sizes are above the threshold for renal filtration. After 48 h, 6-16% of the dose was excreted in the feces. Therefore, the primary route for elimination of these molecules was via intestinal excretion, believed to be the primary route by which large molecules that cannot be excreted through the kidney can escape the body. [138]

Biodistribution experiments of DOX-conjugated bow-tie polyester dendrimer-PEO performed in BALB/c mice bearing s.c. C-26 tumors showed an elimination half-life of 16 ± 1 h for hydrazone-linked bow-tie DOX conjugate [139]. In previous studies, blood elimination half-life of 31 ± 2 h was observed for drug-free bow tie PEO-polyester dendrimer [138]. The long circulation half-life of conjugates contrasts with the short half-life of the free drug, which is <10 min. The tumor concentrations of DOX measured 48 h after administration of either DOX-conjugated bow-tie polyester dendrimer-PEO (20 mg/kg DOX) or free DOX (6 mg/kg) were approximately nine times higher for mice treated with DOX-conjugated bow-tie polyester dendrimer-PEO on a percent injected dose per gram of tumor basis. The enhanced tumor uptake of the dendrimer bound drug is a reflection of its longer circulation half-life, which exploits passive targeting by means of the EPR effect [139]. Animals serum analysis determined a significant increase in the serum creatine kinase, lactic dehydrogenase, and serum transaminase values in animals that received the 40 and 60 mg/kg doses of DOX-conjugated bow-tie polyester dendrimer-PEO compared with animals that received saline or the 20 mg/kg dose, indicating the presence of damage to muscle tissue and to the liver at these dose levels. So it was concluded that the maximum tolerated single dose is between 20 and 40 mg/kg DOX equivalents or between ~200 and 500 mg/kg DOX-conjugated bow-tie polyester dendrimer-PEO in healthy BALB/c mice [139]. To determine the optimal dosing schedule for antitumor therapy, BALB/c mice bearing s.c. C-26 tumors were administered a single dose of DOX-

conjugated bow-tie polyester dendrimer-PEO (10 mg/kg DOX) on various days after tumor inoculation. Five different groups of mice were treated with a single i.v. injection of polymer on day 2, 4, 8, 12, or 16 after their tumors were implanted. Dosing schedule experiment showed that Mice treated on day 8 responded the most favorably to treatment, a result that was statistically different from the mice treated on days 4, 12, and 16. A dose-response experiment was performed by monitoring tumor growth and survival of BALB/c mice treated with a single dose of DOX-conjugated bow-tie polyester dendrimer-PEO 8 days after implantation of a s.c. C-26 tumor. Remarkably, at the highest dose administered (20 mg/kg DOX equivalents), complete tumor regression was observed, resulting in 100% survival of mice in this treatment group over the 60-day experiment. In contrast, none of free DOX (6 mg/kg) administered mice was survived at day 25. The activity of the DOX-conjugated bow-tie polyester dendrimer-PEO in vivo, despite its reduced in vitro toxicity relative to free DOX, is convincing evidence of the dendrimer's ability to modulate the pharmacokinetic profiles of attached anticancer drugs [139].

Collectively, DOX conjugated [G-3]-(PEO_{5k})₈-[G-4]-(OH)₁₆ bow-tie structure illustrated some significant advantages for example water solubility even at DOX concentrations of 6 mg/mL, pH-dependent release, no significant toxicity of carrier, long circulation half-life of conjugates, and enhanced tumor uptake. In spite of reduced in vitro toxicity, the DOX-conjugated bow-tie polyester dendrimer-PEO showed higher antitumor activity in vivo. These results introduce DOX-conjugated bow-tie polyester dendrimer-PEO as a promising anticancer system [138, 139].

Liver-targeting potential of galactose conjugated PEG-*b*-PAMAM-DOX_n prodrug (Compound 17) has been confirmed using contrast-enhanced MRI carried out on Female ICR mice [141]. Comparison of signal enhancement in liver for Gal-PEG-*b*-PAMAM-Gd and mPEG-*b*-PAMAM-Gd complexes showed the maximum liver ENH of both agents after 6 h of injection. Then, a rapid decrease of ENH has been observed for mPEG-*b*-PAMAM-Gd. In contrast, Gal-PEG-*b*-PAMAM-Gd has shown a gradual decrease of ENH due to the high affinity of ASGP receptor at the liver surface to galactosyl residues in Gal-PEG-*b*-PAMAM-Gd, proving its active liver-targeting potential. In vivo antitumor evaluations indicated inhibition of tumor growth after Gal-PEG-*b*-PAMAM-DOX_n administration (Figure 35). Gal-PEG-*b*-PAMAM-DOX_n showed better in vivo antitumor efficacy than free DOX, suggesting its great potential as a polymeric antitumor prodrug. In mice treated with free DOX, increasing tendency has been found in tumor size after observed antitumor activity up to the tenth day. These data offer Gal-PEG-*b*-PAMAM-DOX_n as useful targeting anticancer agent [141]. Properties reported for Gal-PEG-*b*-PAMAM-DOX_n including stability in pH 7.4, triggered drug release in pH 5.6-6.5 and sensitivity of drug vehicle to lower pH of tumor cells, receptor mediated liver targeting, higher in vivo antitumor efficacy in spite of lower in vitro activity compared to free drug make this system interesting for anticancer investigations. Additionally, biodistribution and pharmacokinetics studies can develop this system [141].

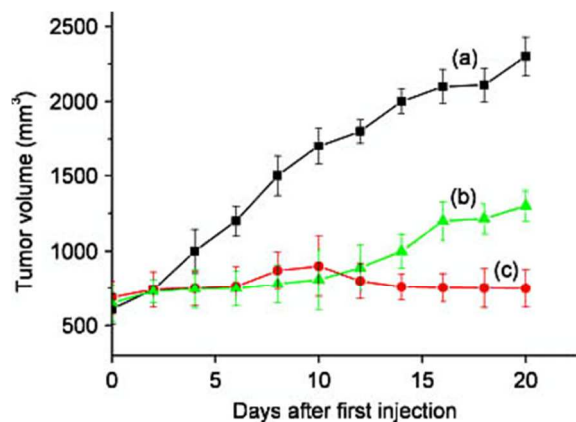


Figure 35. In vivo antitumor efficacy of (a) PBS, (b) DOX and (c) Gal-PEG-b-PAMAM-DOX_n (mean \pm SD, n = 8). Reprinted with permission from ref. 141. Copyright (2010) Society of Chemical Industry

Determined by in vivo experiments, the tumor weights in mice treated with mPEGylated L-lysine Dendron-DOX conjugate nanoparticle (Compound 18) were obviously lower compared with the tumors from free drug DOX treatment group [143]. The high antitumor activity of the DOX-conjugated nanoparticle has been attributed to neutral charged surface, longer blood circulation, potential higher accumulation in tumor via EPR effect and the accelerated release of DOX from endosomes. Also less body weight shift has been observed for the group administrated DOX-conjugated nanoparticle compared to the free DOX treated ones, indicating better drug tolerability. As shown in Figure 36, histologically, for mice administrated free drug DOX, the heart toxicity induced by DOX was observed due to the necrosis (grade 1) with acute inflammatory cells infiltration at epicardium and cardiac myocyte under epicardium. In contrast, the mice administrated with drug-free peptide dendron and peptide Dendron-DOX conjugate based nanoparticle were normal and no visible difference was observed compared to the control [143].

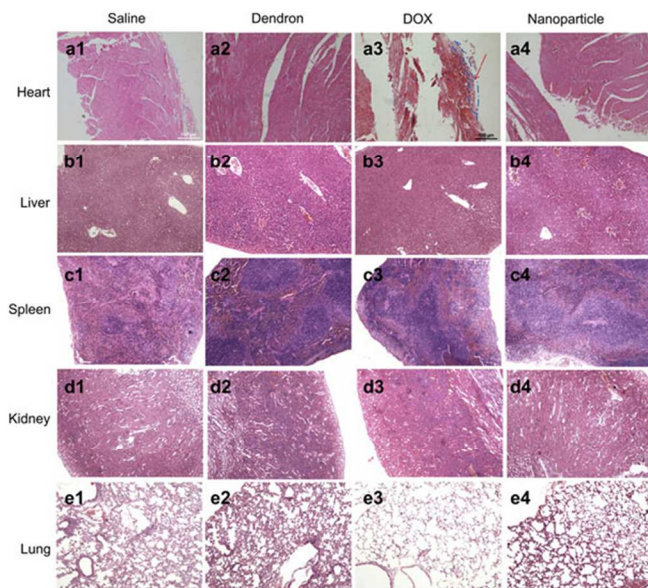


Figure 36. Histological analysis for different organs of normal mice administrated control (Saline), drug-free peptide dendron (Dendron), free drug DOX (DOX) and mPEGylated peptide dendron -DOX conjugate based nanoparticle (Nanoparticle) (heart: $\times 200$, other tissues: $\times 100$). The analysis showed that the free drug DOX resulted in heart toxicity due to the observed necrosis (grade 1) with acute inflammatory cells infiltration in epicardium and cardiac myocyte under epicardium (a3). In contrast, organs of mice administrated saline, drug-free mPEGylated peptide dendron and mPEGylated peptide dendron -DOX conjugate based nanoparticle did not exhibit signs of toxicity. Reprinted with permission from ref. 143. Copyright (2012) Elsevier Ltd.

According to in vivo experiments, higher antitumor activity has been obtained for DOX-conjugated mPEGylated L-lysine Dendron nanoparticle [143]. Lower tumor weights have been observed in mice administrated with DOX-conjugated nanoparticles in comparison with the tumors from free drug DOX treatment group. This result is caused by neutral charged surface, longer blood circulation, potential higher accumulation in tumor via EPR effect and the accelerated release of DOX from endosomes [150]. Also less body weight loss has been observed for the group administrated DOX-conjugated nanoparticle compared to the free DOX treated ones, indicating better drug tolerability. Histological analysis on normal mice demonstrated the heart toxicity for mice administrated free drug DOX [143]. The toxicity has been attributed to the necrosis (grade 1) with acute inflammatory cells infiltration at epicardium and cardiac myocyte under epicardium (Figure 36). In contrast, no toxicity has been observed in mice administrated with drug-free nanoparticles and peptide Dendron-DOX nanoparticle. Low molecular weight of mPEG-peptide dendron and its biodegradability, high accumulation of DOX-conjugated nanoparticles in tumor tissue but lower accumulation in normal tissue via EPR effects, and sensitivity of drug vehicle to lower pH of tumor cells promote the clearance from organism and thereby enhance the in vivo biocompatibility [143]. The overall structural design of mPEGylated L-lysine Dendron-DOX conjugate and its properties such as nontoxicity of vehicle, pH-sensitive manner of drug release, enhanced tumor inhibition in vivo in spite of lower in vitro cytotoxicity in comparison with free DOX, better drug tolerability, enhanced in vivo biocompatibility, and reduced side effects provide this prodrug as safe and efficient anticancer drug delivery system [143]. From in vivo studies on mice bearing 4T1 breast tumor model, She et al. showed that the tumors treated with dendronized heparin-DOX nanoparticle (Compound 19) exhibited a significantly stronger response than the tumors treated with saline only or free drug DOX [146]. Particularly, after 25 days therapy, the statistically significant was obtained for mice treated with nanoparticles to the control and DOX treated group due to the much smaller tumor volume, as shown in the tumor growth curves (Figure 37a, $p < 0.001$). The tumor sizes from mice administrated dendronized heparin-DOX conjugate based nanoparticles were obviously smaller than those from free drug DOX treatment group and controls. (Figure 37b), which was proportional to the observed relative tumor volume results (Figure 37a). Simultaneously, the tumor weights in mice treated with nanoparticles were obviously lower compared with the tumors from free drug DOX treatment group ($p < 0.05$) and control ($p < 0.001$) (Figure 37c) [146]. The high antitumor activity of the nanoparticle was attributed to negatively charge surface, longer blood circulation, potential higher accumulation in tumor via EPR effect and the accelerated release of DOX from endosomes [151]. Regarding advantages of non-toxicity of carrier, pH-sensitive drug release manner, and higher antitumor activity in vivo, dendronized heparin-DOX may be therefore a potential nanoscale drug delivery vehicle

for breast cancer therapy. Certainly, pharmacokinetics studies make this system more helpful for cancer therapy purposes [146].

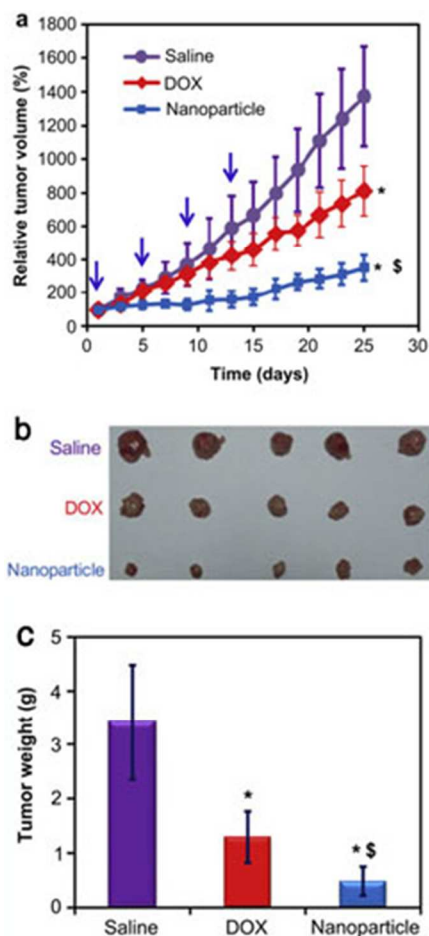


Figure 37. In vivo tumor growth inhibition of nanoparticle. Comparison of the tumor inhibition effect of dendronized heparin-DOX conjugate based nanoparticle with drug (Nanoparticle) versus free drug DOX (DOX) and saline in the breast tumor model ($n = 5$). The nanoparticle demonstrated significant tumor inhibition ($*p < 0.001$, compared to saline[§]; $p < 0.001$, compared to free drug DOX) (a). At the end of this experiment, tumor tissues were collected from each sacrificed animal after 25 days treatment, photographed (b) and weighted ($*p < 0.01$, compared to saline; $§p < 0.05$, compared to free drug DOX) (c). Reprinted with permission from ref. 146. Copyright (2012) Elsevier Ltd.

Although these DOX-conjugated linear-dendritic polymer systems demonstrated low in vitro cytotoxicities in comparison with free drug [136, 141, 143, and 146], the larger accumulation in tumor tissue in vivo could counter balance the low in vitro toxicity. High molecular weight polymers preferentially accumulate in solid tumor tissue due to a combination of the leaky character of tumor blood vessels formed during neo-angiogenesis and to limited lymphatic drainage. The combination of these two factors is responsible for the enhanced permeability and retention effect (EPR) observed with tumor tissue, which leads to a passive targeting of drugs to tumors. In addition, the larger hydrodynamic volume of polymers contributes to the increased plasma half-life of the drug-polymer conjugates, increasing the probability of accumulation of the therapeutic agent in the tumor tissue by means of the EPR effect. Drugs have also been conjugated to polymers to improve their water solubility properties, to decrease their toxicity due to local accumulation of the drug prior to reaching the target tissue, and to protect them from possible enzymatic degradation or hydrolysis. So these DOX-conjugated linear-dendritic systems are promising because they allowed slow elution of doxorubicin into the tumor after administrated, since the nanoparticle with much longer blood circulation time and higher accumulation in tumor tissue via EPR effect [136, 141, 143, and 146].

Table 4. Doxorubicin-conjugated linear-dendritic block copolymers

Carrier name	Size (nm)	In vitro activity	In vivo activity	advantages	ref
3-arm PEO-(bis-MPA) dendrimer	n	Less cytotoxicity compared to free drug on B16F10, MDA-MB-435, and MDA-MB-231 cell line	no significant accumulation in any vital organ, including the liver, heart, and lungs evaluated on CD-1 female mice	biocompatibility of carrier, pH-dependent release, no significant accumulation in vital organs, and longer circulatory half-life than free drug	136
	8	Lower cytotoxic activity ($IC_{50}=1.4 \pm 0.2 \mu\text{g/ml}$) compared to free DOX ($IC_{50}=0.08 \pm 0.02 \mu\text{g/ml}$) on MDA-MB-231 cancer cells	Higher antitumor effects compared to free DOX on BALB/c mice bearing s.c. C-26 tumors	water solubility even at DOX concentrations of 6 mg/mL, pH-dependent release, no significant toxicity of carrier, long circulation half-life of conjugates, and enhanced tumor uptake and higher antitumor activity in vivo	138, 139

Gal-PEG-b-PAMAM	n	Reduced cytotoxic activity compared to free drug against Bel-7402 cells	better in vivo antitumor efficacy than free Dox on Female ICR mice	stability in pH 7.4, triggered drug release in acidic pH, receptor mediated liver targeting, higher in vivo antitumor efficacy	141
mPEGylated poly(L-lysine) dendron	220	lower cytotoxicity (IC_{50} = 151 ng/mL) compared with free DOX (IC_{50} = 25.9 ng/mL) on mouse breast cancer cell line (4T1)	Higher antitumor activity in comparison with free DOX	nontoxicity of vehicle, pH-sensitive manner of drug release, enhanced tumor inhibition in vivo, reduced side effects	143
Heparin-poly(L-lysine)	90	lower cytotoxicity (IC_{50} of 300 ng/mL) compared with free DOX (IC_{50} of 27 ng/mL) against mouse breast cancer cell line (4T1)	higher antitumor activity on mice bearing 4T1 breast tumor model compare to free drug	non-toxicity of carrier, pH-sensitive drug release manner, and higher antitumor activity in vivo	146
MPEG-b-PAMAM	60	Higher in vitro cytotoxicity for nanoparticles compared to free DOX and free HCPT in MCF-7 and HepG2 cell lines	n	co-delivery of two anticancer drugs (DOX and HCPT), high drug loading content, pH-dependent manner of drug release, higher cellular uptake compared to free HCPT, higher in vitro cytotoxicity	147
MPEG-b-PAMAM-LA	140 (CMC=13.30 $\mu\text{g mL}^{-1}$)	Being more effective after a longer period of incubation on HeLa cells and A549 cells	n	High drug loading content, pH and reduction-sensitive DOX release behavior, higher in vitro cytotoxic effect with the elongation of the incubating time	78

n: not reported

6. Cisplatin

Cisplatin (cis-dichlorodiammine platinum (II)) (CDDP) is one of the most potent anticancer agents available today and is widely used in the treatment of many malignancies, including testicular, ovarian, bladder, head and neck, small cell and nonsmall cell lung cancers because of its potent activity to cross-link DNA upon entering the cells. It preferentially binds to the N7 atoms of guanine bases in DNA double-helix strands, thereby preventing the strands from uncoiling and separating. This prohibits the division of the cells and ultimately results in cellular apoptosis. [152–156] However, its clinical use is limited due to its significant toxic side effects, such as acute nephrotoxicity and chronic neurotoxicity. CDDP shows a rapid distribution over the whole body and high glomerular clearance within 15 min after intravenous injection. A total of 90% of the cisplatin is bound to plasma proteins in the blood and, thus, does not enter the cells; leading to less therapeutic efficacy. Therefore, many efforts have been devoted to develop a drug delivery system aimed at increasing the blood circulation period and accumulation in solid tumors [157–159].

6-1. Cisplatin-conjugated linear-dendritic block copolymers

6.1.1. Physicochemical properties

Using linear-dendritic polycitric acid-polyethylene glycol-polycitric acid (PCA-PEG-PCA) copolymers ($M_w \sim 2000$ Da), Haririan et al. prepared conjugates of PCA-PEG-PCA-CDDP (Compound 22) in an aqueous media [160]. Drug loading of about 6% weight of platinum/weight of the conjugates was gained for conjugates. By in vitro platinum release tests, it was found that the release rate in the acidic pH (5.4) was slightly greater and faster than the neutral pH (7.4) attributed to the catalytic effect of the acidic conditions on the ease of displacement of water molecules with chloride or carboxylate ions inside the cisplatin cavity [160]. It was observed that when the conjugates were formed from the dendrimers, an increase in the particle size were seen in the conjugates (141 nm) as contrasted with the dendrimers (85 nm). This phenomenon can result from the crosslinking of the dendrimers with cisplatin which intercalates between two of the dendrimer molecules [160]. In our previous study, we used polycitric acid-polyethylene glycol-polycitric acid (PCA-PEG-PCA) linear-dendritic copolymers to solubilize and functionalize multi-walled carbon nanotubes (MWCNTs) by noncovalent interactions [161]. We showed that a potential anticancer drug cisplatin can be conjugated to the carboxyl functional groups of the dendritic blocks of PCA-PEG-PCA linear-dendritic copolymers and then the prodrugs interacted with the MWCNTs noncovalently leading to formation of MWCNT/PCA-

PEG-PCA-CDDP hybrid nanomaterial-based drug delivery systems (HNDDSs) (Compound 23). Based on our previous investigations the cavity of the polymer-functionalized carbon nanotubes are able to host nanoparticles of up to 15 nm in diameter, due to their high solubility and opened cavity. Since the size of an individual PCA-PEG-PCA linear-dendritic copolymer is less than 10 nm, [162,163] they can transfer conjugated CDDP molecules to the cavity of MWCNT/PCA-PEG-PCA hybrid nanomaterials (Figure 37b). As exhibited by the TEM images, the synthesized hybrid nanomaterials “transfer” CDDP molecules not only by conjugation to the linear-dendritic copolymers on their surface but also in their cavity. Drug release studies at 37 °C and pH 7.4 showed the slow rate of release with cumulative release percent around 40% after 168 h [161].

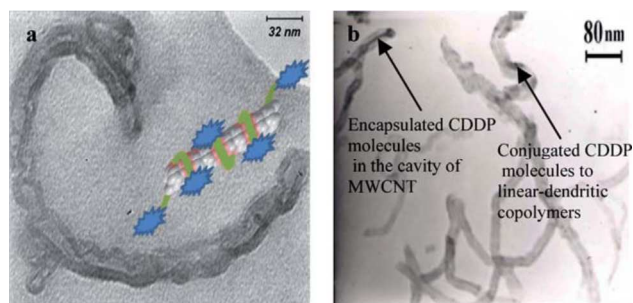


Figure 38. TEM images of a) MWCNT/PCA-PEG-PCA and b) MWCNT/PCA-PEG-PCA-CDDP. Reprinted with permission from ref. 161. Copyright (2011) The Royal Society of Chemistry

In other study, we reported conjugation of CDDP with PCA-PEG-PCA/CNT/ γ -Fe₂O₃NP hybrid nanomaterials (Compound 23) [164]. Deposition of γ -Fe₂O₃ nanoparticles onto the surface of CNTs led to magnetic CNT/ γ -Fe₂O₃NP and then, non-covalent interactions between PCA-PEG-PCA and CNT/ γ -Fe₂O₃NP resulted in PCA-PEG-PCA/CNT/ γ -Fe₂O₃NP hybrid nanomaterials with improved water solubility, functionality, and potential application to target anticancer drugs. According to TGA analysis the weight percent of PCA-PEG-PCA linear-dendritic copolymers adsorbed onto the surface of CNTs is around 45%. While the molecular weight of CNTs is much more than that of linear-dendritic copolymers, it can be found that a large number of linear-dendritic copolymers are attached onto the surface of a CNT [164]. Based on TGA thermal analysis, the weight percent of CDDP in the CDDP/PCA-PEG-PCA/CNT/ γ -Fe₂O₃NP drug delivery system is around 7%. DLS experiments show that the average diameter of CNT/ γ -Fe₂O₃NP hybrid nanomaterials in water changes from 977 to 190 nm upon interaction with PCA-PEG-PCA linear-dendritic copolymers, confirming that conformation of CNTs converts from the linear to globular form. This is of great importance, because the shape and size of nanomaterial- and especially CNT-based drug delivery systems affect their toxicity efficiently so that carcinogenicity of CNTs sometimes is assigned to their long length and is compared with the asbestos fibers. It should be kept in mind that another reason for diminishing the size of CNT/ γ -Fe₂O₃NP hybrid nanomaterials could be separation of their bundles toward individual objects, due to the noncovalent interactions with linear-dendritic copolymers. The size of the CDDP/PCA-PEG-PCA/CNT/ γ -Fe₂O₃NP drug delivery system in water is 11 nm bigger than that of the PCA-PEG-PCA/CNT/ γ -Fe₂O₃NP hybrid nanomaterial, proving that the interaction of CDDP/PCA-PEG-PCA anticancer prodrug with the surface of CNT/ γ -Fe₂O₃NP is weaker than that of the PCA-

PEG-PCA linear-dendritic copolymer. This result confirms that CDDP molecules are conjugated with the carboxyl functional groups of PCA blocks and limit interactions between linear-dendritic copolymers and hydroxyl functional groups of iron oxide nanoparticles anchored onto the surface of CNTs [164]. VSM curves showed that the saturation of magnetization of PCA-PEG-PCA/CNT/ γ -Fe₂O₃NP hybrid nanomaterials was smaller than that of CNT/ γ -Fe₂O₃NP, but both had similar properties (Figure 39). This proved that the magnetic properties of CNT/ γ -Fe₂O₃NP were not influenced by the self-assembly of PCA-PEG-PCA linear-dendritic copolymers on their surfaces indicating that PCA-PEG-PCA/CNT/ γ -Fe₂O₃NP hybrid nanomaterial can be used as a promising material in cancer diagnosis and therapy [164].

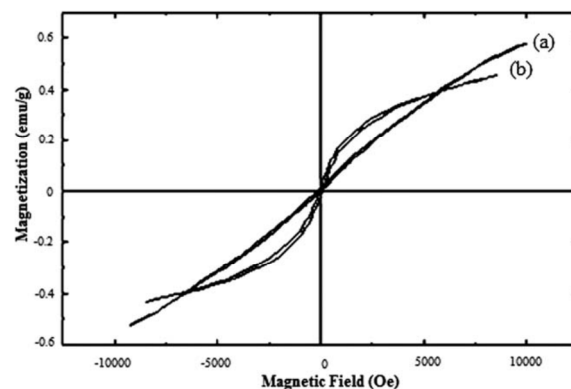


Figure 39. Hysteresis loop by VSM of: (a) CNT/ γ -Fe₂O₃NP and (b) PCA-PEG-PCA/CNT/ γ -Fe₂O₃NP. Reprinted with permission from ref. 164. Copyright (2011) The Royal Society of Chemistry

6.1.2. In vitro evaluations

In vitro cytotoxicity assay evaluated in CT26 cells (24 h incubation) demonstrated IC₅₀ of 0.8252 μ g mL⁻¹ for PCA-PEG-PCA (G2) – CDDP conjugates (Compound 22), which was 9 fold lower in comparison with free cisplatin. IC₅₀ determined for PCA-PEG-PCA(G2)–CDDP conjugates in HT1080 cell lines (48 h incubation) was 0.973 μ g mL⁻¹, which was 8.4 fold lower than that determined for free cisplatin [160]. These significantly higher toxicities were explained by two factors: 1) higher uptake of the conjugates as contrasted with the free cisplatin due to the citric acid content of the conjugates together with the greater demands of cancer cells for such energy sources during the time of incubation. 2) Increased liberation of the drug attributed to lysosomal enzymes existing inside the cell which gradually breakdown the bond between cisplatin and the dendrimers [160].

Regarding nontoxicity of PCA-PEG-PCA and the in vitro results gained for the conjugates of cisplatin-PCA-PEG-PCA including greater and faster drug release rate in acidic pH, and greater cytotoxicity compared to free cisplatin, it is hoped that these conjugates would be able to maintain the observed potency in vivo and retain the parent drug conjugated at the surface of the dendrimers in the physiologic plasma condition. Future in vivo studies will be able to clarify the potentiality of these entities in the cure of both sensitive and resistant cancerous cells [160].

In vitro cytotoxicity studies on murine colon adenocarcinoma tumor C26 cancer cells demonstrated higher cytotoxicity for MWCNT/PCA-PEG-PCA-CDDP HNDDSs (Compound 23) in comparison with free drug [161]. This was attributed to the complementary roles of

carbon nanotubes and PCA-PEG-PCA linear-dendritic copolymers. MWCNTs raise the rate of the “transferring” of the linear-dendritic copolymers from the cell membrane. On the other hand, PCA-PEG-PCA linear-dendritic copolymers improve the water solubility of the MWCNTs and due to their citric acid backbone PCA-PEG-PCA probably can be used as the source of energy by the cells that cause to insert MWCNTs in the cell metabolism [161]. In summary, results from this study showed slow rate of cisplatin release at physiological conditions and higher cytotoxicity for MWCNT/PCA-PEG-PCA-CDDP in comparison with free drug which make this system useful for anticancer drug delivery. More studies in pharmacokinetics and antitumor effect in vivo are required for developing this system in cancer therapy [161].

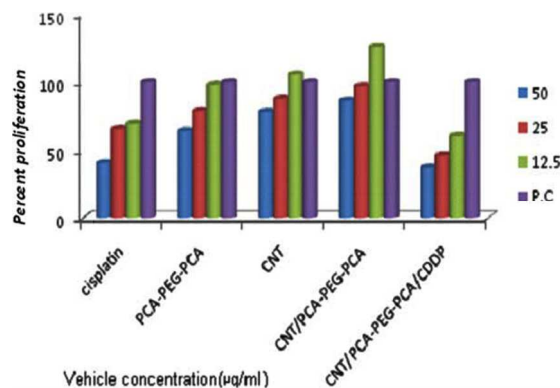


Figure 40. Percentage survival of C26 cancer cells, assessed by the MTT assay, after exposure to free CDDP, opened MWCNT, PCA-PEG-PCA, MWCNT/PCA-PEG-PCA and MWCNT/PCA-PEG-PCA-CDDP at 12.5, 25 and 50 $\mu\text{g mL}^{-1}$ ($n = 3$). P.C. is the positive control. Reprinted with permission from ref. 161. Copyright (2011) The Royal Society of Chemistry

In vitro cytotoxicity tests conducted on the mouse tissue connective fibroblast adhesive cell line (L929) demonstrated that a 100 $\mu\text{g ml}^{-1}$

concentration of CDDP/PCA-PEG-PCA/CNT/ $\gamma\text{-Fe}_2\text{O}_3\text{NP}$ (Compound 24) killed more than 95% of cancer cells (Figure 40) [164]. This high toxicity was explained by fast transferring through the cell membrane caused by CNT, and high water solubility and capability to insert in the cell metabolism caused by PCA-PEG-PCA [164].

Noncovalent interactions between carbon nanotubes and linear-dendritic copolymers lead to hybrid nanomaterials having a hybrid of properties such as fast transferring through the cell membrane, high functionality, water solubility, biocompatibility, and ability to target drugs to tumors. Sufficient in vitro cytotoxicity makes this system attractive for future in vivo studies [164].

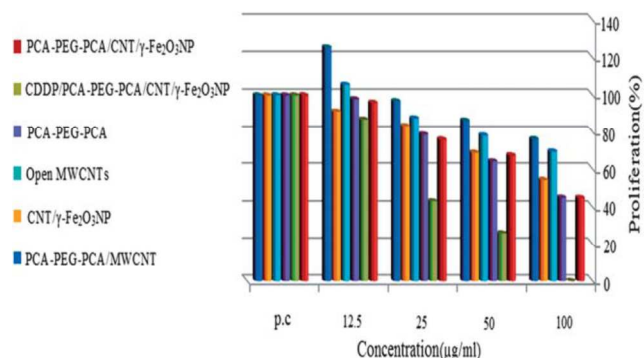


Figure 41. The MTT assay results for opened MWCNT, CNT/ $\gamma\text{-Fe}_2\text{O}_3\text{NP}$, PCA-PEG-PCA, PCA-PEG-PCA/CNT, PCA-PEG-PCA/CNT/ $\gamma\text{-Fe}_2\text{O}_3\text{NP}$ and CDDP/PCA-PEG-PCA/CNT/ $\gamma\text{-Fe}_2\text{O}_3\text{NP}$ hybrid nanomaterials. Reprinted with permission from ref. 164. Copyright (2011) The Royal Society of chemistry

Table 5. Cisplatin-conjugated linear-dendritic block copolymers

Carrier name	Size (nm)	In vitro activity	In vivo activity	advantages	ref
PCA-PEG-PCA	141	Significantly higher cytotoxicity in CT26 cells (IC_{50} of $0.8252 \mu\text{g mL}^{-1}$ for conjugates, 9 fold lower than free cisplatin) and in HT1080 cell lines (IC_{50} of $0.973 \mu\text{g mL}^{-1}$ for conjugates, 8.4 fold lower than free cisplatin)	n	nontoxicity of carrier, greater and faster drug release rate in acidic pH, and greater cytotoxicity compared to free cisplatin	160
MWCNT/PCA-PEG-PCA	371	higher cytotoxicity for HNDDSs in comparison with free drug on murine colon adenocarcinoma tumor C26 cancer cells	n	slow rate of cisplatin release at physiological conditions and higher cytotoxicity compared to free drug	161
PCA-PEG-PCA/CNT/ $\gamma\text{-Fe}_2\text{O}_3\text{NP}$	200	Higher cytotoxicity against the mouse tissue connective fibroblast	n	fast transferring through the cell membrane, high functionality, water	164

Fe ₂ O ₃	adhesive cell line (L929)	solubility, biocompatibility, sufficient in vitro cytotoxicity
n: not reported		

7. Camptothecin

Camptothecin (CPT), a natural plant alkaloid extracted from *Camptotheca acuminata*, is a promising antitumor agent that acts by stabilizing a topoisomerase I-induced single strand break in the phosphodiester backbone of DNA, thereby preventing religation. This causes to destroy DNA strands during DNA replication in the cell cycle, which leads to cell death if the broken DNA is not repaired [165–167]. The drug is a pentacyclic indole alkaloid, with the terminal ring converting readily between the lactone in acidic environments (pH < 5) to the carboxylate (pH > 8) form. In order for CPT to be active, the lactone form must dominate. The opening of the lactone ring at physiological pH and above, which produces the less active and high toxic carboxylate form prevents the clinical application of CPT in cancer therapy. Moreover, poor solubility in water and in physiological acceptable organic solvents restricts practical use of the active lactone form of CPT [168–170]. Attempts to overcome these limitations have involved conjugation of camptothecin to biocompatible polymers (prodrug approach) [171], and encapsulation into liposomes [172], polymeric micelles [173], dendrimers [174], and nanoparticles [175].

7-1. Camptothecin-conjugated linear-dendritic block copolymers

7.1.1. Physicochemical properties

Camptothecin has been conjugated to PEG-block-dendritic polylysine to tailor the hydrophobicity of amphiphilic linear-dendritic PEG-polylysine – CPT conjugates (Compound 25) [79]. By CPT content-controlled self-assembly, nanostructures – nanospheres or nanorods of different diameters and lengths have been obtained. As shown in Figure 42, CPT-PDP containing a disulfide bond and an NHS active ester group has been reacted with PEG-block-dendritic polylysine (PEG₄₅-DPLL-G₂) of different generations. The CPT contents of PEG-polylysine G₀-CPT, PEG-polylysine G₁-DiCPT, PEG-polylysine G₂-TetraCPT and PEG-polylysine G₃-OctaCPT have been 13.4%, 21.4%, 30.6%, and 38.9% by weight, respectively.

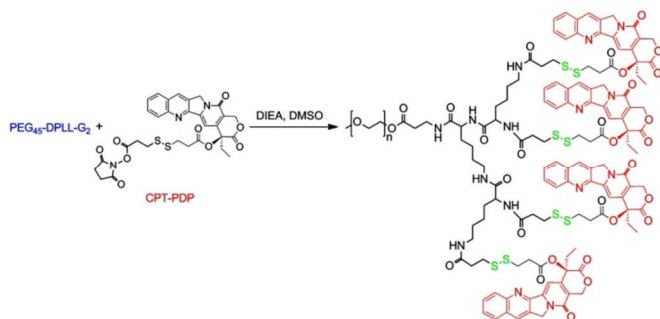


Figure 42. Schematic illustration of PEG-dendritic polylysine (G₂)-camptothecin conjugation reaction (Compound 25). Reprinted with permission from ref. 79. Copyright (2013) Elsevier Ltd.

PEG-polylysine G₀-CPT and PEG-polylysine G₁-DiCPT formed uniform ~100 nm nanospheres. Interestingly, PEG₄₅-TetraCPT and PEG₄₅-OctaCPT formed unusual nanorods. The nanorods of PEG-polylysine G₂-TetraCPT were about 60 nm in diameter and 500 nm long, and those of PEG-polylysine G₃-OctaCPT were about 100 nm in diameter and about 1 μm long. The stability of the nanostructures was studied in PBS at 37 °C by DLS. PEG₄₅-DiCPT nanospheres and PEG₄₅-TetraCPT nanorods were stable for over five days and their sizes did not change over time, whereas PEG₄₅-OctaCPT nanorods aggregated slightly. None of these nanostructures released any CPT under these conditions. In vitro drug release studies showed no CPT release from PEG-polylysine-CPT formulations due to conjugation of CPT molecules by disulfide bonds which can be cleaved intracellularly by GSH indicating stability of formulations at the physiological conditions but quickly releasing the drug CPT once in the cytosol. GSH-mediated release was evidenced by addition of DTT, a strong reducing agent similar to GSH, which caused to immediately release of CPT-thioester (CPT-SH) [79].

7.1.2. In vitro evaluations

MTT assay on MCF-7 cells determined the IC₅₀ value 0.138 μg/mL for PEG₄₅- polylysine G₁-DiCPT, 0.073 μg/mL for PEG₄₅- polylysine G₂-TetraCPT and 0.070 μg/mL for PEG₄₅- polylysine G₃-OctaCPT, which are higher than that of free CPT (0.008 μg/mL) [79].

7.1.3. In vivo evaluations

Pharmacokinetics in BALB/c mice determined elimination half-life times (t_{1/2}) of 5.82 h for PEG-polylysine G₂-TetraCPT, which was significantly greater than those of PEG-polylysine G₁-DiCPT (1.61 h) and PEG-polylysine G₃-OctaCPT (1.70 h) [79]. The prolonged circulation time of the PEG-polylysine G₂-TetraCPT nanorods has been attributed to their elongated shape, which might align or tumble in the flow to reduce clearance by the liver or spleen. Biodistribution studies after 4 h i.v. administration to BALB/c mice demonstrated nanostructures presence in the spleen. Also accumulation of some PEG-polylysine G₁-DiCPT in the liver (15.75 ± 3.85% ID/g tissue), and significant amount of PEG-polylysine G₃-OctaCPT in the lung (64.89 ± 2.63%) was observed [79]. PEG-polylysine G₂-TetraCPT had lower concentrations in liver and spleen than PEG-polylysine G₁-DiCPT. After 24 h, PEG-polylysine G₁-DiCPT almost disappeared from all the organs. The level of PEG-polylysine G₃-OctaCPT in the lung was also greatly reduced and little remained in the spleen (10.53 ± 1.31% ID/g of tissue) and liver (3.55 ± 0.57% ID/g tissue). PEG-polylysine G₂-TetraCPT was still found in the spleen (22.05 ± 6.33% ID/g tissue) and blood (3.59 ± 0.29% ID/g blood) [79]. Collectively, high drug content, stability of formulations at the physiological conditions, and reduction-sensitive drug release profile which leads to fast release in cytosol made this system suitable for drug delivery. It was demonstrated that PEG-polylysine G₂-TetraCPT conjugate nanorods with proper lengths can unite the two opposites in cancer-drug delivery: long blood circulation versus fast cellular uptake and drug retention in circulation versus

intracellular drug release, ideal for efficient tumor-drug delivery [79].

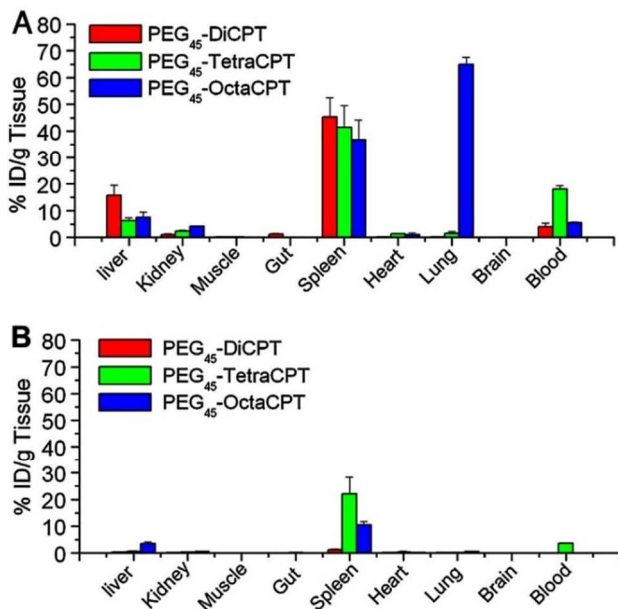


Figure 43. The biodistribution at 4 h (A) or 24 h (B) post i.v. administration of the PEG-xCPT nanostructures. Dose, 10 mg CPT-eq./kg, n = 4. Reprinted with permission from ref. 79. Copyright (2013) Elsevier Ltd.

8. Conclusion

In summary, linear-dendritic block copolymers show great potential in anticancer drug delivery applications. The high architectural control and the option to tailor the properties of the linear-dendritic copolymers to the specific requirements of cancer therapy including prolonged circulation times, increased drug solubility, reduced drug toxicity, selective delivery to tumors by active targeting with covalently bonded tumor-targeting agents or passive targeting resulted from the enhanced permeability and retention (EPR) effect make these nanostructures promising carriers for variety of anticancer drugs. The reported data demonstrate that in most studies PEG has been utilized as linear segment of linear-dendritic anticancer carriers because of its biocompatibility and hydrophilic properties. The chemotherapeutic agents can be loaded either as conjugated to the functional groups on the dendritic blocks or encapsulated by the hydrophobic interior of the dendritic segments of block copolymers. Several strategies have been employed for delivery of loaded chemotherapeutic agents such as pH-, enzyme-, light-, and glutathione-dependent manners. In many cases, slow drug release in physiological conditions, improved selectivity and higher drug accumulation in tumor tissues, and reduced drug toxicities were observed for drug loaded linear-dendritic copolymers indicating these nanostructures as promising vehicles for anticancer agents. Although a large number of studies, investigating in vitro and in vivo antitumor efficacy of anticancer drugs loaded by linear-dendritic copolymers are available, more research works focusing on the biodistribution, pharmacokinetic studies, toxicity problems and side effects are needed. Clearly, more studies lead to better knowledge in the design of linear-dendritic based anticancer drug delivery systems in order to achieve more targeting properties and higher antitumor effects, and avoid the uptake in vital organs and side effects that can be used to assist in the optimization of clinical protocols.

Table 6. Camptothecin-conjugated linear-dendritic block copolymers

Carrier name	Size (nm)	CMC	In vitro activity	In vivo activity	advantages	ref
PEG-polylysine	100	PEG45-polylysine G1-DiCPT=0.114 mg/mL, PEG45-polylysine G2-TetraCPT=0.074 mg/mL, PEG45-polylysine G3-OctaCPT=0.025 mg/mL	Lower cytotoxicity against MCF-7 cells, IC ₅₀ = 0.138 µg/mL for PEG45-polylysine G1-DiCPT, 0.073 µg/mL for PEG45-polylysine G2-TetraCPT and 0.070 µg/mL for PEG45-polylysine G3-OctaCPT, and 0.008 µg/mL for free CPT	After 24 h i.v. administration to BALB/c mice, greatly reduced level of PEG-polylysine G ₃ -OctaCPT in the lung, spleen, and liver. But remaining of PEG-polylysine G ₂ -TetraCPT was in the spleen and blood	high drug content, stability of formulations at the physiological conditions, and reduction-sensitive drug release	79

9. Acknowledgment

Authors would like to thank Iran Nano Council to support this work financially.

Notes and references

^aDepartment of Chemistry, Faculty of Science, Lorestan University, Khorramabad, Iran

^bInstitut für Chemie und Biochemie, Freie Universität Berlin, Germany

Corresponding author:

Mohsen Adeli: ^bDepartment of Chemistry, Faculty of Science, Lorestan University, Khorramabad, Iran

E-mail: mohadeli@yahoo.com or m.aadeli@fu-berlin.de

10. References

- [1] Diao, Y.Y.; Li, H.Y.; Fu, Y. H.; Han, M.; Hu, Y. L.; Jiang, H. L.; Tsutsumi, Y.; Wei, Q. C.; Chen, D. W.; Gao, J. Q. *Int. J. Nanomed.*, 2011, **6**, 1955.
- [2] Oerlemans, C.; Bult, W.; Bos, M.; Storm, G.; Nijssen, J. F.; Hennink, W. E. *Pharm. Res.*, 2010, **27**, 2569.
- [3] López-Gómez, M.; Malmierca, E.; de Górgolas, M.; Casado, E. *Crit. Rev. Oncol./Hematol.*, 2013, **88**, 117.
- [4] Brannon-Peppas, L.; O. Blanchette, J. *Adv. Drug Deliv. Rev.*, 2004, **56**, 1649.
- [5] Feng, S. S.; Chien, S. *Chem. Eng. Sci.*, 2003, **58**, 4087.
- [6] Zeng, X.; Morgenstern, R.; Nyström, A. M. *Biomaterials*, 2014, **35**, 1227.
- [7] Nobs, L.; Buchegger, F.; Gurny, R.; Allemann, E. *Bioconj. Chem.*, 2006, **17**, 139.
- [8] Clementi, C.; Miller, K.; Mero, A.; Satchi-Fainaro, R.; Pasut, G. *Mol. Pharm.*, 2011, **8**, 1063.
- [9] Brambilla, D.; Luciani, P.; Leroux, J.-C. *Contr. Rel.*, 2014, **190**, 9.
- [10] Adeli, M.; Sarabi, R.S.; Farsi, R.Y.; Mahmoudi, M.; Kalantari, M.J. *Mater. Chem.*, 2011, **21**, 18686
- [11] Lu, S.; Neoh, K. G.; Huang, C.; Shi, Z.; Kang, E. T. *J. Colloid Interface Sci.*, 2013, **412**, 46.
- [12] Kraus, A.; Wortmann, L.; Hermanns, L.; Feliu, M.; Vahter, M.; Stucky, S.; Mathur, M.; Fadeel, B. *Nanomed.: Nanotech., Biology Med.*, 2014, **10**, 1421.
- [13] Jin, R.; Lin, B.; Li, D.; Ai, H. *Cur. Opin.Pharm.*, 2014, **18**, 18.
- [14] Su, M.; Liu, H.; Ge, L.; Wang, Y.; Ge, S.; Yu, J.; Yan, M. *Electrochim. Acta*, 2014, **146**, 262.
- [15] Wang, X.; Sun, X.; Lao, J.; He, H.; Cheng, T.; Wang, M.; Wang, S.; Huang, F. *Colloids Surf. B: Biointerfaces*, 2014, **122**, 638.
- [16] Cao, X.; Tao, L.; Wen, S.; Hou, W.; Shi, X. *Carbohydr. Res.*, 2014, DOI: 10.1016/j.carres.2014.06.030.
- [17] Adeli, M.; Beyranvand S.; Kabiri R. *Polym. Chem.*, 2013, **4**, 669.
- [18] Batigelli, A.; Ménard-Moyou, C.; Bianco, A. *J. Mater. Chem. B*, 2014, **2**, 6144.
- [19] Ke, X. Y.; Ng, V. W. L.; Gao, S. J.; Tong, Y. W.; Hedrick, J. L.; Yang, Y. Y.; *Biomaterials*, 2014, **35**, 1096.
- [20] Pourjavadi, A.; Adeli, M.; Yazdi, M. *New J. Chem.* 2013, **37**, 295.
- [21] Ang, C.Y.; Tan, S.Y.; Zhao, Y. *Org. Biomol. Chem.*, 2014, **12**, 4776.
- [22] Chegeni B.K.; Kakanejadifard A.; Abedi F.; Kabiri R.; Daneshnia F.; Adeli M. *Colloid Polym. Sci.*, 2014, **292**, 3337.
- [23] Sunoqrot, S.; Bugno, J.; Lantvit, D.; Burdette, J. E.; Hong, S. J. *Control. Release*, 2014, **191**, 115.
- [24] Guillaudeau, S.J.; Fox, M.E.; Haidar, Y.M.; Dy, E.E.; Szoka, F.C.; Fréchet, J.M. *Bioconj. Chem.*, 2008, **19**, 461.
- [25] Grotzky, A.; Altamura, E.; Adamcik, J.; Carrara, P.; Stano, P.; Mavelli, F.; Nauser, T.; Mezzenga, R.; Schlüter, A. D.; Walde, P. *Langmuir*, 2013, **29**, 10831.
- [26] Zhang, X.; Guo, S.; Fan, R.; Yu, M.; Li, F.; Zhu, C.; Gan, Y. *Biomaterials*, 2012, **33**, 7103.
- [27] Maeda, H. *J. Control. Release*, 2012, **164**, 138.
- [28] Fang, J.; Nakamura, H.; Maeda, H. *Adv. Drug Deliv. Rev.*, 2011, **63**, 136.
- [29] Oberoi, H. S.; Laquer, F. C.; Marky, L. A.; Kabanov, A. V.; Bronich, T. K. *J. Control. Release*, 2011, **153**, 64.
- [30] Liu, Y.; Miyoshi, H.; Nakamura, M. *Int. J. Cancer*, 2007, **120**, 2527.
- [31] Hosseini, F.; Panahifar, A.; Adeli, M.; Amiri, H.; Lascialfari, A.; Orsini, F.; Doschak, M.R.; Mahmoudi, M. *Colloids Surfaces B: Biointerfaces*, 2013, **103**, 652.
- [32] Adeli, M.; Ashiri, M.; Chegeni, B. K.; Sasanpour, P. *J. Iran. Chem. Soc.*, 2013, **10**, 701.
- [33] Jhavery, A.; Deshpande, P.; Torchilin, V. J. *Contr. Rel.*, 2014, **190**, 352.
- [34] Ferrari, M. *Nature Rev. Cancer*, 2005, **5**, 161.
- [35] Davis, M.E.; Chen, Z.; Shin, D.M. *Nature Rev. Drug Disc.*, 2008, **7**, 771.
- [36] Gitsov, I.; Berlinova, I.V.; Vladimirov N.G. *J. Polym. Sci., Part A: Polym. Chem.* 2015, **53**, 178.
- [37] Gillich, T.; Acikgöz, C.; Isa, L.; Schlüter, A. D.; Spencer, N. D.; Textor, M. *ACS Nano*, 2013, **7**, 316.
- [38] Gitsov, I.; Wooley, K. L.; Hawker, C. J.; Fréchet, J. M. J. *Polym Prepr* 1991, **32**, 631.
- [39] Gitsov, I.; Wooley K.L.; Fréchet J.M.J. *Angew. Chem. Int. Ed. Engl.*, 1992, **31**, 1200.
- [40] Carlmark, A.; Malmström E.; Malkoch, M. *Chem. Soc. Rev.*, 2013, **42**, 5858.
- [41] Gitsov, I. *J. Polym. Sci.: Part A: Polym. Chem.*, 2008, **46**, 5295.
- [42] Lambrych, K. R.; Gitsov, I. *Macromolecules*, 2003, **36**, 1068.
- [43] Dong, C. M.; Liu, G. *Polym. Chem.*, 2013, **4**, 46.
- [44] Nanjwade, B.K.; Bechra, H.M.; Derkar, G.K.; Manvi, F.V.; Nanjwade, V. K. *Eur. J. Pharm. Sci.*, 2009, **38**, 185.
- [45] Mignani, S.; El Kazzouli, S.; Bousmina, M.; Majoral, J.P. *Adv. Drug Deliv. Rev.*, 2013, **65**, 1316.
- [46] Gajbhiye, V.; Palanirajan, V.K.; Tekade, R.; Jain, N.K. *J. Pharm. Pharmacol.*, 2009, **61**, 989.
- [47] Adeli, M.; Fard, A.K.; Abedi, F.; Chegeni, B.K.; Bani, F. *Nanomed. Nanotech. Biol. Med.*, 2013, **9**, 1203.
- [48] Adeli, M.; Zarnegar, Z.; Dadkhah, A.; Hossieni, R.; Salimi, F.; Kanani, A. *J. Appl. Polym. Sci.*, 2007, **104**, 267.
- [49] Baars, M.W.P.L.; Kleppinger, R.; Koch, M.H.J.; Meijer, E.W. *Angew. Chem. Int. Ed.*, 2000, **39**, 1285.
- [50] Stiriba, S.E.; Kautz, H.; Frey, H. *J. Am. Chem. Soc.*, 2002, **124**, 9698.
- [51] Krämer, M.; Stumbé, J.F.; Türk, H.; Krause, S.; Komp, A.; Delineau, L.; Prokhorova, S.; Kautz, H.; Haag, R. *Angew. Chem.*, 2002, **114**, 4426.
- [52] Chang, Y.; Park, C.; Kim, K.T.; Kim, C. *Langmuir*, 2005, **21**, 4334
- [53] Zhu, C.; Hard, C.; Lin, C.; Gitsov I. *J. Polym. Sci., Part A: Polym. Chem.*, 2005, **43**, 4017
- [54] Gitsov, I. *Advances in Dendritic Macromolecules*, G.R. Newkome, Ed., Elsevier Science, Amsterdam, 2002, **5**, 45.
- [55] Chapman, T.M.; Hillyer, G.L.; Mahan, E.J.; Shaffer, K.A. *J. Am. Chem. Soc.* 1994, **116**, 11195.
- [56] Gitsov, I.; Ivanova, P.T.; Fréchet, J.M.J. *Macromol. Rapid. Comm.* 1994, **15**, 387.
- [57] Blasco, E.; Pinol, M.; Oriol, L. *Macromol. Rapid Commun.*, 2014, **35**, 1090.
- [58] Wurm, F.; Frey, H. *Prog. Polym.Sci.*, 2011, **36**, 1.
- [59] Nguyen, P. M.; Hammond, P. T. *Langmuir*, 2006, **22**, 7825.
- [60] Zhua, J.; Shi, X. *J. Mater. Chem., B* 2013, **1**, 4199.
- [61] Mignani, S.; Majoral, J. P. *New J. Chem.*, 2013, **37**, 3337.
- [62] Zhou, Z.; D'Emanuele, A.; Lennon, K.; Attwood, D. *Macromolecules*, 2009, **42**, 7936.
- [63] Kojima, C.; Suehiro, T.; Watanabe, K.; Ogawa, M.; Fukuhara, A.; Nishisaka, E.; Harada, A.; Kono, K.; Inui, T.; Magata, Y. *Acta Biomater.*, 2013, **9**, 5673.
- [64] Menjoge, A. R.; Rangaramanujam M. Kannan, R. M.; Tomalia, D. A. *Drug Discovery Today*, 2010, **15**, 171.
- [65] Singh, P.; Gupta, U.; Asthana, A.; Jain, N. K. *Bioconjugate. Chem.*, 2008, **19**, 2239.
- [66] Li, M. H.; Choi, S. K.; Thomas, T. P.; Desai, A.; Lee, K. H.; Kotlyar, A.; Holl, M. M. B.; Baker Jr., J. R. *Eur. J. Med. Chem.*, 2012, **47**, 560.
- [67] Chang, Y.; Meng, X.; Zhao, Y.; Li, K.; Zhao, B.; Zhu, M.; Li, Y.; Chen, X.; Wang, J. *J. Colloid Interface Sci.*, 2011, **363**, 403.
- [68] Yang, W.; Cheng, Y.; Xu, T.; Wang, X.; Wen, L. *P. European J. Med. Chem.*, 2009, **44**, 862.
- [69] Sousa-Herves, A.; Riguera, R.; Fernandez-Megia, E. *New J. Chem.*, 2012, **36**, 205.
- [70] Whitton, G.; Gillies, E.R. *J. Polym. Sci., Part A: Polym. Chem.*, 2015, **53**, 148.

- [71] Thomas, T. P.; Patri, A. K.; Myc, A.; Myaing, M. T.; Ye, J. Y.; Norris, T. B.; Baker Jr., J. R. *Biomacromol.*, 2004, **5**, 2269.
- [72] Neerman, M. F.; Chen, H. T.; Parrish, A. R.; Simanek, E. E. *Mol. Pharm.*, 2004, **1**, 390.
- [73] Torchilin V. *Adv. Drug Deliv. Rev.*, 2011, **63**, 131.
- [74] Buczkowski, A.; Sekowski, S.; Grala, A.; Palecz, D.; Milowska, K.; Urbaniak, P.; Gabryelak, T.; Piekarski, H.; Palecz, B. *Int. J. Pharm.*, 2011, **408**, 266.
- [75] Wang, Y.; Guo, R.; Cao, X.; Shen, M.; Shi, X. *Biomaterials*, 2011, **32**, 3322.
- [76] Namazi, H.; Jafarirad, S. *Int. J. Pharm.*, 2011, **407**, 167.
- [77] Stover, T. C.; Kim, Y. S.; Lowe, T. L.; Kester, M. *Biomaterials*, 2008, **29**, 359.
- [78] Zhang, Y.; Xiao, C.; Li, M.; Ding, J.; He, C.; Zhuang, X.; Chen, X.; *Polym. Chem.*, 2014, **5**, 2801.
- [79] Zhou, Z.; Ma, X.; Jin, E.; Tang, J.; Sui, M.; Shen, Y.; Van Kirk, E. A.; Murdoch, W. J.; Radosz, M. *Biomaterials*, 2013, **34**, 5722.
- [80] Li, Y.; Xiao, K.; Luo, J.; Xiao, W.; Lee, J. S.; Gonik, A. M.; Kato, J.; Dong, T. A.; Lam, K. S. *Biomaterials*, 2011, **32**, 6633.
- [81] Kono, K.; Kojima, C.; Hayashi, N.; Nishisaka, E.; Kiura, K.; Watarai, S.; Harada, A. *Biomaterials*, 2008, **29**, 1664.
- [82] Gillies, E.R.; Fréchet, J.M.J. *Pure Appl. Chem.*, 2004, **76**, 1295.
- [83] Lim, J.; Simanek, E. E. *Adv. Drug Deliv. Rev.*, 2012, **64**, 826.
- [84] Xiao, K.; Luo, J.; Fowler, W. L.; Li, Y.; Lee, J. S.; Xing, L.; Cheng, R. H.; Wang, L.; Lam, K. S. *Biomaterials*, 2009, **30**, 6006.
- [85] Negishi, T.; Koizumi, F.; Uchino, H.; Kuroda, J.; Kawaguchi, T.; Naito, S.; Matsumura, Y.; *British J. Cancer*, 2006, **95**, 601.
- [86] Nederberg, F.; Appel, E.; Tan, J. P. K.; Kim, S. H.; Fukushima, K.; Sly, J.; Miller, R. D.; Waymouth, R. M.; Yang, Y. Y.; Hedrick, J. L. *Biomacromol.*, 2009, **10**, 1460.
- [87] Lim, J.; Lo, S. T.; Hill, S.; Pavan, G. M.; Sun, X.; Simanek, E. E. *Mol. Pharm.*, 2012, **9**, 404.
- [88] Gaucher, G.; Marchessault, R. H.; Leroux, J. C. *J. Control. Release*, 2010, **143**, 2.
- [89] Majoros, I. J.; Myc, A.; Thomas, T.; Mehta, C. B.; Baker Jr., J. R. *Biomacromol.*, 2006, **7**, 572.
- [90] Luo, J.; Xiao, K.; Li, Y.; Lee, J. S.; Shi, L.; Tan, Y. H.; Xing, L.; Cheng, R. H.; Liu, G. Y.; Lam, K. S. *Bioconjugate. Chem.*, 2010, **21**, 1216.
- [91] Poon, Z.; Lee, J. A.; Huang, S.; Prevost, R. J.; Hammond, P. T. *Nanomed.: Nanotechnol., Biology Med.*, 2011, **7**, 201.
- [92] Qiao, H.; Li, J.; Wang, Y.; Ping, Q.; Wang, G.; Gu, X. *Int. J. Pharm.*, 2013, **452**, 363.
- [93] Unezaki, S.; Maruyama, K.; Hosoda, J.; Nagai, I. *Int. J. Pharm.*, 1996, **144**, 11.
- [94] Kim, S.C.; Kim, D.W.; Shim, Y.H.; Bang, J.S.; Oh, H.S.; Wan Kim, S.; et al. *J. Control Release*, 2001, **72**, 191.
- [95] Stevens, P.J.; Sekido, M.; Lee, R.J. *A Pharm. Res.*, 2004, **21**, 2153.
- [96] Yoo, H.S.; Park, T.G. *J. Control Release*, 2004, **96**, 273.
- [97] Kukowska-Latallo, J.F.; Candido, K.A.; Cao, Z.; Nigavekar, S.S.; Majoros, I.J.; Thomas, T.P.; et al. *Cancer Res*, 2005, **65**, 5317.
- [98] Chamorro, C.; Boerman, M.A.; Arnusch, C.J.; Breukink, E.; Pieters, R.J. *Biochim. Biophys. Acta (BBA): Biomembranes*, 2012, **1818**, 2171.
- [99] Aryal, S.; Grailer, J. J.; Steeberband, S. P. D. A.; Gong, S. J. *Mater. Chem.*, 2009, **19**, 7879.
- [100] Chen, J.; Xing, M. M. Q.; Zhong, W. *Polymer*, 2011, **52**, 933.
- [101] Al-Jamal, K. T.; Al-Jamal, W. T.; Wang, J. T. W.; Rubio, N.; Buddle, J.; Gathercole, D.; Zloh, M.; Kostarelos, K. *ACS Nano*, 2013, **7**, 1905.
- [102] Wu, Z.; Zeng, X.; Zhang, Y.; Feliu, N.; Lundberg, P.; Fadeel, B.; Malkoch, M.; Nyström, A. M. *J. Polym. Sci. Part A: Polym. Chem.*, 2012, **50**, 217.
- [103] Minotti, G.; Menna, P.; Salvatorelli, E.; Cairo, G.; Gianni, L. *Pharmacol. Rev.*, 2004, **56**, 185.
- [104] Deng, Z.; Yan, F.; Jin, Q.; Li, F.; Wu, J.; Liu, X.; Zheng, H. *J. Control. Release*, 2014, **174**, 109.
- [105] Li, G. Y.; Song, S.; Guo, L.; Ma, S. M. *J. Polym. Sci. Part A: Polym. Chem.*, 2008, **46**, 5028.
- [106] Wang, Y.; Cao, X.; Guo, R.; Shen, M.; Zhang, M.; Zhu, M.; Shi, X. *Polym. Chem.*, 2011, **2**, 1754.
- [107] Gillies, E. R.; Fréchet, J. M. J.; *Bioconjugate. Chem.*, 2005, **16**, 361.
- [108] Xiao, K.; Luo, J.; Li, Y.; Lee, J. S.; Fung, G.; Lam, K. S. *J. Control. Release*, 2011, **155**, 272.
- [109] Wu, X.; He, X.; Zhong, L.; Lin, S.; Wang, D.; Zhu, X.; Yan, D. *J. Mater. Chem.*, 2011, **21**, 13611.
- [110] He, X.; Wu, X.; Cai, X.; Lin, S.; Xie, M.; Zhu, X.; Yan, D. *Langmuir*, 2012, **28**, 11929.
- [111] Adeli, M.; Mirab, N.; Alavidjeh, M. S.; Zahra Sobhani, Atyabi, F. *Polymer*, 2009, **50**, 3528.
- [112] Kam, N. W. S.; Liu, Z.; Dai, H. J. *Am. Chem. Soc.*, 2005, **127**, 12492.
- [113] Maleki, M.; Adeli, M.; Kakanejadifard, A.; Movahedi, S.; Bani, F. *Polymer*, 2013, **54**, 4802.
- [114] Yarotski, D. A.; Kilina, S. V.; Talin, A. A.; Tretiak, S.; Prezhdo, O. V.; Balatsky, A. V.; et al. *Nano Let.*, 2009, **9**, 12.
- [115] Adeli, M.; Soleyman, R.; Beiranvand, Z.; Madani, F. *Chem. Soc. Rev.*, 2013, **42**, 5231.
- [116] Yuksel, M.; Colak, D.G.; Akin, M. et al. *Biomacromolecules*, 2012, **13**, 2680.
- [117] Durmaz, H.; Dag, A. Tunca, U.; Hizal, G. *J. Polym. Sci. A: Polym. Chem.*, 2012, **50**, 2406.
- [118] Bahun, G. J.; Adronov, A. *J. Polym. Sci. A: Polym. Chem.*, 2010, **48**, 1016.
- [119] Liu, P. *Eur. Polym. J.*, 2005, **41**, 2693.
- [120] Dalton, A. B.; Stephan, C.; Coleman, J. N.; McCarthy, B.; Ajayan, P. M.; Lefrant, S. *J. Phys. Chem., B* 2000, **104**, 10012.
- [121] Chen, J.; Liu, H.; Weimer, W. A.; Halls, M. D.; Waldeck, D. H.; Walker, G. C. *J. Am. Chem. Soc.*, 2002, **124**, 9034.
- [122] Adeli, M.; Mirab, N.; Zabihi, F. *Nanotechnology*, 2009, **20**, 485603.
- [123] Liu, C.-C.; Sadhasivam, S.; Savitha, S.; Lin, F.-H. *Talanta*, 2014, **122**, 195.
- [124] Khandare, J.J.; Jalota-Badwar, A.; Satavalekar, S.D. et al. *Nanoscale*, 2012, **4**, 837.
- [125] Adeli, M.; Beyranvand, S.; Hamid, M. J. *Mater. Chem.*, 2012, **22**, 6947.
- [126] Simonyan, A.; Gitsov, I. *Langmuir*, 2008, **24**, 11431.
- [127] Gitsov, I.; Lambrych, K.R.; Remnant, V.A.; Pracitto, R. *J. Polym. Sci. Part A Polym. Chem.*, 2000, **38**, 2711.
- [128] Adeli, M.; Haag, R. *J. Polym. Sci. Part A Polym. Chem.*, 2006, **44**, 5740.
- [129] Hed, Y.; Zhang, Y.; Andrén, O. C. J.; Zeng, X.; Nyström, A. M.; Malkoch, M. *J. Polym. Sci. Part A: Polym. Chem.*, 2013, **51**, 3992.
- [130] Fomina, N.; Sankaranarayanan, J.; Almutairi, A. *Adv. Drug Deliv. Rev.*, 2012, **64**, 1005.
- [131] Liu, G.; Liu, W.; Dong, C.M. *Polym. Chem.*, 2013, **4**, 3431.
- [132] Sun, L.; Zhu, B.; Su, Y.; Dong, C. M. *Polym. Chem.*, 2014, **5**, 1605.
- [133] Liu, G.; Liu, W.; Dong, C. M. *Polym. Chem.*, 2013, **4**, 3431.
- [134] Fomina, N.; Sankaranarayanan, J.; Almutairi, A. *Adv. Drug Deliv. Rev.*, 2012, **64**, 1005.
- [135] Sun, L.; Ma, X.; Dong, C. M.; Zhu, B.; Zhu, X. *Biomacromol.*, 2012, **13**, 3581.
- [136] De Jesús, O. L. P.; Ihre, H. R.; Gagne, L.; Fréchet, J. M. J.; Szoka Jr., F. C. *Bioconjugate. Chem.*, 2002, **13**, 453.
- [137] Gillies, E. R.; Fréchet, J. M. J. *J. Am. Chem. Soc.*, 2002, **124**, 14137.
- [138] Gillies, E. R.; Dy, E.; Fréchet, J. M. J.; Szoka, F. C. *Mol. Pharm.*, 2005, **2**, 129.
- [139] Lee, C.; Gillies, E. R.; Dy, E.; Fox, M. E.; Cramer, A. T.; Fréchet, J. M. J.; Dy, E. E.; Szoka, F. C. *Proc. Nat. Acad. Sci. USA*, 2006, **45**, 16649.
- [140] Lee, C.C.; Cramer, A.T.; Szoka, F.C.; Fréchet, J.M.J. *Bioconj. Chem.*, 2006, **17**, 1364.
- [141] Huang, J.; Gao, F.; Tang, X.; Yu, J.; Wang, D.; Liu, S.; Li, Y. *Polym. Int.*, 2010, **59**, 1390.
- [142] Spiess, M.; *Biochemistry*, 1990, **29**, 10009.
- [143] She, W.; Luo, K.; Zhang, C.; Wang, G.; Geng, Y.; Li, L.; He, B.; Gu, Z. *Biomaterials*, 2013, **34**, 1613.
- [144] del Barrio, J.; Oriol, L.; Sanchez, C.; Serrano, J.L.; Di Cicco, A.; Keller, P.; et al. *J. Am. Chem. Soc.*, 2010, **132**, 3762.
- [145] MacKay, J.A.; Chen, M.; McDaniel, J.R.; Liu, W.; Simnick, A.J.; Chilkoti, A. *Nat. Mater.*, 2009, **8**, 993.
- [146] She, W.; Li, N.; Luo, K.; Guo, C.; Wang, G.; Geng, Y.; Gu, Z. *Biomaterials*, 2013, **34**, 2252.
- [147] Zhang, Y.; Xiao, C.; Li, M.; Chen, J.; Ding, J.; He, C.; Zhuang, X.; Chen, X.; *Macromol. Biosci.*, 2013, **13**, 584.
- [148] Bae, Y.; Nishiyama, N.; Fukushima, S.; Koyama, H.; Yasuhiro, M.; Kataoka, K. *Bioconjugate.Chem.*, 2005, **16**, 122.
- [149] Shenderova, A.; Burke, T. G.; Schwendeman, S. P. *Pharm. Res.*, 1999, **12**, 241.
- [150] Davis, M. E. *Nat. Rev. Drug Discovery.*, 2008, **7**, 771

ARTICLE

- [151] Zhu, S.; Hong, M.; Tang, G.; Qian, L.; Lin, J.; Jiang, Y.; Pei, Y. *Biomaterials*, 2010, **31**, 1360.
- [152] Mattheolabakis, G.; Taoufik, E.; Haralambous, S.; Roberts, M. L.; Avgoustakis, K. *Eur. J. Pharm. Biopharm.*, 2009, **71**, 190.
- [153] Boulikas, T.; Vougiouka, M. *Oncol.Rep.*, 2004, **11**, 559.
- [154] Aryal, S.; Hu, C. M. J.; Zhang, L. *ACS Nano*, 2010, **4**, 251.
- [155] Wang, D.; Lippard, S. J. *Nat. Rev. Drug Discovery*, 2005, **4**, 307.
- [156] Galanski, M.; Arion, V. B.; Jakupec, M. A.; Keppler, B. K. *Curr. Pharm. Des.*, 2003, **9**, 2078.
- [157] Osada, K.; Christie, R. J.; Kataoka, K. *J. R. Soc. Interface.*, 2009, **6**, S325.
- [158] Casolaro, M.; Cini, R.; Del Bello, B.; Ferrali, M.; Maellaro, E. *Biomacromol.*, 2009, **10**, 944.
- [159] Gianasi, E.; Wasil, M.; Evagorou, E. G.; Kedde, A.; Wilson, G.; Duncan, R. *Eur. J. Cancer.*, 1999, **35**, 994.
- [160] Haririan, I.; Alavidjeh, M. S.; Khorramizadeh, M. R.; Ardestani, M. S.; Ghane, Z. Z.; Namazi, H. *Int. J. Nanomed.*, 2010, **5**, 63.
- [161] Adeli, M.; Hakimpoor, F.; Ashiri, M.; Kabiri, R.; Bavadi, M. *Soft Mater.*, 2011, **7**, 4062.
- [162] Naeini, A. T.; Adeli, M.; Vossoughi, M. *Nanomed.: Nanotechnol., Biol. Med.*, 2010, **6**, 556.
- [163] Naeini, A. T.; Adeli, M.; Vossoughi, M. *Eur. Polym.J.*, 2010, **46**, 165.
- [164] Mehdipoor, E.; Adeli, M.; Bavadi, M.; Sasanpour, P.; Rashidian, B. *J. Mater.Chem.*, 2011, **21**, 15456.
- [165] Kusari, S.; Zühlke, S.; Spitteller, M. *J. Nat. Prod.*, 2009, **72**, 2.
- [166] Berrada, M.; Serreqi, A.; Dabbarh, F.; Owusu, A.; Gupta, A.; Lehnert, S. *Biomaterials*, 2005, **26**, 2115.
- [167] Cheng, Y.; Li, M.; Xu, T. *Eur. J. Med. Chem.*, 2008, **43**, 1791.
- [168] Tyner, K. M.; Schiffman, S. R.; Giannelis, E. P. *J. Control.Release*, 2004, **95**, 501.
- [169] Zhang, L.; Hu, Y.; Jiang, X.; Yang, C.; Lu, W.; Yang, Y. *H. J. Control.Release*, 2004, **96**, 135.
- [170] Min, K. H.; Park, K.; Kim, Y. S.; Bae, S. M.; Lee, S.; Jo, H. G.; Park, R. W.; Kim, I. S.; Jeong, S. Y.; Kim, K.; Kwon, I. C. *J. Control. Release*, 2008, **127**, 208.
- [171] Schluep, T.; Cheng, J.; Khin, K. T.; Davis, M. E. *Cancer Chemother.Pharmacol.*, 2006, **57**, 654.
- [172] Modi, S.; Xiang, T. X.; Anderson, B. D. *J. Control.Release*, 2012, **162**, 330.
- [173] Kawano, K.; Watanabe, M.; Yamamoto, T.; Yokoyama, M.; Opanasopit, P.; Okano, T.; Maitani, Y. *J. Control.Release*, 2006, **112**, 329.
- [174] Sadekar, S.; Thiagarajan, G.; Bartlett, K.; Hubbard, D.; Ray, A.; McGill, L. D.; Ghandehari, H. *Int. J. Pharm.*, 2013, **456**, 175.
- [175] Martins, S.M.; Sarmiento, B.; Nunes, C.; Lúcio, M.; Reis, S.; Ferreira, D. C. *Eur. J. Pharm. Biopharm.*, 2013, **85**, 488.